CHAPTER 4

EXPERIMENTAL PROGRAMME AND PROCEDURES

4.1 Experimental Procedure of Soil Suction Imposition under a Temperature Field. Psychrometer calibrations

4.1.1 General aspects of soil water potential. Background of application and measurement of soil suction

Water in an unsaturated clayey soil is linked to the solid phase by both capillary absorption and surface adsorption due to the presence of active clay minerals (hydrogen bonding, hydration of cations, charged surface dipole and van der Waal's attraction: Mitchell, 1993), as well as by osmotic effects due to bulk water composition. Due to the difficulty of describing the different terms involved in the status of water in soils, an energy concept or soil-water potential is preferred to specify the amount of water held in a soil. The movement of water in the liquid phase in an unsaturated soil is thus explained in terms of this transport potential. In addition, this water potential is recognised as a fundamental concept to understand hydro-mechanical behaviour and the stress state in unsaturated soils, either by surface effects or by osmotic properties capable of maintaining water inside the soil structure. It is convenient to consider the potential of soil water per unit quantity of pure water (specific Gibbs energy) as the sum of several contributions defined with respect to a reference state with zero potential, usually taken as a flat surface of free pure water within a bath (Aitchinson *et al*., 1965 in Mitchell, 1993). Thus, the total potential Ψ of the soil constituent water at temperature T, is the amount of work that must be done per unit amount of pure water (usually weight) by means of externally applied forces in order to transport reversibly and isothermally an infinitesimal quantity of water from a pool of pure water at a specified elevation, the same temperature T and at atmospheric pressure to the soil liquid phase at the point under consideration.

The aim of the psychrometric technique is to measure the potential of water vapour existing in equilibrium with soil water. On the other hand, the vapour equilibrium technique imposes a soil water potential by means of the migration of water molecules through the vapour phase from a reference salt solution of known potential to the soil pores, until equilibrium is reached. At that instant, the condition for two phases to be in equilibrium with respect to the water species is that the chemical potential of these species should have the same value in the two phases (Guggenheim, 1967). The differential form of vapour chemical potential or molar Gibbs function is obtained from the fundamental equation (Castellan, 1971): $d\mu_v(u_v,T) = dg_v(u_v,T) = -\overline{S}_v dT + \overline{V}_v du_v$, where $\overline{S}_v$ and $\overline{V}_v$ are the molar entropy and molar volume of vapour, and u_v the vapour pressure. Assuming that vapour behaves as an ideal gas: $u_v = \rho_v RT/M_w = RT/\overline{V}_v$, where M_w is the molecular mass of water, ρ_v the vapour density, R the molar gas constant and T the absolute temperature. Admitting an ideal solution concept, the chemical potential of the liquid water is given by (Guggenheim, 1967; Castellan, 1971): $\mu_w(u_w,T,x_w) = \mu_w^o(u_w,T) + RT\ln x_w$, in which the first term $d\mu_w^o(u_w,T) = -\overline{S}_w^o dT + \overline{V}_w^o du_w$ is the chemical potential of the pure water species in the same (u_w, T) state as the liquid phase and x_w is the mole fraction of pure water solvent in the liquid mixture. $\overline{S}_w^o$ and $\overline{V}_w^o = M_w v_w$ are the molar entropy and molar volume of the pure solvent component, where $v_w = 1/\rho_w$ is the water specific volume. Assuming an isothermal evolution dT = 0, liquid incompressibility and after integration between a flat surface reference state (u_{wo}, x_{wo} and u_{vo}) and an experimentally accessible measuring state (u_w, x_w and u_w), phase equilibrium yields:

$$\overline{V}_w^o du_w + RTd(\ln x_w) - \frac{RT}{u_v} du_v = 0\,; \quad (u_w - u_{wo}) + \frac{RT}{\overline{V}_w^o} \ln\left(\frac{x_w}{x_{wo}}\right) - \frac{RT}{\overline{V}_w^o} \ln\left(\frac{u_v}{u_{vo}}\right) = 0 \tag{4.1}$$

The relative humidity due to soil matrix $h_m = u_v/u_{v1}$ is obtained from the previous equation admitting equality of liquid composition between the reference state (state with subscript 1) and the measuring system (state without subscript): $x_w = x_{w1} \leq 1$, where x_{w1} is the soil-water or reference state mole fraction. The flat surface reference liquid water pressure in equilibrium with atmospheric mixture pressure outside the porous medium is $u_{w1} = u_{da} + u_{v1}$, where u_{da} and u_{v1} are dry air mixture pressure and saturating water vapour pressure, respectively. The water pressure in the accessible measuring state within the porous medium in equilibrium with the same external dry air mixture pressure is $u_w = u_a - s = u_{da} + u_v - s$, where $s = (u_a - u_w)$ stands for matric suction or capillary pressure. Eq. (4.1) transforms to:

$$s = -\frac{\rho_w RT}{M_w} \ln h_m + (u_v - u_{v1})\,; \quad \ln h_m \approx -\frac{M_w s}{\rho_w RT} \tag{4.2}$$

The first relationship is equivalent to that described in Stallman (1964) (referred in Bear, 1972), where the term $(u_v - u_{v1})$ is usually neglected, transforming to the second expression or Kelvin's equation (Bear, 1972; Coussy, 1995; Coussy *et al*., 1998).

If matric component of water potential Ψ_m (surface and capillary sorption phenomena) is defined in terms of the molar Gibbs function g_{vm} of water in porous medium referred to that of a pool with identical solution composition and at the same temperature (reference state with subscript 1), a pressure definition of this component is obtained using Eq. (4.2):

$$\Psi_m = \frac{\Delta g_{vm}}{gM_w} = \frac{RT}{gM_w} \ln\left(\frac{u_v}{u_{v1}}\right) = \frac{RT}{gM_w} \ln h_m\,; \quad \Psi_m = \frac{(u_v - u_{v1}) - s}{\gamma_w} \tag{4.3}$$

where g is the gravitational constant and the last expression includes part of the pneumatic potential between the measuring system u_v and the reference state u_{v1}. According to this last expression it is assumed that the dry mixture pressure u_{da} in the reference state outside the porous medium is the same mixture pressure within the soil. Special care needs to be taken when measuring and imposing different energy status to soil water at high suction levels, where the classical mechanical air and water pressure interfacial concept reflected by Eq. (4.2) and Eq. (4.3) is not associated with a real physical meaning and to an experimentally accessible measuring state. It is not appropriate to relate hygroscopic humidity at suction levels of 100 MPa, that reasonably occur at 47% of relative humidity, with an equivalent negative water pressure that makes no physical sense, since physical properties of water that fills intra-aggregate pore spaces are different from water that flows at inter-aggregate level. Furthermore, negative absolute water pressures are difficult to conceptualise as indicated by Gray and Hassanizadeh (1991), where bulk water pressures approaching triple point pressure (0.611 kPa) seem to imply a condition of nearly no water phase present. However, water under tension with absolute negative pressure is assumed to remain in a meta-stable state (due to the presence of potential cavitation nuclei) when the phase boundary is transgressed without the liquid changing phase. Under these circumstances and the development of curved liquid-gas interfaces, it is possible to reach a state normally associated with a stable vapour phase (the one with lower chemical potential) without the vapour phase developing (Apfel, 1970 in Marinho and Chandler, 1995). Nevertheless, this liquid meta-stability can be destroyed if vapour cavities are formed within the liquid itself or at its boundaries (Trevena, 1987 in Marinho and Chandler, 1995). Indirectly measured values of tensile strength of water using different methods, which represent the overall ability of the water-container system to resist tension applied to the water, are compiled in Marinho and Chandler (1995), Guan and Fredlund (1997) and Guan *et al*. (1998), where relatively scattered values lower than -2 MPa are usually reported. This way, from now on, when referring to high

suction levels in a mechanistic pressure sense, they must be understood in a conceptualisation of soil-water energy status.

The relative humidity due to osmotic suction $h_\pi = u_{v1}/u_{vo}$ can be obtained from Eq. (4.1) admitting that the flat surface measuring state contains dissolved salts with a soil-water mole fraction x_{w1} different from that of the reference flat surface of pure water $x_{wo} = 1$. In the reference state $u_{wo} = u_{da} + u_{vo}$ and in the measuring state $u_{w1} = u_{da} + u_{v1}$. Substituting in Eq. (4.1) results:

$$(u_{v1} - u_{vo}) + \frac{RT}{\overline{V}_w^o} \ln x_{w1} - \frac{RT}{\overline{V}_w^o} \ln h_\pi = 0 \; ; \quad h_\pi \approx x_{w1} \tag{4.4}$$

where the term $(u_{v1} - u_{vo})$ is usually neglected transforming to the second expression or Raoult's law for ideal solutions (Castellan, 1971). This last expression shows the decrease in the relative humidity due to increasing dissolved salts in the bulk pore-water of the soil. An expression for the osmotic potential component Ψ_π is obtained following a similar procedure to that of Eq. (4.3), incorporating the pneumatic potential between the measuring system u_{v1} and the reference state u_{vo}:

$$\Psi_\pi = \frac{\Delta g_{v\pi}}{g M_w} = \frac{RT}{g M_w} \ln\left(\frac{u_{v1}}{u_{vo}}\right) = \frac{RT}{g M_w} \ln h_\pi \; ; \quad \Psi_\pi = \frac{(u_{v1} - u_{vo}) + \dfrac{RT}{\overline{V}_w^o} \ln x_{wl}}{\gamma_w} \tag{4.5}$$

Special care has been taken in the different experimental techniques, to try not to confuse the various water potential components. When suction is related to vapour equilibrium and psychrometric techniques, the water potential refers to the total component that includes the interaction with soil matrix and with the solute it contains, which is associated with the relative humidity of the pore air vapour $h_r = h_m h_\pi$. If suction is related to air overpressure technique described in section 3.1.2.1, then the water potential corresponds to the matric component, which at the same time is related to the matric relative humidity h_m that has no direct measurable physical meaning unless the osmotic suction is first determined. The squeezing technique of pore water reports this osmotic component, which is usually admitted to be independent of water content. The relative humidity related to this last component is directly measurable and corresponds for Boom clay powder to an approximate value of $h_\pi \approx 0.997$ (refer to section 2.2.2).

4.1.2 Vapour equilibrium technique

The thermodynamic relation between total suction of soil moisture $\psi = -(\Psi_m + \Psi_\pi)\gamma_w$ and the relative humidity of pore-water vapour h_r is given by the psychrometric law (Fredlund and Rahardjo, 1993): $\psi = -RT \ln h_r / (M_w v_w)$, obtained from Eq. (4.3) and Eq. (4.5). The suction water content relationship can be determined by exerting a controlled potential varying the relative humidity of the air of a sample and by measuring at equilibrium its gravimetric water content and total volume. To control the suction potential a constant relative humidity environment can be created by using colligative properties of salt solutions. In this way, the clay exchanges pure water until it reaches a thermodynamic equilibrium with the vapour pressure of the solution.

If an involatile solute is dissolved in a liquid under a solvent mole fraction x_l, the equilibrium vapour pressure u_v over the solution is observed to be less than over the pure liquid at the same temperature u_{vo} (Castellan, 1971). Since the solute is involatile, the vapour consists of pure solvent, which is usually confined together with a foreign inert dry air mixture at u_{da}. The requirement for the two phases to be in equilibrium with respect to the water species is that the chemical potential of the water should have the same value in both phases (Guggenheim, 1967; Castellan, 1971): $\mu_l(u_w,T,x_l) = \mu_v(u_v,T)$, where $\mu_l(u_w,T,x_l)$ is the chemical potential of the solvent species in the liquid

phase at a temperature T and under a flat surface pressure of $u_w = u_v + u_{da}$, and $\mu_v(u_v,T)$ is the chemical potential of the solvent in the vapour. For a non-electrolytic and non-ideal solution, which does not follow Raoult's law over the entire range of concentrations, and assuming the vapour as an ideal gas of pure solvent having a pressure u_v, the above condition becomes (Castellan, 1971):

$$\mu_l^o(u_w, T) + RT \ln a_l(x_l, T) = \mu_v^o(T) + RT \ln u_v(u_w) \tag{4.6}$$

where a_l is the activity of the solvent that is a function of temperature and composition, and the superscript refers to the standard chemical potential of the substance, which is a function of temperature and pressure in liquids and only of temperature in ideal gases. Subtracting the equation for pure solvent ($a_l = 1$) in equilibrium with vapour at u_{vo} from the preceding one, the analogue of Raoult's law for a non-ideal solution is obtained: $a_l(x_l, T) = u_v(x_l)/u_{vo}(T)$, which is the activity of a solvent (equivalent to the relative humidity of the equilibrated vapour that is usually accepted to be pressure independent). In solutions exhibiting negative deviations from Raoult's law, i.e. $a_l < x_l$, the solvent has a lower escaping tendency than an ideal solution at the same concentration. Real solutions behave ideally as the concentration becomes more dilute, $a_l = 1$ as $x_l \to 1$, thus being Raoult's law a limiting law.

In the preceding discussion of the liquid-vapour equilibrium, it was assumed that there was a foreign gas in the system. If the vapour is confined together with a foreign inert gas, the case of water vapour mixed with dry air at u_{da}, it has no important effect that apparently changes the behaviour outlined in the previous paragraphs. However, the vapour pressure u_v depends on the pressure exerted on the liquid phase (Castellan, 1971; Bear, 1972). This can be explained in terms of Eq. (4.6), where for constant temperature results:

$$\left(\frac{\partial \mu_l^o}{\partial u_w}\right)_T = RT\left(\frac{1}{u_v}\frac{\partial u_v}{\partial u_w}\right)_T ; \left(\frac{\partial u_v}{\partial u_w}\right)_T = \frac{\overline{V}_w^o}{\overline{V}_v(u_v)} = \frac{\rho_v(u_v)}{\rho_w} \tag{4.7}$$

where the second expression assumes vapour behaving as an ideal gas $u_v = RT/\overline{V}_v$. This last expression states that vapour pressure increases with the total pressure acting on the liquid, i.e. more solvent evaporates when more foreign gas is added; the increase being very small since ρ_v is much less than ρ_w.

It is important to clarify that to impose total suction one can use saturated saline solutions or select one type of aqueous solution, to which the solute quantity is progressively varied in order to achieve the predetermined soil-water potential. In this research, the second option was selected because it is easier to handle one reference saline electrolyte solution such as NaCl and to know the influence of the temperature on its properties (solubility and activity). Eq. (4.6) still holds for electrolyte solutions, expressing the activity a_l of the solution in terms of the geometric mean of the individual ion activities. For the electrolyte NaCl solution of dissociated ions the activity of the electrolyte can be related to the mean ionic molality, which at the same time is a function of the solute molality (Castellan, 1971). The relation between the relative vapour pressure or activity of a NaCl aqueous electrolytic solution and the molality of the solute m (mol of NaCl/kg of pure water, which is numerically equal to the mean ionic molality in a 1:1 electrolyte such as NaCl), as a function of the temperature T(°C), is given by the following empirical expression (Mac Mullin, 1969 in Horvath, 1985) valid for $m \geq 3.0$mol/kg:

$$a_l(m, T) = u_v(m)/u_{vo}(T) = 1 - 0.035m - m(m-3)(1.9772\times10^{-3} - 1.193\times10^{-5}T) \tag{4.8}$$

Mole fraction of water x_l can be obtained from molality, assuming a molecular mass of pure water of $M_w = 18.015$ kg/kmol: $x_l = 55.508/(55.508+m)$. Fig. 4.1 represents the activity of the electrolyte

solution for different temperatures and water mole fractions according to Eq. (4.8), which is valid for $x_l \leq 0.9487$. This system shows negative deviations from ideal solutions, being the activity less than the water mole fraction. For values $x_l > 0.9487$ experimental points at different temperatures have been adapted from Lang (1967). In the original work of this author, water potentials of NaCl solutions were reported as function of the molality ($0.05 \leq m \leq 2.0$) at different temperatures between 0°C and 40°C. These experimental results, previously converted to relative vapour pressures by means of the psychrometric law, are also plotted in Fig. 4.1, where it can be seen that the solution behaves ideally as the concentration of the solute approaches zero. If the molality of the solution is m < 3.0 mol/kg, it is accurate enough to take an activity not dependent on temperature. The following expression fits the experimental data in this range:

$$a_l(m) = u_v / u_{vo} = 1 - 0.035m - 1.1421 \times 10^{-3} m(m-3) \tag{4.9}$$

Eq. (4.8) is valid for unsaturated solutions, because there is a limiting value for salt concentration, which corresponds to the equilibrium condition of a solution saturated with respect to NaCl (refer to Fig. 4.1). The dependence of NaCl solubility on temperature can be stated by the following expression (molecular mass of the salt of 58.443 kg/kmol), similar to that proposed by Langer (1982) by fitting experimental data: m = (6.0461-0.039264T)/(1-0.0069059T), where m is the electrolyte molality and T is the temperature in °C.

The energy status or total suction ψ that is imposed to the soil water can be related through the psychrometric law to the relative vapour pressure of the soil pores, which at the same time is controlled by the activity of the NaCl solution:

$$\psi = -\frac{RT}{v_w M_w} \ln a_l \tag{4.10}$$

If it is assumed an exponential relationship for the water density (ρ_w in kg/m^3) dependent only on the temperature (T in °C) and fitting experimental results from Batchelor (1983) and Perry (1992) between 5°C and 100°C at a pressure of 0.1 MPa, the following expression results: $\rho_w = 1007.9 e^{-4.5731 \times 10^{-4} T}$. Using this last relation and substituting the different constant values, Eq. (4.10) can be written to give a fixed relationship between total suction in kPa, temperature in °C and NaCl aqueous solution activity:

$$\psi = -465.17(T + 273.15) e^{-4.5731 \times 10^{-4} T} \ln a_l \tag{4.11}$$

Fig. 4.2 shows a plot of Eq. (4.11) in combination with Eq. (4.8) or alternatively Eq. (4.9) for four different temperatures, representing the molality of NaCl versus the imposed soil total suction. Molality can easily be converted to g of solute per 1000 g of pure water multiplying it by the molecular mass of NaCl. Experimental points of Lang (1967) at two different temperatures are also plotted.

4.1.3 Suction imposition test series at different temperatures

The objective of this test series was to determine soil water potential relationships at different temperatures in terms of gravimetric water content and degree of saturation. A range of relative humidity $0.80 \leq u_v / u_{vo} \leq 0.98$, which correspond to the following total suction limits 3.2 MPa < ψ < 32 MPa, was generated using the sodium chloride solutions. The practical range of vapour equilibrium technique with this salt solution is indicated in Fig. 4.2. Suction inferior limit was chosen as 3 MPa due to the difficulty of controlling with accuracy high relative humidity values by NaCl solutions, which require small amounts of solute. As indicated in this figure, the slope of

the calibration curve is steeper, hindering suction control at low levels. It is preferred to use in this range other type of salt solution, i.e. saturated salt solutions with a relative humidity of $u_v/u_{vo} \geq 0.85$ (for example, saturated solutions of KCl with $u_v/u_{vo} = 0.85$, $ZnSO_4.7H_2O$ with $u_v/u_{vo} = 0.90$, $Na_2SO_3.7H_2O$ with $u_v/u_{vo} = 0.95$ or $CuSO_4.5H_2O$ with $u_v/u_{vo} = 0.98$; Vicol, 1990). The suction upper limit is defined by the salt solubility, which in the case of NaCl is limited to a relative humidity of $u_v/u_{vo} = 0.75$ at 25°C. Fig. 4.3 represents the variation of relative humidity for saturated NaCl solutions at different temperatures, according to Eq. (4.8) and to IUPAC reference solutions and Wexler and Seinfeld (1991) (referred in Lide and Frederikse, 1997). For higher suction values, up to approximately 350 MPa, solutions of H_2SO_4 are more appropriate (Esteban, 1990; CIEMAT Report in Volckaert *et al.*, 1996a).

Cylindrical soil specimens (diameter of 15.0 mm and height of 12.0 mm) were static and uniaxially compacted at an hygroscopic humidity of (3.0±0.3)% (relative humidity of the laboratory of 47%) and at seven different initial dry unit weights of 14.7, 15.7, 16.7, 17.7, 18.6, 19.6 and 20.6 kN/m^3. Soil samples were equilibrated in hermetic wide mouthed jars of 500×10^3 mm^3 capacity at a specified temperature and relative humidity of the air. The gravimetric hygroscopic humidity of NaCl powder was approximately 0.611% (oven drying at 105°C) at the same relative humidity of the laboratory, with a maximum limit of insoluble impurities of 0.005% of dry weight. These specifications have been taken into account in preparing salt solutions. Each jar was filled with 400×10^3 mm^3, leaving an air volume of 100×10^3 mm^3 and a surface area of 5.17×10^3 mm^2 for equalisation. The initial soil volume and exposed area are 2.12×10^3 mm^3 and 0.919×10^3 mm^2, respectively. After compaction, soil specimens were placed inside a glass cup, which in turn were put into the jars. The soil samples were allowed to equilibrate with the vapour pressure of the solution under different temperatures: 22°C (controlled room temperature to ±1°C) and 40°C, 60°C and 80°C by introducing the jars in a thermostatic oven (the cabinet maintained the desired temperature to ±1°C). Fig. 4.4 shows the jar, the rigid compaction mould and the glass cup used in a typical vapour equilibrium test.

One of the major concerns was the time required for vapour pressure equilibrium. Preliminary results of this test series indicated that changes in water content beyond the first week were negligible; hence, samples were allowed to equilibrate for a period of two weeks. After equalisation, the glass cup containing the sample was quick and carefully transferred to a digital analytical balance of 0.1-mg accuracy. This operation took less than 5 s in order to minimise moisture loss from the soil, specially under elevated temperatures. The estimated gravimetric water content loss at 80°C is less than 0.02%, deduced by observing the time evolution of the weight for 5 more seconds. After weighing, samples were carefully measured with a micrometer resolution of 10 μm (volumetric resolution of 0.20%). In this way, gravimetric water content and degree of saturation were determined at various applied total suctions and temperatures. In each of the vapour equilibrium stages different saline solutions were used in order to avoid changes in the concentration of the solutions, which could affect suction imposition due to solvent evaporation, specially under elevated temperatures.

Two types of test series were carried out: multi-stage and single-stage. In a multi-stage procedure, the same soil specimen underwent a main wetting phase followed by a main drying phase. The objective of this type of test, which was carried out only at 22°C, was to examine hysteresis effects in the water potential relationships. These tests started from a total suction value of 102 MPa (corresponding to the relative humidity of the laboratory) and the samples were progressively wetted following these suction steps: 31.6 MPa, 10.0 MPa, 7.9 MPa, 6.3 MPa and 3.2 MPa. After each equalisation stage the weight of the specimen was measured to determine the moisture change. At the end of the test series, the final water content was calculated by oven drying (ASTM D2216), and the water content of the seven samples after each equalisation stage was determined by backcalculation.

Single stage procedure was preferred in the test series at higher temperatures: 40°C, 60°C and 80°C. Hotter specimen swell more, being the volume change determination more difficult to accomplish, mainly in the high-porosity fabrics at elevated temperatures, which tend to crumble. On the other hand, soil samples equalised at a given temperature, are incorporated to the laboratory temperature during the weight and measurement process, being therefore preferable to put another prepared sample into the jar than continuing with the same soil subjected to a cooling path. Different soil samples were prepared at an initial suction value of 102 MPa for the different suction steps: 31.6 MPa, 10.0 MPa, 7.9 MPa, 6.3 MPa and 3.2 MPa. At the end of each equilibrium stage the seven samples with different packings were carefully weighed and measured, and the water content of the different specimens determined. Water potential relationships at different temperatures using the proposed methodology are presented in section 5.1.5.

4.1.4 Psychrometer calibrations and measurements

Thermocouple and transistor psychrometers were used to complement the retention curve information of vapour equilibrium points as described before, mainly in the total suction range from 15 MPa to 0.3 MPa. Transistor psychrometers (SMI type: Dimos, 1991; Woodburn *et al*., 1993) were employed in the upper limit ranging from 15 MPa to 4 MPa, measuring total suction of compacted cylindrical soil specimens (diameter of 15.0 mm and height of 12.0 mm), which were fabricated from wetted powder (refer to section 2.3.2) at a maximum water content of w = 19.0%. After this stage, soil powder was allowed to air dry at specified humidity between w = 10.6% and the upper limit indicated previously, and then compacted at predetermined void ratios ranging from 0.502 to 0.824.

Careful transistor psychrometer calibrations, that is determining the relationship between microvolts output from the transistors and a known total suction value, have been carried out according to the standard procedure adopted by Dimos (1991) for this kind of equipment. This relationship is affected by changes in several factors, which were discussed by Dimos (1991) and Truong and Holden (1995), such as temperature, hysteresis, change of calibration with time, equalisation period, drop shape and gap size. Several NaCl solutions, giving the standard range indicated in Fig. 4.2, were used to obtain the calibration curve for each probe. Woodburn and Lucas (1995) have extended this range up to 70 MPa, disconnecting the probes from the standard logger and reading the outputs using a millivoltmeter. The psychrometers were first equilibrated overnight at zero suction with distilled water (≤ 3 μS/cm) and the output adjusted to the initial offset. Afterwards the different outputs were recorded following one-hour stabilisation period for the increasing suction steps, starting from 100 kPa to 10 MPa salt solutions in a monotonic path to avoid hysteresis in the results. Fig. 4.5a shows the calibration curves at a controlled temperature of (22±1)°C, where total suction values are plotted against output voltages. Calibrations at different temperatures ranging from 20°C up to 27°C have been done by Troung and Holden (1995), showing a small zero-shift that did not exceed ±0.05 pF and no temperature effect on sensitivity. Specimens were tested at 22°C following the same equalisation period and calibration path, i.e. dry specimens were measured after wet ones.

Thermocouple psychrometers (Wescor HR-33T dew point microvoltmeter) were used on Boom clay powder in the lower limit ranging from total suction values of 0.3 MPa to 5 MPa. The practical limit over which total suction measurements can be made with this type of equipment is between 0.3 MPa and 7 MPa. However, above 4 MPa the repeatability of the outputs is not very good (Dimos, 1991; Ridley and Wray, 1996), specially when working with the dew point method (some output variability above 3.5 MPa). Below 0.3 MPa, psychrometer measurements should be carefully evaluated for validity (Lee and Wray, 1995). The psychrometer calibration procedure uses the same jars and solution volumes adopted for soil vapour equilibrium technique. Stainless steel screen psychrometers, which took less than one hour to reach equilibrium, were installed in the sealed jars such that the screen flat bottom was just touching the solution. However, the probes were allowed to equilibrate for at least 24 hours, to investigate time shift on outputs. The effect of the gap distance between source and sensor was discussed by Ridley and Wray (1996). A monotonic calibration path

starting from 0.1 MPa to 3.2 MPa was followed to avoid hysteresis effects at a controlled temperature of (22±1)°C. Average results obtained from three output readings (one after an hour and two at 24 hours) have been represented in Fig. 4.5b for the different probes used in the experiments and for two operation modes: psychrometric and dew point methods. Standard calibration curves at 25°C for the different modes are also plotted (Wescor HR-33T Instruction Manual), as well as a sensitivity range obtained from Wan (1996) for the psychrometric mode over a study of 40 probes at 25°C. Zero-shift error observed at zero suction, as well as probably some sensitivity shift with respect to the standard calibration, are due to time deterioration effects as a consequence of dust accumulation and corrosion of the measuring junction that can affect the heat exchange characteristics of the sensor (Ridley and Wray, 1996). Thermocouple sensitivity is also a function of the temperature of the psychrometer. Psychrometric mode calibration curves have been studied by Brown and Bartos (1982) (referred in Ridley and Wray, 1996) at various temperatures ranging from 0°C to 35°C, with the maximum variability in data occurring at higher temperatures. However, temperature dependence of soil water potential up to 50°C has been successfully investigated by Mohamed *et al.* (1992) and Wan (1996), using temperature calibrated psychrometers (psychrometric mode).

Boom clay powder at $\gamma_d \approx 10.8$ kN/m^3 and starting at an initial water content of 27.4% was controlled air dried to a final target of 15.4%. Soil powder was thoroughly mixed with demineralised water according to the procedure outlined in section 2.3.2 and maintained in the sealed jar for 24 hours before the suction measurement. Afterwards, it was allowed to air dry in the open jar controlling the target humidity by weight. After this operation, an equalisation stage of 24 hours was allowed. Probes were installed inside the soil mass and the water content of a representative amount of soil was determined after the equalisation stage. Average testing results of three outputs, one after an hour and two at 24 hours, are presented in Fig. 5.2 and Fig. 5.6 using both operation modes.

4.2 Testing Programme and Test Paths

This section describes the methods and stress paths that were followed within the testing programme. As this research is mainly focused on the volumetric behaviour of unsaturated clays (swelling, collapse and shrinkage behaviour) under suction, stress and temperature changes, two types of tests were performed: oedometer and isotropic tests. Advantages and limitations of both tests were analysed in section 3.1.1. Tests were performed initially under isothermal conditions at different temperatures and in a second stage, after gaining certain work experience, non-isothermal paths were considered in order to obtain additional information on aspects of behaviour related to temperature.

4.2.1 Test paths and methodology

4.2.1.1 Oedometer test paths

A series of oedometer tests were conducted on two soil packings described in section 2.3.2. Several types of suction, stress and temperature paths have been followed:

- isothermal wetting and drying cycles at constant net vertical stress and at two different temperatures (22°C and 80°C) (refer to Fig. 4.6 and Fig. 4.7);
- isothermal loading-unloading cycles at constant matric suction and at two different temperatures (22°C and 80°C) (refer to Fig. 4.8 and Fig. 4.9);
- drained heating-cooling cycles under constant matric suction and net vertical stress (refer to Fig. 4.10); and
- isothermal constant volume and suction controlled swelling pressure paths at two different temperatures (22°C and 80°C) (stress paths are presented in Fig. 6.72 and Fig. 6.73).

With reference to the first type of tests, samples at two different temperatures (22°C and 80°C) were loaded at approximately constant water content (around 15%) and at constant air pressure (u_a = 0.50 MPa) until the desired net vertical stresses were reached (indicated with letter i in Fig. 4.6 and Fig. 4.7). Loading stages for the denser overconsolidated samples were the following (refer to Fig. 4.6): 0.026 MPa, 0.085 MPa, 0.30 MPa and 0.55 MPa (at 0.45 MPa only two suction steps were performed at both temperatures). For the high-porosity samples the loading stages were the following ones: 0.085 MPa, 0.30 MPa, 0.60 MPa and 1.20 MPa (refer to Fig. 4.7). A wide range of initial overconsolidation ratios OCR_{vo} have been analysed for the low porosity packing, ranging from 173 to 8.2 at 22°C and from 157 to 7.4 at 80°C. These last estimations are based on an average unsaturated preconsolidation pressure of 4.50 MPa at 22°C and 4.07 MPa at 80°C, according to test results presented in Fig. 2.15. In the case of the high-porosity packing, overconsolidation ratios varied between 14.9 and 1.1 at 22°C and between 13.9 and 1 at 80°C. Maximum fabrication preconsolidation net vertical stress is around 1.27 MPa at 22°C and around 1.18 MPa at 80°C, as indicated in Fig. 2.15. Afterwards, matric suction paths were applied systematically by maintaining a constant air pressure of u_a = 0.50 MPa in the upper coarse porous stone and controlling the water pressure acting on the bottom high air-entry value ceramic disc. Water pressure is applied instantaneously and maintained during the equalisation period. The following suction steps were followed in the first wetting path: 0.45 MPa, 0.20 MPa, 0.06 MPa and 0.01 MPa. Subsequently, the process was reversed applying the same suction steps. The second wetting path continued the same steps indicated previously. A second drying path was followed in order to arrive to the target matric suction before continuing with the loading-unloading cycles (indicated with letter f in Fig. 4.6 and Fig. 4.7). Wetting and drying paths represented in different planes involving other state variables (matric suction and net mean stress or mean intergranular stress) are presented in Fig. 6.1 to Fig. 6.4.

Net vertical stress increase and decrease paths under constant matric suction and different temperatures are represented in Fig. 4.8 for the high-density packing and in Fig. 4.9 for the high-porosity fabric. Equipment deflections resulting from each load increment were corrected for compliance of the loading system according to Fig. 3.9. Duration of the different equalisation stages is presented in section 4.4.3. A relatively large number of loading steps were used in order to avoid the sudden decrease in suction associated with each undrained load application. For some tests, net vertical load increase was applied in equal increments usually between 0.05 MPa and 0.10 MPa and in some, by using load increment ratios between 0.10 and 0.25. Net vertical load decrease was achieved in equal decrements of around 0.20 MPa or in constant decrement ratios between 0.25 and 0.40. Stress increment ratios when adopting a step-loading approach present certain influence in the compression results, resulting in smaller compressions for the smaller increment ratios (Das, 1983b). These discrepancies have been explained for virgin states by Sivakumar (1993) in terms of the loading-collapse LC yield locus proposed by Alonso *et al.* (1990). Advantages of continuous loading systems over step-loading approaches have been discussed by Sivakumar (1993) and Cui and Delage (1996). According to these last authors, the step-loading technique overestimates the compressibility and underestimates the yield stress, because virgin states are reached under lower values of suction than intended. Nevertheless, the same stress increment criteria and step loading duration have been followed when comparing compressibility results at different temperatures. In addition, it is expected that differences associated with these two experimental procedures are smaller at nearly saturated states, which is the case of the tests performed, where degrees of saturation are usually maintained above 90%.

Net vertical stress loading and unloading were achieved by applying specified air pressure values acting on the diaphragm and piston systems, according to the calibration values presented in section 3.2.4.1. Different matric suction levels have been selected for the high-density packing: 0.01 MPa, 0.20 MPa, 0.30 MPa and 0.45 MPa. These loading paths were sufficiently extended in order to cause the soil to yield and detect rigidity changes that permit to obtain yield points and virgin states. Maximum net vertical stress values are indicated in Fig. 4.8. Unloading paths were accomplished until maintaining the same initial stress level, indicated with letter i in the same figure. Matric suction levels for the high- porosity packing were maintained at 0.01 MPa, 0.06 MPa, 0.20 MPa and

0.45 MPa; and maximum net vertical stress values, selected with the same previous criterion, are indicated in Fig. 4.9. A second loading-unloading cycle was also performed in all the tests related with the looser packing.

Drained heating and cooling paths were accomplished on heavily overconsolidated samples that were brought to the desired matric suction in the first wetting path and then subjected to temperature cycles under constant net vertical stress and matric suction. Equipment dilatation resulting from each temperature increment was corrected according to section 3.2.4.2. A net vertical stress of (σ_v-u_a) = 0.026 MPa has been applied and two constant matric suctions of 0.06 MPa and 0.20 MPa have been selected, according to Fig. 4.10. The following temperature steps were applied upon heating: 22°C, 40°C, 60°C and 80°C. After an initial quasi-undrained heating at a rate varying between 0.16 °C/min and 0.38 °C/min, temperature is maintained for 6 to 15 days and pore air and water pressures allowed to equalise under controlled matric suction. The cooling and subsequent heating paths follow the temperature steps indicated in the same figure. Quasi-undrained cooling rates depend on initial temperature according to Fig. 3.2, typical values being -0.23 °C/min at a starting temperature of 80°C and around -0.13 °C/min at a temperature of 60°C. Drained stages in cooling paths were maintained for 2 to 5 days.

In the constant volume paths the height of the specimens is forced to remain constant throughout the main wetting-drying cycle, recording the variation of the net vertical stress exerted on a stationary load cell. Wetting paths at the following matric suction steps were applied under a constant air overpressure of u_a = 0.50 MPa: 0.45 MPa, 0.20 MPa, 0.06 MPa and 0.01 MPa. After the wetting stage, suction was increased in the same increments to obtain the shrinkage pressure curve under null volume change without exceeding the air-entry value of the packing. The process is interrupted when shrinkage affects constant volume conditions. Swelling and shrinkage pressure paths represented in different stress state variable planes are presented in Fig. 6.76 to Fig. 6.78. The equalisation stages continued for 3 to 5 days until some steady state is registered. Nevertheless, some secondary stress relaxation effects are present and try to overlap themselves with the primary collapse and shrinkage phenomena. With the idea of reducing these secondary effects, lower equalisation periods to that of swelling/collapse under constant load tests have been selected. Continuous records of net vertical stress, net horizontal stress and water content changes, as well as apparatus deformability affecting null volume condition, were obtained throughout the experiments.

4.2.1.2 Isotropic test paths

Several types of suction, stress and temperature paths have been followed:

- wetting-drying cycles at constant net mean stress and at a constant temperature of 22°C (refer to Fig. 4.11);
- loading-unloading cycles at constant matric suction and at a constant temperature of 22°C (refer to Fig. 4.11 and Fig. 4.12); and
- heating-cooling cycles at constant matric suction and net mean stress (refer to Fig. 4.12).

Wetting and drying cycles, under constant isotropic stress and temperature, have been applied by varying matric suction to both soil packings. The samples were isotropically loaded at constant water content until the desired net mean stresses were reached. Afterwards, the suction paths were imposed step by step (0.45 MPa, 0.20 MPa, 0.06 MPa and 0.01 MPa) by applying a constant air overpressure of u_a = 0.50 MPa to the coarse porous rings and controlling the water pressure acting on the high air-entry value ceramic discs.

Following wetting-drying paths, the samples were isotropically loaded in different steps by increasing cell pressure, while holding constant both water and air back pressures. Net mean load increase in the mini isotropic cell was applied in equal increments of 0.05 MPa, while in the triaxial cell it was by using a load increment ratios between 0.04 and 0.11. Maximum net mean stresses are indicated in Fig. 4.11 and Fig. 4.12. Net mean load decrease was achieved in equal decrements of around 0.20

MPa in the mini isotropic cell and 0.40 MPa in the triaxial cell. Loading steps were allowed to equalise for several days according to equalisation periods detailed in section 4.4.3 to ensure nearly complete dissipation of any excess pore water pressure.

The same high-porosity packing was further subjected to drained heating-cooling cycles (refer to Fig. 4.12) at a constant matric suction of 0.20 MPa and under constant isotropic net mean stresses of $(\sigma_m\text{-}u_a)$ = 1.00 MPa (normally consolidated state) and $(\sigma_m\text{-}u_a)$ = 0.10 MPa (overconsolidated state). The drainage lines were kept open throughout the tests. The temperature was raised in steps starting from 22°C at a minimum rate of 0.08°C/min. Every 10°C the quasi-undrained temperature increase was stopped to allow for full equilibration of pore pressure that results from the higher expansion coefficient of soil water compared to that of soil skeleton (around 1 week of drained heating conditions). This way, experiments are initially not true drained tests with restricted drainage due to soil permeability and ceramic disc impedance effects. During this quasi-undrained stage, matric suction diminishes due to water pressure build-up, which is equivalent to a decrease in the effective (or intergranular) stress under nearly saturated conditions. The increase of pore water pressure with no change in boundary confining stress is analysed in section 7.2.1. Maximum temperatures have been limited to 60°C in the first heating-cooling cycles (refer to path B-C-D-E-F in Fig. 4.12), due to certain problems associated with diffused air accumulation with their consequences on the loss on continuity in the liquid water source and the evaporation of the interstitial water that induces a non-controlled shrinkage on the sample (refer to Fig. 7.27). In the thermal cycle performed on the overconsolidated sample at a lower isotropic load, the temperature was increased up to 50°C, with the idea of diminishing problems associated with soil water evaporation and minimising the irreversible disturbances induced on the sample. Additional aspects on evaporative fluxes and their control are presented in section 4.5.1. Cooling paths following the same temperature steps were performed with quasi-undrained typical rates of around -0.23°C/min in the range between 60°C and 40°C.

4.2.2 Oedometer and isotropic testing programme

4.2.2.1 Oedometer testing programme

4.2.2.1.1 Test programme on high-density packings

Twelve complete wetting-drying tests (137 suction equalisation stages), both in a single cycle or in two cycles, seven loading-unloading cycles (109 loading steps), and two heating-cooling paths (16 temperature steps) were conducted in the research programme with the high-density (heavily overconsolidated) packing. Three series of constant volume swelling pressure tests were also carried out. A periodic record of volumetric strains and water content changes has been followed throughout the tests. Systematically the stability of the pressure and temperature systems has been checked and when necessary they have been amended in order to maintain stress path stability. Table 4.1 summarises the main characteristics of the different tests (identification, stress paths, and time that is spent on each test), which lasted around 70 weeks working with an average of 4 cells. Test identification has been accomplished according to the following: 'C' refers to isothermal tests at 22°C ('H' is the equivalent identification for 80°C and 'CH' corresponds to non-isothermal paths), '17' refers to γ_d = 16.7 kN/m^3 and '0.026' refers to a constant net vertical stress of $(\sigma_v\text{-}u_a)$ = 0.026 MPa ('SP' corresponds to a swelling pressure path). Characteristics and comments on testing periods are described in section 4.4.3.

Test series were first performed on 20-mm high samples (height to radius ratio: h/r = 0.80). However, this height was further changed to 10 mm after observing excessive long equalisation periods (approximately 2.9 weeks per suction step), as well as detecting important ring friction effects (refer to section 4.5.1). However, the new height is sufficiently large for accurate strain measurements (volumetric strain resolution: 0.025%).

Table 4.1 Test series on heavily overconsolidated dense packings.

Test identification	Stress paths	Description	Period (weeks)
C17-0.026A	Wetting-drying (2 cycles)	h/r=0.80; conv. cell; 13 suction steps; ring friction effects; long term equalisation	36.7
C17-0.026B	Wetting	h/r=0.40; failed after 4 suction steps (electrical power interruption)	6.0
C17-0.026C	a)Wetting-drying-wetting	h/r=0.40; 11 suction steps	10.6
	b)Loading-unloading	15 loading steps at s=0.30MPa (max.1.00 MPa)	5.3
H17-0.026A	Wetting-drying (2 cycles)	h/r=0.80;13 suction steps; ring friction effects; long term equalisation; high evaporative fluxes	39.6
H17-0.026B	Wetting	h/r=0.40; failed after 4 suction steps (electrical power interruption)	6.3
H17-0.026C	a)Wetting-drying-wetting	h/r=0.40; 11 suction steps	14.7
	b)Loading-unloading-loading	14 loading steps at s=0.30MPa (max.0.80 MPa)	4.7
C17-0.085A	a)Wetting-drying (2 cycles)	h/r=0.40; 16 suction steps	22.9
	b)Loading-unloading	17 loading steps at s=0.01MPa (max.0.63 MPa)	8.1
C17-0.085B	a)Wetting-drying-wetting	h/r=0.57; lateral stress cell; ring friction effects; 12 suction steps	15.0
	b)Loading-unloading(2 cycl.)	26 loading steps at s=0.20MPa (max.0.80 MPa)	12.5
H17-0.085	a)Wetting-drying-wetting	h/r=0.40; 10 suction steps	17.7
	b)Loading-unloading	16 loading steps at s=0.01MPa (max.0.72 MPa)	8.0
C17-0.300	Wetting-drying-wetting	h/r=0.40; 10 suction steps	12.7
H17-0.300	Wetting-drying-wetting	h/r=0.40; 10 suction steps	13.1
C17-0.550	a)Wetting-drying (2 cycles)	h/r=0.40; 12 suction steps	5.2
	b)Loading-unloading	11 loading steps at s=0.45MPa (max.1.70 MPa)	3.7
H17-0.550	a)Wetting-drying (2 cycles)	h/r=0.40; 12 suction steps	6.0
	b)Loading-unloading	10 loading steps at s=0.45MPa (max.1.70 MPa)	3.3
CH17-0.026A	a)Wetting	h/r=0.40; thermal cell; 3 suction steps	4.1
	b)Heating-cooling (2 cycles)	7 temperature steps at s=0.20 MPa	2.7
CH17-0.026B	a)Wetting	h/r=0.40; thermal cell; 4 suction steps	5.4
	b)Heating-cooling (2 cycles)	9 temperature steps at s=0.06 MPa	8.5
C17-SPA	Wetting	h/r=0.40; 2 suction steps (load cell compliance)	0.7
C17-SPB	Wetting	h/r=0.40; 4 suction steps	1.3
C17-SPC	Wetting-drying	h/r=0.57; lateral stress cell; 7 suction steps	5.3

Many of the long term tests failed by different causes: electrical power interruption and its repercussions on heating and pneumatic systems, progressive ceramic disc desaturation or cavitation of water pressure system due to diffused air accumulation, mercury pots leakage affecting water pressure stabilisation and irreversible disturbances that could not be adequately corrected. Two failed tests occurred when performing the series on the denser samples, mainly due to electrical power interruption affecting the pneumatic system that acts independently from the mercury pot system. Nevertheless, many of the failed tests were used to state the reproducibility with different equipment and the repeatability with the same cell of different wetting paths. In general, quite good repeatability and consistency are observed in Fig. 4.13 and Fig. 4.14 in terms of volumetric strain and water content evolutions, when comparing different wetting paths carried out at the same temperature, with the same height to radius ratio and in the same cell. Some scatter is only appreciable, mainly in the hotter specimen, in the first equalisation stage because of some small variations in the initial conditions associated with the setting up phase. However, these deviations are progressively reduced in successive stages, when more homogeneous conditions have been

established. Some scatter has also been observed when comparing the most unfavourable cases of a sample tested with two different equipment (conventional and thermal cell reproducibility) and at the same temperature (22°C). Nevertheless, as the deviations are only observed in some cases (identified with '?' in the previous figures), they appear not to be systematic and can be attributed to certain variations in the initial conditions with their consequences on the first equalisation stages, as well as to the sensitivity and the resolution of the loading platen system of the thermal equipment at low stress levels (around 5 kPa according to section 4.1.2.2).

4.2.2.1.2 Test programme on high-porosity packings

Sixteen complete wetting-drying tests (154 suction equalisation stages), both in a single cycle or in two cycles, and nine loading-unloading cycles (144 loading steps) were conducted in the research programme with the high-porosity packing. Five series of constant volume swelling pressure tests were also performed. Table 4.2 summarises the main characteristics of the different tests, which lasted around 50 weeks working with an average of 4 cells. Test identification has been accomplished according to the criteria outlined in the previous section, where '14' refers to $\gamma_d = 13.7$ kN/m^3. Comments on testing periods are presented in section 4.4.3. Failed tests, which are also described in Table 4.2 indicating the cause of failure, have been advantageous for quality control to analyse the repeatability in a same type of equipment, as well as for detecting spurious problems associated with soil shrinkage and free water evaporation. Fig. 4.15 to Fig. 4.18 represent strain and water content evolution for different tests at constant net vertical stress, where both tendencies of swelling and collapse behaviour showed an adequate repeatability. In general, tests at 22°C present a better repeatability if compared to tests performed at higher temperatures, where the first stages are affected by the setting up and initial conditions that are more difficult to control in the case of the hotter samples.

Two tests are represented in Fig. 4.16 and Fig. 4.17 that failed at high temperatures by dissolved air accumulation below the ceramic porous stones. This accumulation that is difficult to control is mainly associated with the cavitation of the water pressure system and to the consequent evaporation of soil free water. Under these circumstances, spurious shrinkage phenomena are present and can be confused with primary collapse phenomena occurring in the first wetting stages. Nevertheless, these spurious phenomena are detected in the following suction step when observing lower collapse volumetric strain rates (refer to 'failed sample' in the aforementioned figures). Under these circumstances, water does not present the necessary continuity to transfer the boundary conditions to the soil mass and consequently to induce the collapse phenomenon. These spurious phenomena can also be detected due to the smaller water content changes that were observed in the following suction step (refer to 'failed sample' in Fig. 4.16) since water volume changes are mainly associated with the evaporation of the liquid and not to the capability of soil to retain water. In accordance to the previous exposition, it is probable that in test H14-0.600A (refer to Fig. 4.17), the primary collapse at the beginning of the stage is later affected by a progressive shrinkage of the sample, which is difficult to detect a priori. In the second stage, the increasing diffused air accumulation and the consequent difficulty of water to enter, makes difficult to arrive to a matric suction equalisation and the development of collapsible strains.

4.2.2.2 Isotropic testing programme

A series of four isotropic tests was performed on both packings, which are described in Table 4.3. Test identification has been accomplished according to the following criteria: 'I' corresponds to isotropic tests, '17' refers to $\gamma_d = 16.7$ kN/m^3 and '14' to $\gamma_d = 13.7$ kN/m^3, and '0.085' refers to a constant net mean stress of $(\sigma_m - u_a) = 0.085$ MPa ('IDT' corresponds to a dummy sample isotropic test). Loading-unloading paths could not be carried out on series I17-0.085B due to irreversible disturbances affecting soil sample. Series IDT of heating-cooling cycles were performed on a dummy stainless steel sample in order to calibrate the equipment and the transducers and to know

Table 4.2 Test series on high-porosity packings.

Test identification	Stress paths	Description	Period (weeks)
C14-0.085A	Wetting	h/r=0.40; failed after 2 suction steps (mercury pot leakage and water pressure drop)	1.6
C14-0.085B	a)Wetting-drying-wetting	h/r=0.40; 11 suction steps	10.3
	b)Loading-unloading (2cycl.)	20 loading steps at s=0.06MPa (max.0.60 MPa)	8.4
H14-0.085A	Wetting-drying	h/r=0.40; failed after 6 suction steps (mercury pot leakage and water pressure drop)	4.6
H14-0.085B	a)Wetting-drying-wetting	h/r=0.40; 11 suction steps	9.1
	b)Loading-unloading (2cycl.)	18 loading steps at s=0.06MPa (max.0.60 MPa)	6.1
C14-0.300A	Wetting	h/r=0.40; failed after 2 steps (mercury pot leakage and water pressure drop)	1.3
C14-0.300B	a)Wetting-drying (2 cycles)	h/r=0.40; 13 suction steps	8.4
	b)Loading-unloading (2cycl.)	13 loading steps at s=0.45MPa (max.1.00 MPa)	4.7
H14-0.300A	Wetting	h/r=0.40;failed after 2 suction steps (diffused air accumulation and progressive shrinkage)	1.0
H14-0.300B	a)Wetting-drying (2 cycles)	h/r=0.40; 13 suction steps	14.4
	b)Loading-unloading (2cycl.)	14 loading steps at s=0.45MPa (max.1.20 MPa)	4.3
C14-0.600A	Wetting	h/r=0.40; 4 suction steps (repeatability test)	3.3
C14-0.600B	a)Wetting-drying (2 cycles)	h/r=0.40; 11 suction steps	9.4
	b)Loading-unloading (2cycl.)	14 loading steps at s=0.20MPa (max.1.50 MPa)	5.1
C14-0.600C	a)Wetting-drying (2 cycles)	h/r=0.57; lateral stress cell; 11 suction steps	10.0
	b)Loading-unloading (2cycl.)	17 loading steps at s=0.20MPa (max.1.60 MPa)	7.0
H14-0.600A	Wetting	h/r=0.40; 2 suction steps (diffused air accumulation)	2.4
H14-0.600B	Wetting-drying	h/r=0.40; failed after 5 suction steps (mercury pot leakage and sample shrinkage)	7.6
H14-0.600C	Wetting	h/r=0.40; failed after 1 suction step (electrical power interruption)	1.7
H14-0.600D	a)Wetting-drying (2 cycles)	h/r=0.40; 11 suction steps	10.4
	b)Loading-unloading (2cycl.)	16 loading steps at s=0.20MPa (max.1.60 MPa)	4.9
C14-1.200	a)Wetting-drying-wetting	h/r=0.40; 10 suction steps	13.2(*)
	b)Loading-unloading (2cycl.)	15 loading steps at s=0.01MPa (max.1.90 MPa)	4.5
H14-1.200A	a)Wetting-drying	h/r=0.40; failed after 7 suction steps	10.5(*)
H14-1.200B	a)Wetting-drying-wetting	h/r=0.40; 10 suction steps	9.7
	b)Loading-unloading (2cycl.)	17 loading steps at s=0.01MPa (max.2.20 MPa)	5.1
C14-SPA	Wetting-drying	h/r=0.40; 6 suction steps	2.0
C14-SPB	Wetting-drying-wetting	h/r=0.57; lateral stress cell; 10 suction steps (problems with lateral stress stability)	4.7
C14-SPC	Wetting-drying	h/r=0.57; lateral stress cell; 7 suction steps (pellet fabric starting at hygroscopic humidity)	4.7
C14-SPD	Wetting-drying	h/r=0.57; lateral stress cell; 7 suction steps	4.6
H14-SP	Wetting-drying-wetting	h/r=0.40; 10 suction steps	3.1

Table 4.3 Isotropic tests on high-density and high-porosity packings.

Test identification	Stress paths	Description	Period (weeks)
I17-0.085A	a)Wetting-drying (2 cycles)	12 suction steps in mini isotropic cell	14.1
	b)Loading-unloading	17 loading steps at s=0.20MPa (max.0.80 MPa)	5.6
I17-0.085B	Wetting-drying-wetting	10 suction steps in triaxial cell; failed test	20.4
IDT	Heating-cooling (4 cycles)	22 temperature steps (max. 80°C)	9.0
I14-0.600	a)Wetting-drying (2 cycles)	11 suction steps in triaxial cell	15.9
	b)Loading	6 loading steps at s=0.20 MPa (max.1.00 MPa)	6.0
	c)Heating-cooling (2 cycles)	12 temperature steps at s=0.20MPa and (σ_m-u_a) = 1.00 MPa (max.60°C)	11.1
	d)Unloading + equalisation	2 unloading steps at s=0.20MPa up to 0.10MPa	3.4
	e)Heating-cooling (1 cycle)	6 temperature steps at s=0.20MPa and (σ_m-u_a) = 0.10 MPa (max.50°C)	6.1

4.3 Sample Preparation Techniques

4.3.1 Stress paths for sample preparation (oedometer tests)

Special attention has been given to the procedure of manufacturing soil samples at a specified dry unit weight, water content and temperature, in order to obtain an adequate sample homogeneity and repeatability. All samples were prepared in an identical fashion in order to maintain similar initial conditions. A variable peak stress - constant stroke static compaction procedure on the dry-side has been followed until a specified final volume is achieved. By means of this procedure, no trimming of the specimen is needed, which would be very difficult to accomplish in the case of the denser samples. Static compaction methods compared to dynamic methods are considered to give the best uniformity and repeatability (Sivakumar, 1993). Specimens 50.0 mm in diameter and 10.0 mm high for temperature controlled oedometer testing were compacted in a single layer and from one end in the two-split hermetic mould and heating chamber presented in Fig. 3.4. The experimental setup for the sample preparation tests in the hermetic mould inside the heating chamber is presented in Fig. 4.19a. Samples 70.0 mm in diameter and 20.0 mm high were prepared following the single layer compaction procedure detailed in section 2.3.1.2.1 in the lateral stress compaction equipment described in section 3.2.3.2. Fig. 4.19b presents the experimental setup for the sample preparation tests in the lateral stress ring.

In preparing specimens, the required quantity of demineralised water to achieve a starting water content of (15.0±0.3)% was added to the air-dried powder, following the powder preparation procedure detailed in section 2.3.2. This humidity approximately corresponds to an initial total suction of 2.3 MPa at 22°C and around 1.9 MPa at 80°C (refer to Fig. 5.18). Oedometer rings were greased with Teflon® grease and weighed prior to being placed into the mould. The required quantity of soil was poured into the pre-assembled oedometer mould. A metallic disc having approximately the same diameter of the ring and a height of 10.0 mm is installed in order to prevent the piston entering the 20-mm high oedometer ring. The initial height to radius ratio h/r relation is approximately 0.48 in the 50-mm ring and around 0.68 in the lateral stress ring, which ensure a low loss of energy input due to boundary friction. The mould was then placed in the triaxial frame and the top piston pushed in at a constant rate of 0.50 mm/min axial displacement until the flanges were in contact with the rest of the mould wall. The entrapped air is progressively released by the air pressure valve indicated in Fig. 3.4, which is immediately closed in order not to lose water content, specially under high temperature. The force of compaction determined by a load cell and the corresponding piston travel are measured at different intervals of displacements. Maximum fabrication (preconsolidation) net vertical stress is (4.50±0.16) MPa at 22°C and (4.07±0.12) MPa at

80°C for the heavily overconsolidated packing. Maximum net horizontal stress measured at ambient temperature for the same high-density fabric is around (1.74±0.09) MPa. In the case of the high-porosity fabric, maximum net vertical stress is (1.27±0.07) MPa at 22°C and (1.18±0.04) MPa at 80°C. Maximum net horizontal stress at ambient temperature for the high-porosity packing is (0.47±0.03) MPa. In order to reduce some rebound upon unloading, the piston is blocked and stress level approximately maintained for about 5 min. However, some net stress relaxation is detected, mainly affecting the lateral stress measuring system. Target height deviations due to specimen swelling after removal of vertical stress, affect target dry unit weights within ±0.20 kN/m^3 for the high-density fabric and around ±0.10 kN/m^3 for the high-porosity fabric.

Stress paths and soil conditions for the low-density and high-density packings during sample preparation under different temperatures are presented in Fig. 4.20 and Fig. 4.21, respectively. Sample preparation paths, for both thermal/conventional and lateral stress cells, can be described in the following steps with reference to the previous figures:

- **1**: Pre-compaction of powder at a seating net vertical stress of 0.80 MPa. Initial total suction is approximately 2.3 MPa. The estimated dry unit weight is around 13 kN/m^3.
- **1-2c**: One layer static compaction to the target density at constant water content and ambient temperature. A rate of 0.5 mm/min on a triaxial press was adopted.
- **1-2h**: Heating up to 80°C at constant water content in the hermetic mould maintained in the silicone oil bath at controlled temperature. The mould is then used to compact the soil at the predetermined density following the same rate indicated previously. Static compaction is performed, realising some pressurised air entrapped by the hermetic piston.
- **2c-3c (2h-3h)**: Stress relaxation while loading piston is blocked. Net vertical stress unloading path. Lateral stress relaxation probably related to an incipient passive failure under a Mohr-Coulomb criterion.
- **3c-4c (3h-4h)**: After compaction, the sample is weighed and the thickness measured (only for the specimens at ambient temperature) and the oedometer ring is transferred from the compaction mould to the oedometer cell. Water loss is prevented by covering the upper part with a plastic film, while mounting the different parts. Maximum temperature and water content changes during transferring and setting up are detailed in section 4.4.2.1.
- **4c-5c (4h-5h)**: Air and diaphragm pressures are applied. Loading path at constant water content (and approximately constant suction) up to the target net vertical stress. Water pressure is applied in order to impose an initial matric suction on the sample of 0.45 MPa. Suction controlled isothermal wetting path at constant net vertical stress.

4.3.2 Examination of static compaction techniques for isotropic tests (triaxial equipment)

Similar stress paths have been followed for the isotropic test sample preparations. Sample compaction for the mini isotropic cell with compression in a single layer from both ends is described in Cruz (1996). Specimens 38.0 mm in diameter and 76.0 mm high for the triaxial equipment were statically compacted in a stainless steel rigid mould in three layers using static one-dimensional compression. Compression of the first layer was performed at 0.50 mm/min until the desired volume, controlled by the flanges of the compaction piston, was reached. The sample would be then unstressed and the surface scarified. The same quantity of soil mass is poured in and compression of the second layer achieved by another flanged piston. Once the last layer has been compacted, the vertical stress is held for about 5 min. Air escaped between the piston and the mould. A three-piece split mould 200-mm long (refer to Fig. 4.25) previously greased with Teflon® grease has been used in order to facilitate the withdrawal of each part once compaction has been achieved, mainly in the case of the high-density specimens. Variable peak stress – constant stroke compaction procedure has been selected in order to arrive at a specified volume that allows a simpler assembly without trimming and a better adaptation to the geometry of the equipment. Maximum net vertical stress of approximately 5.79 MPa for the denser specimen and around 1.52 MPa for the high-porosity fabric were registered, which are larger

than the corresponding oedometer ones due to ring friction effects. However, a constant peak stress criterion has been preferred by Sivakumar (1993) and Cui and Delage (1996), because it provides the same maximum stress level in all the layers, improving even more the homogeneity of the samples.

The following compaction procedures were compared, compaction in a single layer (height to radius ratio of h/r = 4.0) and compaction in three layers (h/r = 1.33), both with compression from one end. The second procedure results in a better sample uniformity but is affected by marked interfaces between layers, although the surface was scarified before adding the same quantity of material for the next layer. Mechanical characteristics of sample uniformity were examined with isotropic compression tests, studying overall radial deformation patterns. As observed in Fig. 4.22, considerable non-uniformity is present when compacting in one layer, presenting higher compressibility in the less compacted lower part due to certain efficiency loss in the vertical load by friction effects (refer to Eq. (4.13)). However, even with the three layer compaction procedure, perfect homogeneity was difficult to achieve.

4.4 Testing Procedures

4.4.1 Saturation of ceramic discs. Water volume changes

Complete saturation and properly deairing is necessary to achieve a specified bubbling pressure. The method of deairing the ceramic disc is by solution of air under high water pressures. The oedometer cells were filled with deaired water and pressurised under a constant value of 1.0 MPa in the case of the 0.50 MPa air-entry value ceramic discs and of 3.0 MPa for the 1.50 MPa air-entry value filters. Special chambers were developed to saturate and pressurise the ceramic discs outside the triaxial cell. Most of the free air was removed from the porous ceramic by flushing through under a high flow gradient to atmospheric pressure. The steady-state seepage through the filter is used to evaluate the permeability of the disc and ensure that it is not cracked. After this stage, the valve connected to atmosphere was closed and the pressure in the system allowed to build-up to the cell pressure and left for several hours, in order to dissolve air entrapped in microscopic crevices (Ridley and Wray, 1996). The water compartment was then flushed through and the cell pressure allowed dissipating to atmospheric level. Under these conditions, it is expected that occluded bubbles at pseudo-equilibrium state try to diffuse and coalesce to come out of solution into the atmosphere at a very low rate, being replaced by water if the disc is inundated. However, pseudo-equilibrium conditions may exist even for larger periods than that involved in the disc saturation phase. For high temperature testing, the pressurising process was repeated several times. The ceramic discs were then checked for blow-through pressure at different temperatures. An open graduated burette was connected to the water compartment and an air pressure up to 0.50 MPa was then applied within the cell. Non drainage would be an indication that air-entry value had not been exceeded. Ceramic filters were re-saturated after each long-term test, specially under high temperature testing. In between the periods of consecutive tests the filters were kept under water in order to avoid their drying and connected to an open water system. If not inundated, continuous air passages could form, if no water is present to replace occluded bubbles diffusing into the atmosphere.

Measurements of water volume where mainly affected by soil free water evaporation and diffused air accumulation. Water volume change experiences three different behaviours: a transient phase due to progressive drainage, a quasi-linear steady-state condition due to diffusion of air and evaporation of free water, and a cyclic volume change with a period of 24 hours due to temperature fluctuations. The magnitude of this last volume change is around ± 25 mm^3 (approximately within the resolution of the system) for a temperature variation of ± 1°C. Daily cyclic temperature variations were minimised by systematically registering water volume changes at specified hours. Typical steady-state evaporative fluxes are presented in section 4.5.2, whereas typical dissolved air fluxes are indicated in section 3.2.5. During testing diffused air was periodically flushed, collected and measured from the base of the filter

following the procedures outlined in section 3.2.5.2, specially under high temperature testing and in the first wetting stages.

4.4.2 Specimen mounting

4.4.2.1 Specimen mounting in oedometer cells

The apparatus was prepared well in advance of sample preparation. Drainage lines were flushed with deaired water. The meniscus shape of the water volume change device was set in the appropriate direction and the whole water system was pressurised up to 50 kPa, unless a drainage line connecting the header tank to the ceramic disc compartment at 15 kPa. For high temperature testing, all the pieces (upper porous stone, top cap, top cell, ring fixing element and dial gauge) were partially mounted and heated to the target temperature. During the transference and assembly period of the hot sample, the different elements (upper porous stone, ring fixing element and dial gauge) were placed on the top plate that covers the heating chamber, which is at a temperature of approximately 80°C. In addition, during this assembly period, the top cell and cap are placed in an oven at 80°C. This way, it is ensured that all the different elements are assembled at a temperature similar to that of the test. Thus, spurious expansions of the different elements while thermal equilibrium is reached are minimised. These effects are of consideration in constant volume swelling pressure paths at high temperatures, since they can affect stress evolution. Nevertheless, these effects generally tend to appear at the initial wetting stages (usually during the first 10 min), showing a clear tendency that can be usually corrected when comparing to test evolution at ambient temperature (quasi-linear swelling trend or increase in the net vertical stress).

Once the sample has been compacted as described in section 4.3.1 and removed from the mould it is quickly installed in the oedometer cell and protected with an upper plastic film to minimise water content losses due to evaporation. Any excess water left over the ceramic disc is removed with an absorbent paper, but a thin film of water is still left, in order to avoid any desaturation of the disc and ensure an adequate contact with soil water. The initial weight of the sample at 22°C is measured just before installing it in the cell. The low air-entry filter and ring-fixing element are installed over the sample and then the top cap (connected to the air pressure line) is placed on the top of the filter. After this stage, the top cell is quickly assembled and a small seating pressure of around 5 kPa is applied, until platen movement occurs. Once contact has been established and initial position registered, the vertical stress and air pressure are raised together in steps of 50 kPa until the desired air pressure is reached. The difference between the vertical stress and the air pressure is maintained within 25 kPa. Afterwards, the vertical pressure is raised to the desired value under quasi-undrained conditions (water content is assumed approximately constant) and the compressive strains monitored. Water pressure is further increased up to 50 kPa and the wetting stage is started.

Water content losses and temperature changes were controlled by minimising the time during which the soil was exposed to the atmosphere. Fig. 4.23 shows the temperature evolution of the high-density sample at two points (central zone and border in contact with the ring) once it is withdrawn from the mould. In addition, the temperature evolution of the soil inside the mould is indicated once it is removed from the heater. Water content changes during this transference are also indicated in the previous figure. This loss can be associated with changes in the initial suction, according to the retention curve of the high-density packing presented in Fig. 5.18. The minimum time that takes withdrawing the mould from the heater, as well as removing the sample from the mould and installing it in the hot cell at 80°C, is 30 s. This fast process requires two people working in different activities with a pre-assembled equipment. Transferring the specimen from the mould into the cell induces a maximum change of temperature of around -5°C (approximately -10°C in the centre of the specimen and -2°C in the border in contact with the ring). Water content changes up to this moment are between -0.6% and -0.9% (estimated total suction between 2.6 MPa and 3.0 MPa). Immediately, the sample is covered with a plastic film to try to diminish the loss of humidity, while the fixing element of the ring

is fastened (dashed lines in Fig. 4.23). Afterwards, the plastic film is removed, the upper coarse porous stone installed, and the top cell mounted. From this moment on, the evaporation process is controlled because the nearly hermetic top cell is covering the sample. The assembly process is extended for 100 s more and finished when matric suction is applied. With the idea of improving the initial conditions of the sample, the powder mixture is prepared at a slightly higher water content (around 15.5%). This way, it is intended that initial water contents being within the usual range for this type of tests (15.0±0.3)%.

The mounting procedure for the lateral stress cell is as described for the conventional and thermal oedometer cells. Main differences refer to the disassembling of the metallic base cell and the compaction mould, once sample preparation is finished. The compaction equipment utilises a steel casing, which connects the base plate with the loading cap (piston guide) and that is further required to complete oedometer cell assembly. The lateral stress ring with the sample is quickly installed over the porous stone to diminish the effects of lateral stress relaxation. Special care has been taken in fixing lateral stress ring with ceramic disc base plate, in order not to disturb the initial conditions of the ring wall that controls the lateral pressure system. Wheatstone bridge output before the assembly of the ring is registered and unbalances due to ring setting up are compensated by a potentiometer acting on the zero-offset.

Specimen mounting in swelling pressure tests follows a similar procedure to that indicated for the thermal and lateral stress cells. The assembled cell with the miniature load cell and LVDT are quickly placed in the compression frame, according to what it is observed in Fig. 4.24a for the thermal cell and in Fig. 4.24b for the lateral stress cell.

After completing test paths, the samples were removed from the cells, measured, weighed and calculated their water contents. Local water contents by cutting the sample into three vertical layers were determined in the 20-mm high sample. About 2 mm were removed from the bottom to eliminate any disturbances from this end in contact with the ceramic disc. Maximum variations in the final water content are within 0.17% for the high-density packing (the bottom part presents 25.59% and the upper 25.42% for test series C17-0.085B; 21.85% and 21.84% for test series C17-SPC). Maximum variations are within 0.44% for the high-porosity packing (the bottom part presents 23.87% and the upper 23.43% for series C14-0.600C; 28.94% and 28.64% for series C14-SPB). Although samples present higher water contents in the bottom part, relatively homogeneous conditions are reached.

4.4.2.2 Specimen mounting in triaxial cell

4.4.2.2.1 General aspects of mounting procedure

Mounting procedures for the mini isotropic cell are described in Cruz (1996). However, some of the setting up stages indicated for the triaxial equipment can also be applied for the mini cell. A systematic and ordered procedure has been followed for the preparation of the sample and the assembly of the different mechanical elements. The main steps followed during this operation are described next, where only the assembly for silicone oil confining fluid is discussed. The process is similar, although more reduced, when air is used, eliminating the corresponding stages of the heating circuit. The whole setting up process takes approximately 60 min for two people working in an organised manner and having all the pieces of assembly prepared and marked to fit in the correct position.

- Acquisition system and transducers have been previously powered on to allow A/D converter to come into thermal equilibrium and minimise temperature effects on offsets.
- Drainage lines of the bottom fixed piston and the movable upper cap are filled with deaired water. Water volume change measuring system is pressurised up to 50 kPa, unless a drainage line connecting the header tank at 15 kPa with the conduits of the upper cap and bottom piston.

- The heating and expansion chamber, as well as the ram-feeding pump to compensate fluid losses and the cooling circuit, are filled with silicone oil by means of the high-pressure gear pump. Trapped air is released by the upper purge located in the heating chamber.
- The bottom porous stone with its portable base plate (previously filled with water) is placed on a thin film of water at atmospheric pressure. A thin film of water is also left over the top of both ceramic filters during the sample setting up process, preventing the possibility of their drying and ensuring a better contact with soil water. The sample is prepared as described in section 4.3.2, weighed and measured (micrometer resolution of 0.01mm). The initial water content is calculated from the same soil batch. Detected variations in dry unit weight are due to some specimen swelling after removal of the mould confinement. The specimen is wrapped within a plastic film to avoid water content losses.
- The surface of the specimen is painted in the zones of local axial and radial measurements with anaerobic catalysed silicone rubber, which vulcanises at room temperature. This preparation of the surface avoids the sliding of the silicone membrane with respect to the sample in the zones where the axial transducers will stick.
- The sample is placed between both bottom and top plate assemblies (refer to Fig. 3.23), which must be adequately oriented in order not to interfere the water and air drainage lines of the top cap with the LVDTs and their electrical connections. Top ram with the alignment device is maintained fixed in position with an auxiliary device in order not to gravitate on the specimen. Air lines of the upper piston are maintained closed in order not to dry the sample. Enough length is left in air and water drainage lines so that they do not produce non-wished stresses on the specimen. The weight of the specimen cap produces an axial stress on the specimen of less than 5 kPa. A thin coating of silicone grease is placed on both top and bottom caps. As soon as the specimen is brought into contact with the porous stones connected to an open system of water pressure, it begins to absorb water due to its initial suction. It is important to diminish the time to initiate the test, with the idea of minimising disturbances on the initial conditions.
- The silicone membrane, which is not pre-soaked to avoid water absorption, is installed on a two-split stretcher with two Viton® o-rings of 2.6×28 mm. Membranes of 36.5 mm unstretched inner diameter and with a thickness of 0.75 mm were specially developed for high temperature and long term testing. Silicone membranes were prepared by extrusion using the anaerobic catalysed silicone compound, which allows supporting temperatures over 150°C without appreciable changes in their properties. Silicone rubber with its catalytic component vulcanises at room temperature in approximately 45 min. The fabrication process includes the same three-split mould used for the compaction, as well as a stainless steel piston of 36.5 mm in diameter smeared with talcum powder, which lodges in a base plate of equal diameter and an upper ring that serves as a guide. Silicone mixture, deaired with a vacuum pump, is poured into the base plate tank. During the vulcanisation period, the piston is pushed slowly until it evacuates, by means of small lateral grooves, all the material contained in the base plate. The liquid fills the space between the mould and the piston reaching a height of 150 mm. Once the process is finished, it is let rest for 12 hours until the material presents a non-sticky surface. Fig. 4.25 shows the membrane inside the mould.
- The silicone membrane is installed with o-rings fitting in the grooves of both caps. Membrane is cut at a distance of around 3 mm from the o-ring position. The outside of the silicone membrane is coated with anaerobic catalysed silicone in the zone of measurements, ensuring that no sliding takes place between membranes. Silicone grease between the two rubber membranes slightly prevents air penetration in the case of using this cell fluid in early testing stages.
- The second latex membrane is installed in the same two-split stretcher and fitted over the previous one in order to cover and exceed it. This membrane has a thickness not exceeding 1% of the diameter of the specimen and an inner diameter of 90% of that of the sample, following ASTM-D2850. New 2.6×28 mm o-rings are installed on the latex membrane, which rest on the greased caps. This way, an effective seal is ensured at each end. The second membrane is necessary to fix the plastic elements that support the axial displacement transducers, since there is no fast action glue that can be utilised on the silicone membrane.
- The zones of laser measurements are coated with acrylic painting. This waterproof cover has a permanent white colour that does not lose properties with time nor with temperature.

- Both top collars and base plates of axial LVDTs are stuck with a special alignment device in order to ensure electrical zero position (refer to Fig. 3.24). A single component cyanoacrylate adhesive with operating temperatures up to 120°C and curing time of about 1 min at room temperature, was used to firmly attach the plastic elements to the latex membrane. Care must be exercised in aligning the vertical LVDTs with their respective cores. Fig. 4.26a shows sample preparation up to the present stage.
- Soil sample, bottom and top caps with alignment device, and top ram are carefully transferred to the triaxial cell. At this stage, the weight of the cap and the upper piston act on the sample (around 15 kPa), since it must be released from the auxiliary device during transfer.
- Bottom cap is fixed to the lower piston, taking care of the mounting position of the assembly. Air and water conduits between soil porous stone and the exterior drainage lines are connected and some water is flushed to expel trapped air. A water backpressure of 15 kPa is maintained in an open system.
- Bottom and top thermocouples are positioned and LVDTs connected to the power supply. Setting up process up to the present stage is presented in Fig. 4.26b. Triaxial chamber and top plate are carefully assembled without touching the specimen. The upper o-ring that seals the piston is encased before installing the drainage head, which connects air and water drainage lines with the conduits of the piston. Some water is flushed to expel trapped air and a backpressure of 15 kPa is applied to the upper porous stone. The piston and drainage head are locked maintaining a gap of 5 mm above the specimen cap after checking the alignment. The alignment device attached to the loading ram is located inside the sample top cap to prevent sample tilting during the different equalisation stages. After this process, the sample is prepared for establishing isotropic conditions.
- Polyamide pipes of the heating circuit are connected to the valves installed in the upper part of the equipment. The triaxial chamber is slowly filled with oil by pumping and evacuating the air gradually through the upper part. Once filled, the chamber is purged by the upper vent valve. In order to evacuate the air of the upper conduits, the pump flow is reversed and air is again trapped in the triaxial chamber.
- A small isotropic seating pressure of 20 kPa is applied in order to reduce bedding errors due to some movement of top collar and base plate LVDT fittings. Laser sensors are positioned illuminating the inferior part of the pedestal, which is the reference element throughout the testing period. The horizontal displacement micrometers of these sensors are fixed at the calibration position near electrical zero conditions. Initial values of the different transducers are registered by the data acquisition program. The whole height of the sample from the reference pedestal to top cap is travelled by the laser sensors and the sample profile registered in order to detect specimen tilting and to establish the lateral reference configuration.
- The initial stage is similar to the one-dimensional compression tests, where air and cell pressures are raised simultaneously in steps of around 25 kPa to 50 kPa up to a target air pressure of u_a = 0.50 MPa. The difference between the chamber and the air pressure is maintained within 25 kPa. After this stage, the cell pressure is raised to the desired value under quasi-undrained conditions (water content is assumed approximately constant). Water pressure is further increased up to 50 kPa.

When the test were finished, cell pressure was reduced to 20 kPa over air pressure. Then both pressures were progressively reduced to the water pressure, and afterwards, released to atmospheric condition. Cell chamber was emptied and the sample dismantled from top cap and pedestal. Sample final conditions are presented in Fig. 4.26c. Afterwards, the sample was carefully removed from the membrane and prepared for water content measurements. Confirmation of homogeneity after wetting-drying-wetting paths have been verified on the high-density sample measuring the local water content by cutting the sample into five vertical layers. About 5 mm were removed from the top and bottom to eliminate any disturbance due to high hydraulic gradients at these ends. Maximum water content difference between the bottom and top part is around 1.18% (bottom part: 28.66%; mid-height: 28.05% and top: 27.47%) for test series I17-0.085B. Although the sample presents higher water content in the bottom part, relatively homogeneous conditions are ensured due to the cell design with water pressure controlled at both top and bottom of the specimen.

4.4.2.2.2 Specimen hydration during setting up period

The sample starts drawing in water from the saturated disc when placed in contact with it. An estimation of water volume flowing into the specimen during this setting up period and their consequences on the initial conditions, has been carried out by means of a 1-D numerical simulation using the finite element code and the theoretical bases described in section 4.5.2. A mesh of 26 nodes with 5 elements of 1.48 mm corresponding to the ceramic disc and 20 elements of 1.90 mm up to the mid-height of the triaxial sample, have been considered for the analysis of the isothermal liquid flow. Water vapour flow is allowed and its concentration computed through the psychrometric law. This analysis incorporates characterisation of the ceramic stone through an intrinsic permeability of 1.68×10^{-18} m^2 and a porosity of 0.310 (a high air-entry value has been selected in order to ensure saturated conditions), as well as hydraulic properties of Boom clay based on experimental data reported in chapter 5 (a rigid soil skeleton with a porosity of 0.482 corresponding to the low-density packing is considered):

- intrinsic permeability of 8.50×10^{-19} m^2 with the following power expression for the liquid relative permeability $k_{rl} = S_e^{2.886}$, where S_e is the effective saturation assumed as $S_e = (S_r - 0.087)/0.913$;
- degree of saturation is computed as a function of matric suction through van Genuchten (1980) relation (wetting stage): $S_e = \left[1 + \left((u_a - u_w)/P\right)^{1/(1-\lambda)}\right]^{-\lambda}$, where $\lambda = 0.156$ and P = 0.03 MPa; and
- tortuosity factor affecting water vapour diffusion of $\tau \approx 0.40$ (refer to section 4.5.2.2) for the degree of saturation range involved in the simulation.

A constant atmospheric gas pressure u_a = 0.10 MPa and a constant temperature of 22°C is prescribed throughout (dry air density of ρ_{da} = 1.1804 kg/m^3). Initial conditions have been established as follows: u_w = 0.10 MPa in the ceramic disc and u_w = -1.80 MPa in the triaxial sample (matric suction of 1.90 MPa). Boundary conditions are the following: u_w = 0.10 MPa at $z = 0$ (ceramic disc), and $\omega_g^w = \rho_v/(\rho_v + \rho_{da}) = 0.016$ at z = 45.4 mm (mid-height of triaxial specimen). Mass fraction of water in gas is only prescribed for the open system to vapour corresponding to a relative humidity of ρ_v/ρ_{vs} = 0.986 with $\rho_{vs} = 1.948\times10^{-2}$ kg/m^3 at 22°C.

Isochrones showing the vertical variation of water content are indicated in Fig. 4.27. The triaxial sample in contact with the ceramic disc undergoes hydration during the setting up phase, which affects around 10 mm in contact with the ceramic disc. Total suction at the end of the specimen-mounting phase and at a distance of approximately 5 mm over the ceramic disc is estimated around 1.5 MPa. In addition, air lines opened to the atmosphere can have some influence on sample drying (refer to the simulation case of open system to vapour presented in the previous figure). Air lines are maintained closed during the specimen-mounting phase with the purpose of reducing drying effects, reason why the process is equivalent to the simulated case with closed system to vapour.

4.4.3 Equalisation stages

4.4.3.1 Equalisation periods for wetting-drying paths

According to Table 4.1, equalisation stages for wetting and drying cycles under oedometer conditions of the high-density packing involved the following testing periods in order to maintain a rate of volume change of less than 0.025%/day for the 10-mm high sample and 0.013%/day for the 20-mm high specimen (daily volume change within the resolution of the equipment):

- around (1.30±0.20) weeks at a temperature of 22°C and (1.50±0.20) weeks at 80°C for the 10-mm high sample (higher values correspond to the less loaded conditions);
- around 2.82 weeks at 22°C and 3.05 weeks at 80°C for the 20-mm high sample with h/r = 0.80;
- approximately 1.25 weeks for the 20-mm high sample in the lateral stress cell; and

- 0.35 week for the 10-mm sample and 0.76 week for the 20-mm sample (h/r = 0.57) in the swelling pressure paths.

In some tests reported in Table 4.1, mainly isothermal at 80°C, the duration includes the equilibration period of some reversible disturbances that affected the tests, reason why they are not totally representative of the average equalisation time. It is important to emphasise that test duration at higher temperatures is generally larger, due to certain secondary phenomena that have been detected in the swelling strain evolution under sustained low stress levels (secondary expansion aspects as shown in Fig. 4.13), as well as to ensure a reliable steady state condition for evaporation and air diffusion corrections. Time evolution at low stress levels of volumetric strain and water content changes are represented in Fig. 4.13 and Fig. 4.14. In general, it is observed (mainly at high temperatures) that water content equalisation involves shorter periods than the corresponding volumetric strain stabilisation, due to secondary expansion phenomena not attributable to water entrance but to water internal distribution possibly related to intra-aggregate water adsorption. Tests at higher net vertical stress involved shorter equilibration periods (around 0.50 weeks per equalisation stage for a net vertical stress of 0.550 MPa), because the swelling strain evolution is less sensitive to many secondary phenomena that were observed at low stress levels, as well as because the small daily variations that were detected after the forth day were within the resolution values of the measuring equipment.

Tests carried out on the lateral stress cell, although they present a larger sample height, were performed in relatively shorter periods if compared with other tests on 10-mm samples and 20-mm specimens. In general, after an equalisation period of approximately 5 days, daily variations of the horizontal stress measurements were not clearly detected since they were associated with values smaller than the resolution of the control equipment. This way, temperature disturbances in the laboratory originated adverse conditions that exceeded the values associated with soil changes. In order to diminish these thermal disturbances, the lateral stress cell was maintained inside a temperature controlled water bath. Swelling pressure tests were equalised in shorter periods to diminish secondary relaxation effects on soil structure, as well as to avoid secondary effects in the lateral stress measurement system, where some trend in lateral stress increase with elapsed time have been detected.

Equalisation stages for the high-porosity packing under oedometer conditions involved the following testing periods in order to maintain a rate of volume change of less than 0.025%/day for the 10-mm high sample:

- (0.80±0.15) week at a temperature of 22°C and (0.92±0.15) week at 80°C;
- around 0.91 week for the 20-mm high sample in the lateral stress cell; and
- 0.32 week for the 10-mm sample and 0.67 week for the 20-mm sample (h/r = 0.57) in the swelling pressure paths.

In general, shorter equalisation periods are required for the high-porosity packings, as well as longer stabilisation periods for the high temperature tests. Comments on the lateral stress and swelling pressure tests that were previously indicated are still applicable for the high-porosity packing. Larger equilibration periods were maintained in tests C14-1.200 and H14-1.200, indicated with asterisks in Table 4.2, because these tests were performed during the calibration stage of the triaxial cell that required more dedication. Time evolution of volumetric strain and water content changes are represented in Fig. 4.15 to Fig. 4.18. Secondary expansion phenomena affecting tests at high temperatures were detected at low stress levels (refer to Fig. 4.15), attributable to water internal distribution (water content changes were first stabilised). Secondary compression phenomena (creep) of soil skeleton under high-sustained stress levels, high temperatures and null water content changes were also observed (refer to Fig. 4.17 and Fig. 4.18).

Wetting-drying equalisation stages under isotropic conditions took at least 1.18 weeks for the high-density packing in the mini isotropic cell before the volume change rate and the flow of water in or out the sample were maintained in a daily variation within the resolution of the equipment (0.16%/day for volumetric strain rate and around 0.10%/day for the water content change). Numerical simulations

carried out by Cruz (1996) with the finite element code described in section 4.5.2 for a matric suction step from 1.9 MPa to 0.45 MPa at (σ_m-u_a) = 0.085 MPa, indicated that from the seventh day on more than 90% of the total soil volume and water content changes had taken place. In addition, the average liquid pressure had reached more than 95% of the change associated with suction reduction, and air pressure had dissipated the excess pressure (around 20 kPa), which was generated due to the ascending liquid flow that trapped air in the upper part. Equalisation periods in the triaxial equipment were maintained for 2.04 weeks (high-density packing) and 1.45 weeks (low-density fabric), equivalent to a daily soil volume change of less than 0.10%/day and a water content change of around 0.04%/day.

4.4.3.2 Equalisation periods for loading-unloading paths

High-density and high-porosity samples were subjected to increments of applied stress of (0.36±0.05) week interval in the conventional and thermal oedometer cells to ensure stabilisation of both water exchanges and volume changes to daily variations within equipment resolution, whereas in the lateral stress cell a duration of (0.45±0.04) week was adopted. Preliminary step loading tests (C17-0.085A and H17-0.085) carried out over an equalisation period of around 0.47 week, have shown that primary consolidation is completed within 48 hours. This way, time increments were selected according to the previous values in order not to have significant creep, which would be of certain consideration at higher temperatures (refer to Fig. 4.28). Numerical simulations for step loading equalisation stages carried out by Cruz (1996) ((σ_v-u_a) = 0.085 MPa to 0.150 MPa at constant (u_a-u_w) = 0.20 MPa), established a period of around 2 days for the high-density packing in the mini isotropic cell to arrive to 83.0% of the total soil volume change and 84.8% of the corresponding water content change. Soil volume change and expelled water were recorded and are presented in Fig. 4.28 for selected stages in test series C17-0.026C (conventional cell) and H17-0.026C (thermal cell), in Fig. 4.29 for test series C17-0.085B (lateral stress cell) and in Fig. 4.30 for test series C14-0.600C (lateral stress cell).

A coupled analysis of the isothermal two phase flow (liquid and gas) and skeleton deformation, which takes place during step loading equalisation, has been carried out for test series C14-0.600C ((σ_v-u_a) = 0.80 MPa to 0.90 MPa at constant (u_a-u_w) = 0.20 MPa), using the finite element code described in section 4.5.2. A 1-D mesh of 26 nodes with 5 elements of 1.48 mm corresponding to the ceramic disc, 10 elements of 1.75 mm representing the soil and 10 elements of 1.00 mm corresponding to the upper coarse porous stone, have been considered. Independent variables of the flow formulation are the gas $u_a = u_v + u_{da}$ and liquid pressures u_w. Water vapour flow is allowed and its concentration computed through the psychrometric law. Dissolved air is considered and its concentration computed through Henry's law. The ceramic disc is characterised through a porosity of 0.310 and an intrinsic permeability of 7.46×10^{-18} m^2. A low air-entry value and a low relative water permeability have been selected to ensure dry conditions in the upper coarse porous stone, as well as a tortuosity factor of $\tau \approx 0.50$. Hydraulic properties of Boom clay have been selected according to experimental results reported in chapter 5 (an initial porosity of 0.393 corresponding to the low-density packing is considered):

- intrinsic permeability of 3.00×10^{-19} m^2 with the following power expression for the liquid relative permeability $k_{rl} = S_e^{2.886}$ and $k_{rg} = A(1-S_e)^{2.886}$ for the relative permeability of the gas phase (the effective saturation is assumed as $S_e = (S_r - 0.087)/0.913$ for the liquid permeability and $S_e = S_r$ for the gas permeability and parameter A ≈ 2). For nearly saturated conditions involved in the tests (around 93.9%), parameter A can be increased up to around 100 to take into account some interconnected air voids;
- degree of saturation is computed as a function of matric suction through van Genuchten (1980) relation (drying path): $S_e = \left[1 + \left((u_a - u_w)/P\right)^{1/(1-\lambda)}\right]^{-\lambda}$, where $\lambda = 0.280$ and P = 0.50 MPa; and
- tortuosity factor affecting water vapour diffusion of $\tau \approx 0.30$ (however, lower values are expected according to section 4.5.2.2) (mechanical dispersion is neglected since no significant air flow takes place).

Mechanical behaviour of Boom clay is described following the constitutive model proposed in Alonso *et al.* (1990). To limit the amount of parameter determination, only the elastic part is considered through the following parameters: $\kappa = 0.02$ (elastic compressibility parameter for changes in net mean stress, that is mainly required to model the immediate compression), $\kappa_s = 0.14$ (elastic compressibility parameter for changes in suctions and mainly required to model time-dependent compression due to dissipation of excess water pressures) and a Poisson's ratio of $\nu = 0.25$ (according to section 2.3.1.2.2). Initial conditions (in terms of absolute pressures) have been established throughout as follows: $u_a = 0.60$ MPa, $u_w = 0.40$ MPa, T = 22°C, $\sigma_v = 1.40$ MPa and $\sigma_h = 0.72$ MPa. Flux problem boundary conditions prescribed on the ceramic disc are the following: $u_a = 0.60$ MPa and $u_w = 0.40$ MPa, and on the coarse porous stone: $u_a = 0.60$ MPa and $\omega_g^w = 0.269\times10^{-2}$ (mass fraction of water in gas is prescribed for the open system to vapour corresponding to a relative humidity of $\rho_v/\rho_{vs} = 0.980$ with $\rho_{vs} = 1.948\times10^{-2}$ kg/m^3 at 22°C, and $\rho_{da} = 7.082$ kg/m^3 at 0.60 MPa and 22°C). Mechanical boundary conditions are the following ones: vertical displacement prevented at z = 0 (below the ceramic disc) and a prescribed force imposed at z = 34.9 mm equivalent to an absolute pressure of 1.50 MPa. End execution time is fixed at 12 days.

Time evolution of air and water pressure changes during the application of a loading step and during the subsequent consolidation period at selected nodes (top, mid-height and bottom of the oedometer sample), as well as average lateral stress along the sample height, volumetric strain and water content changes compared to test readings, are presented in Fig. 4.31; whereas, isochrones of air and water pressure changes throughout the sample height are indicated in Fig. 4.32. As the sudden increment of net vertical stress is applied an excess of pore air and water pressure is generated within the sample, and suction in the soil is not regulated by the system. After an initial decrease of matric suction of around 10 kPa, it slowly increases in the sample over the consolidation period. Air pressure change is around $\delta u_a = 25$ kPa, with an approximate quasi-undrained parameter under K_0-loading of $B_{ak} \approx \delta u_a / \delta\sigma_v \approx 0.25$. Water pressure increase is around $\delta u_w = 35$ kPa, with an approximate quasi-undrained parameter of $B_{wk} \approx 0.35$. In addition, some instantaneous increase of the degree of saturation takes place (around 0.36%), which is progressively dissipated until conditions similar to the initial prevail. The excess of air pressure is dissipated to the backpressure value in around 200 min, due to the relatively high value of air permeability assumed despite the nearly saturated state. However, excess pore water pressure takes more time to dissipate to the target water backpressure (after three days a surplus of 3 kPa is still detected at mid-height that represents an 8.6% of the initial change). At the bottom face of the sample (air undrained) excess pore water pressure quickly dissipates to the water backpressure in 400 min, corresponding to 5% of the initial pressure change. At the top face of the sample (water undrained) excess pore water pressures dissipates within 6000 min (5% of the initial pressure change). Inspection of Fig. 4.31 indicates two clear stages in the volumetric strain evolution. Firstly, an immediate reduction in volume upon initial application of the net mean stress provided that some air voids remain interconnected and due to the compression of air bubbles. Secondly, a time-dependent compression is further developed due to water mass movement into air void space, to gradual dissolution of gas bubbles, to time-dependent dissipation of excess pore water pressure with the consequent re-expansion of gas bubbles, and to secondary compression or creep (Olson, 1986). Volumetric strain after an equalisation period of three days is maintained within 83% of the total volume change.

There was some uncertainty if disc clogging caused by ageing effects (refer to section 3.2.4.3) was slowing the rate of water pressure dissipation, due to increasing impeded drainage. This impeded flow through the incompressible high air-entry disc at the base of the specimen is characterised through an impedance-type factor (Fredlund and Rahardjo, 1993): $\lambda = k_d d/(k_w h_d)$, where k_d is the coefficient of permeability of the high air-entry disc, k_w the coefficient of permeability of the unsaturated soil with respect to the water phase ($k_w = 2.4\times10^{-12}$ m/s), d the length of the drainage path in the soil (d = 17.5 mm) and h_d the thickness of the ceramic disc ($h_d = 7.4$ mm). The impedance-type factor varied from 71.9 for $k_d = 7.3\times10^{-11}$ m/s to 3.8 for a disc permeability of $k_d = 3.9\times10^{-12}$ m/s due to clogging, which could promote certain time-lag effect (factors greater than 10 show no appreciable boundary

impedance according to Fredlund and Rahardjo, 1993). Another analysis was carried out with a ceramic disc intrinsic permeability of 4.03×10^{-19} m^2 (refer to Fig. 3.17), which is indicated with dashed lines in Fig. 4.31. No appreciable effects were detected when comparing both simulations with reference to water pressure dissipation, showing no important boundary impedance effects.

An approximate period of step load equalisation for time-dependent dissipation of pore pressure can be estimated applying a generalised form of Terzaghi's consolidation theory to nearly saturated soils with occluded air bubbles (usually for Sr > 85%). The nearly saturated soil is transformed into a material whose pores are fully saturated with an equivalent homogenised compressible fluid, containing uniformly distributed gas bubbles. One-dimensional consolidation equation can be written as (Vaziri and Christian, 1994):

$$\frac{\partial^2 \Delta u}{\partial z^2} = \frac{\gamma}{k}\left(\frac{1}{E_k^{'}} + \frac{n}{B_f}\right)\frac{\partial \Delta u}{\partial t}\ ; \quad \frac{C_v}{\left(1 + nE_k^{'}/B_f\right)}\frac{\partial^2 \Delta u}{\partial z^2} = \frac{\partial \Delta u}{\partial t}\ ; \quad C_{vs}\frac{\partial^2 \Delta u}{\partial z^2} = \frac{\partial \Delta u}{\partial t} \tag{4.12}$$

where k and γ are the permeability and the unit weight of the pore-fluid (liquid and gas), Δu is the change in pore-fluid pressure, C_v the coefficient of consolidation under fully saturated conditions, n the porosity, $E_k^{'}$ the drained constrained modulus, and B_f the pore-fluid bulk modulus. The last expression, subjected to all the assumptions and limitations of the classical consolidation theory, is the generalised form of Terzaghi's equation, which transforms to that for an incompressible pore fluid relative to soil skeleton (water-saturated system) when $nE_k^{'}/B_f \to 0$ .For an air saturated system with $nE_k^{'}/B_f \to \infty$, no consolidation response is obtained.

The relation $nE_k^{'}/B_f$ can be estimated from the undrained pore-pressure parameter under K_0-loading as a result of a vertical stress change $\Delta\sigma_v$ and as suggested by Vaziri and Christian (1994): $B_k = \Delta u/\Delta\sigma_v = 1/\left(1 + nE_k^{'}/B_f\right)$. According to the numerical analysis performed on test series C14-0.600C, an equivalent pore-pressure parameter of the mixture $B_k \approx 0.30$ is obtained for Sr ≈ 93.9%, which results in an estimated $nE_k^{'}/B_f \approx 2.33$. In addition, the pore-fluid (air-water mixture) bulk modulus can be calculated by means of the following expression (Ghaboussi and Kim, 1982): $1/B_f = (1 - Sr_o + hSr_o)\,u_{ao}/(u_w + p_c)^2$, which takes into account the compressibility of the air portion due to free air compression and air dissolving into water (volumetric solubility, h = 0.018). The subscript o denotes initial values and it is assumed that the capillary pressure $p_c = u_a - u_w$ remains constant throughout the process. For $Sr_o \approx 93.9\%$ and u_a = 0.60 MPa, $1/B_f \approx 0.131$ MPa^{-1}. Assuming $E_k^{'} \approx 40$MPa (refer to Fig. 2.35) and n ≈ 0.40, the compressibility relation results in $nE_k^{'}/B_f \approx 2.1$, which is similar to the previous value. The equivalent consolidation coefficient under nearly saturated conditions was calculated to be around $C_{vs} \approx 3\times10^{-3}$ mm^2/s (C_v values for saturated conditions are presented in Fig. 2.35 and can be estimated assuming $k_{ws} = 3\times10^{-12}$ m/s).

Step loading stabilisation period for isotropic tests carried out in the triaxial cell can be calculated by means of this equivalent consolidation coefficient and with a maximum flow path of 38 mm: around 6 days for an average degree of saturation of 95% (refer to Table 4.3). However, it is necessary to consider some impeded flow through the high air-entry disc at the base of the specimen. The impedance-type factor, as previously defined, is around λ = 40.7 for a coefficient of permeability of the high air-entry disc of $k_d = 2.38\times10^{-11}$ m/s that includes some clogging due to ageing effects (refer to Fig. 3.17). The coefficient of permeability of the unsaturated soil is assumed $k_w = 3\times10^{-12}$ m/s, with a drainage length of d = 38 mm and a ceramic disc thickness of h_d = 7.4 mm. As the factor is greater than 10, the equalisation period of 6 days is not significantly affected by the impeded flow (Fredlund and Rahardjo, 1993).

4.5 Test Spurious Problems

4.5.1 Ring friction effects

Friction between the soil and the fixed oedometer ring reduces the net vertical stress acting on the soil compared with the applied stress during compression, and increases the net vertical stress during swelling. This way, expansive soils present a smaller trend to swelling due to this effect, and on the other hand, soils with an open structure present less collapse. This behaviour is observed in Fig. 4.33 for the high-density packing. Lateral friction can be approximately determined based on the measured net lateral stress $K_0(\sigma_v\text{-}u_a)$ and considering a wall friction angle δ assumed to be 90% of the drained friction angle (Olson, 1986), which can be estimated in around $\phi' = 21°$ according to experimental data (Horseman *et al*, 1987; Hueckel and Baldi, 1990; Lagny, 1996). The local side shearing force over a height dz, which affects in $d(\sigma_v\text{-}u_a)$ the applied net vertical stress $(\sigma_v\text{-}u_a)_o$ acting over a sample, can be estimated as:

$$d(\sigma_v - u_a) = \mp \frac{2K_0(\sigma_v - u_a)\tan\delta\, dz}{r}; \quad (\sigma_v - u_a)_z = (\sigma_v - u_a)_o e^{\mp\frac{2K_0\tan\delta\, z}{r}} \tag{4.13}$$

where $(\sigma_v\text{-}u_a)_z$ is the average net vertical stress at any depth z in the sample with radius r. The negative sign applies for compressive samples, whereas the positive applies for expansive behaviour. The average correction λ_c affecting applied vertical stress over the sample height h is then:

$$\lambda_c = \frac{(\sigma_v - u_a)_{ave}}{(\sigma_v - u_a)_o} = \frac{\int_0^h e^{\mp\frac{2K_0\tan\delta\, z}{r}} dz}{h} = \mp\frac{r}{2hK_0\tan\delta}\left(e^{\mp\frac{2hK_0\tan\delta}{r}} - 1\right) \tag{4.14}$$

Though these last expressions are only approximate due to the fact that no consideration is given to soil adhesion and enough deformation is assumed to mobilise full soil/ring friction, they indicate that frictional effects can be minimised by using thin specimens in wide rings, by reducing the soil/ring friction or adhesion with grease and by using floating rings. Corrections also depend on stress paths through K_0 factor, suggesting higher friction effects during rebound or initial wetting than during initial compression or drying.

Estimations of ring friction effects on the high-density packing at constant $(\sigma_v\text{-}u_a) = 0.085$ MPa during initial wetting with an average $K_0 \approx 4.2$ measured in the lateral stress cell, report a correction factor of $\lambda_c \approx 2.49$ in this cell with $h/r \approx 0.57$. The same calculation in the conventional suction controlled cell with a sample height of 10 mm and $h/r \approx 0.40$ report a value of $\lambda_c \approx 1.85$. Comparison of both corrections reflects an average stress ratio of $(\sigma_v - u_a)_{lat.cell}/(\sigma_v - u_a)_{conv.cell} \approx 1.35$; that is as if the net vertical stress acting on the lateral stress oedometer would be 35% greater. On the other hand, average value of $K_0 \approx 1.8$ is lower in the shrinkage path following the initial wetting (friction effect is reversed to a compressive behaviour), reducing the overall friction to an average stress ratio of $(\sigma_v - u_a)_{lat.cell}/(\sigma_v - u_a)_{conv.cell} = 0.72/0.79 \approx 0.91$; that is, as if the net vertical stress in the lateral cell is reduced in a 9% with respect to the corresponding value of the conventional cell. The wetting path following the wetting-drying cycle with average $K_0 \approx 1.8$ presents a similar stress ratio of $(\sigma_v - u_a)_{lat.cell}/(\sigma_v - u_a)_{conv.cell} = 1.45/1.29 \approx 1.12$. The general trend can be observed in Fig. 4.33, where main differences are detected in the first wetting path and friction consequences after this path are of lesser importance.

Ring friction consequences in wetting-drying cycles on the high-density packing at constant $(\sigma_v\text{-}u_a) = 0.026$ MPa are also presented in Fig. 4.33. Stress ratios assuming similar K_0 values are of the order of $(\sigma_v - u_a)_{20mm}/(\sigma_v - u_a)_{10mm} \approx 2.04$ in the first wetting path, explaining the lower swelling strains

observed in the 20-mm specimen. The higher shrinkage detected in the 10-mm high sample could not easily be interpreted, but the subsequent wetting with a stress ratio of $(\sigma_v - u_a)_{20mm} / (\sigma_v - u_a)_{10mm} \approx 1.32$ indicates friction effects of lesser importance, which can be observed in the previous figure. Ring friction effects in wetting-drying cycles on the low-density packing at constant $(\sigma_v - u_a) = 0.600$ MPa, were also studied. For the first wetting path with a collapsible trend at an average $K_0 \approx 0.4$, stress ratio is of the order of $(\sigma_v - u_a)_{lat.cell} / (\sigma_v - u_a)_{conv.cell} \approx 0.98$, which indicates no significant consequences and an adequate reproducibility (refer to Fig. 6.35).

Special care has been taking in minimising ring friction consequences (mainly in high-density packings) in the comparison of temperature effects obtained in different equipment. In this sense, only similar h/r ratios around 0.40 are used in contrasting isothermal test results on heavily overconsolidated samples at different temperatures.

4.5.2 Spurious problems with evaporative fluxes

4.5.2.1 General aspects. Measured evaporative fluxes

This section contains the results of a set of 1-D coupled thermo-hydraulic analysis carried out to simulate evaporative fluxes and suction application during a main wetting path at different temperatures. This analysis incorporates hydraulic and thermal properties of Boom clay, as well as a characterisation of both coarse and ceramic stones. The main goal of the simulation is to determine the feasibility of applied matric suction stabilisation under high temperatures, due to the different water fluxes involved in the process: first an evaporative flux that tries to dry the clay dependent on both soil properties (mainly vapour diffusivity) and boundary conditions (relative humidity of air above the evaporating surface) and second a water flux through the low permeability ceramic disc (mainly dependent on soil and ceramic disc permeability). Measured evaporative fluxes (refer to Fig. 4.34) are compared to model predictions prescribing a constant relative humidity at the upper soil surface and solving coupled heat and mass transfer equations for the soil profile, and this way detecting if it is possible to achieve matric suction equalisation throughout the sample height. The results of numerical analysis are a basic tool for a better understanding of the various interacting processes occurring and are used to gain insight of expected test behaviour. Due to the axisymmetric conditions of the tests, 1-D analyses are only incorporated. It is expected that 2-D axisymmetric analysis will report some small quantitative differences, but that will not be qualitative different from the interacting phenomena effects that are intended to be shown. Evaporative fluxes using a Dalton-type equation with adequate exchange functions and with the vapour pressure at the soil surface determined on the basis of solving coupled heat - mass transfer equations, have been modelled and compared to measured results by Wilson *et al.* (1994).

Fig. 4.34 presents results of evaporative fluxes measured under steady-state conditions for both high-density and high-porosity packings in the main wetting stages (evaporative fluxes in drying paths at nearly saturated conditions are presented in Fig. 5.34). Evaporative fluxes at higher suctions are lower than the corresponding fluxes at nearly saturated conditions. This concept has been explained on the basis of water availability within the soil, where the hydraulic conductive properties of the soil no longer permit a sufficient flow of water to maintain the evaporation (Wilson *et al.*, 1994). Similar conclusions can be obtained based on a Dalton-type surface boundary condition for water vapour flow (Fredlund and Rahardjo, 1993; Wilson *et al.*, 1997):

$$E_v = f_v (u_v - u_v^a); \quad E_v = f_v u_{vo} \left[\exp\left(- \frac{((u_a - u_w) + \pi) v_w M_v}{RT} \right) - h_{ra} \right] \tag{4.15}$$

where E_v is the volumetric evaporative flux, u_v the vapour pressure of the evaporating soil surface, u_v^a the vapour pressure in the air above the evaporating surface and f_v an exchange function which

depends on the mixing characteristics of the air above the evaporating surface. The last expression that assumes approximately the same temperature for air and soil (u_{vo} is the common saturation vapour pressure), indicates a reduction in the evaporation rate from a soil surface that is drying (increasing total suction ψ or decreasing u_v at the soil surface) under constant climate conditions (constant relative humidity of the air h_{ra} above the evaporating soil). Soil evaporation ceases when the relative humidity of the soil reaches equilibrium with the constant relative humidity of the air above the soil.

Experimental results (test series H17-0.026A is not included) have been fitted to the expression: $E_v = a[\exp[-b((u_a - u_w) + \pi)] - h_{ra}]$, with an osmotic suction of $\pi \approx 0.41$ MPa (E_v in $(mm^3/s)/mm^2$ and $(u_a\text{-}u_w)$ in MPa). Values of $a = 2.533\times10^{-4}$ mm/s, $h_{ra} = 0.9945$ and $b = 6.336\times10^{-3}$ MPa^{-1} have been obtained. Theoretical value (calculated at 80°C with Eq. (4.15)) of this last constant is $b = 6.314\times10^{-3}$ MPa^{-1} ($v_w = 1.029\times10^{-3}$ m^3/kg), which is in agreement with the previous result. The value of the exchange function is around $f_v = 5.315\times10^{-3}$ mm/(s.MPa) ($u_{vo} = 47.66$ kPa at 80°C). In addition, a high relative humidity in the air chamber is observed, which ensures an adequate suction stabilisation. When performing curve fitting on test series H17-0.026A, maintaining parameters a and b constant, a lower value of $h_{ra} = 0.9780$ is obtained, which is not adequate for matric suction equalisation, as further indicated. According to Fig. 4.34, some reduction of evaporative flux is detected on the high-porosity packing at higher net vertical stress levels and under lower porosity and higher degree of saturation conditions, possibly due to some influence on vapour transport (retarding effect of the porous medium on vapour diffusivity) at inter-aggregate scale affecting pore geometry (air filled porosity as indicated in Eq. (4.17)).

Problems with matric suction equalisation have been detected in test series H17-0.026A and are presented in Fig. 4.35 and Fig. 4.36. As observed, the excessive evaporation at 80°C does not allow a suitable matric suction equalisation nor to reach high degrees of saturation (values at 80°C are consistently lower than the corresponding ones at 22°C, and maximum degree of saturation is limited up to 98.0% at $(u_a\text{-}u_w) = 0.01$ MPa). Due to this condition, the hotter sample experiences lower swelling strains compared to the colder one, which could be erroneously interpreted (the overconsolidated sample swells more upon wetting at higher temperatures, according to the results presented in Fig. 6.12).

In order to limit water vapour transfer under a high vapour pressure gradient between the air circuit chamber and the specimen, a special salt solution reservoir (shown in Fig. 4.37) and similar to that used by Saix and Jouanna (1990) should be connected to the system, mainly at temperatures higher than 80°C in the oedometer cells. In the case of the triaxial cell it is necessary to provide the reservoir with the solution at the same soil temperature in order to humidify the dry air u_{da} (usually at around $h_r = 50\%$) before connecting it to the air chamber u_a ($h_{ra} > 99\%$ and $\psi < 1.48$ MPa calculated at 50°C), due to evaporation and shrinkage phenomena that have been detected at temperatures higher than 50°C, which can overlap to the primary phenomenon of drained thermal contraction (refer to Fig. 7.27). The specified relative humidity h_{ra} (or the activity a_l of the NaCl solution) to control evaporative flux is associated with the molality of NaCl solution in accordance to Eq. (4.8) and Eq. (4.9).

4.5.2.2 Theoretical bases of the thermo-hydraulic analysis

The theoretical bases of the analysis and the model are briefly reviewed. The analysis performed has taken into account the following coupled phenomena:

- heat transport (heat conduction by Fourier's law, heat convection by liquid water, heat convection by water vapour and phase changes);
- water flow (liquid phase by Darcy's law and water vapour diffusion according to Fick's law and phase changes); and
- air flow (gas phase by generalised Darcy's law and flux of dissolved air through liquid); without loss of generality, this equation may be dropped if a constant pressure is assumed for the gas phase.

The simulation of these interacting phenomena is achieved via a finite element code (CODE_BRIGHT: Olivella, 1995) by solving simultaneously the equations of enthalpy (internal energy) conservation, the water mass conservation and the air mass balance, together with the appropriate equilibrium restrictions and constitutive equations. The formulation uses a multi-phase (solid, liquid and gas) and multi-species (mineral, water and dry air mixture) approach. A compositional approach consisting in balancing the species rather than the phases is adopted to establish mass balance equations. Further details regarding conservation equations are specified in Olivella *et al.* (1994). The liquid phase may contain water and dissolved air and the gas phase may be a mixture of dry air and water vapour. Equilibrium restrictions refer to the concentration of mass water vapour per unit volume of gas via psychrometric law and the ideal law for gases, and to the solubility of air in water controlled by Henry's law. Local equilibrium is assumed throughout and species concentration in the various phases can be considered as dependent variables. Thermal equilibrium between phases is also assumed.

With regard to the thermal constitutive equations, conductive heat flow is assumed to be governed by Fourier's law. The parameters defining thermal conductivity are given by the following geometrical mean approximation: $\lambda = \lambda_{sat}^{Sr}\lambda_{dry}^{(1-Sr)}$, where λ_{sat} and λ_{dry} are the thermal conductivities for saturated and dry conditions, respectively. In order not to present changes in temperature distribution due to drying and wetting processes (thermal and hydraulic coupling), no variations with degree of saturation Sr is introduced in the previous expression, and thus $\lambda_{dry} = \lambda_{sat} = 1.2$ W/(m.K) are assumed constant (corresponding to an approximate Sr = 70%; Volckaert *et al.*, 1996a). Internal energies per unit mass (specific heat capacity) for each phase are assumed to be additive with respect to the species and typical material parameters are presented in Gens *et al.* (1998).

Liquid and gas flow are assumed to be governed by generalised Darcy's law:

$$\mathbf{q} = -\mathbf{K}_\alpha(\nabla P_\alpha - \rho_\alpha \mathbf{g}); \quad \alpha = l, g \tag{4.16}$$

where $\mathbf{K}_\alpha = \mathbf{k}\, k_{r\alpha}/\mu_\alpha$ is the permeability tensor (α stands for either l or g depending whether liquid or gas flow is considered), $\mathbf{k}$ the intrinsic permeability tensor, $k_{r\alpha}$ is the value of relative permeability that controls the variation of permeability in the unsaturated regime and μ_α denotes de dynamic viscosity.

Molecular diffusion of vapour in air is governed by Fick's law:

$$\mathbf{i}_g^w = -\mathbf{D}_g^w \nabla \omega_g^w = -\left(n\rho_g(1-Sr)\tau D_m^w \mathbf{I} + \rho_g \mathbf{D}_g^{'}\right)\nabla \omega_g^w \tag{4.17}$$

where $\mathbf{i}_g^w$ is the non-advective mass flux of water in gas, $\mathbf{D}_g^w$ is the dispersion tensor (molecular diffusion plus mechanical dispersion), ω_g^w the mass fraction of water in gas, τ the tortuosity, D_m^w the molecular diffusion of vapour in air (Geankoplis, 1983) and $\mathbf{D}_g^{'}$ the mechanical dispersion tensor, which can be neglected if no significant air flow takes place and since vapour molecular diffusion is very efficient. The tortuosity factor, which accounts for complexities in pore geometry that influence with a retarding effect vapour transport, can be approximately estimated according to the cross sectional area available for vapour flow: $\tau = [n(1-Sr)]^{2/3}$ (proposed by Lai *et al.*, 1976, and used by Milly, 1984, Nassar and Horton, 1989 and Wilson *et al.*, 1994).

A 1-D mesh of 26 nodes with 5 elements of 1.48 mm corresponding to the ceramic disc, 10 elements of 1.00 mm representing the soil and 10 elements of 1.00 mm corresponding to the upper coarse porous stone, have been considered. Main independent variables of the formulation are the gas (u_a, which can be neglected since it is approximately constant in space and time and is not confined during the test) and liquid (u_w) pressures, this last being the most important one. The high air-entry disc is

characterised through a porosity of 0.310 and an intrinsic permeability of 1.36×10^{-17} m^2 at 22°C (a value of 5.73×10^{-19} m^2 is further used at 80°C in order to consider disc clogging and ageing effects). Depending on the hydraulic characteristics of the ceramic disc, the drawing of water into the sample may lead to some desaturation at the top of it, which can have some influence in the slowing of the hydration process. With this idea, a high air-entry value (10 MPa) has been used. A low air-entry value and a low relative water permeability have been selected to ensure dry conditions in the upper coarse porous stone, as well as a tortuosity factor of $\tau \approx 0.50$ and a porosity of 0.40. Hydraulic properties of Boom clay have been selected according to experimental suction plate test results reported in chapter 5 (a rigid soil skeleton with a porosity of 0.482 corresponding to the low-density packing is considered):

- intrinsic permeability of 8.50×10^{-19} m^2 at 22°C (5.80×10^{-19} m^2 at 80°C, some ageing effect is included) with the following power expression for the liquid relative permeability $k_{rl} = S_e^{2.886}$ and $k_{rg} = A(1-S_e)^{2.886}$ for the relative permeability of the gas phase (the effective saturation is assumed as $S_e = (S_r - 0.087)/0.913$ and parameter $A \approx 1.5$);
- degree of saturation is computed as a function of matric suction through van Genuchten (1980) relation (drying path) $S_e = \left[1 + \left((u_a - u_w)/P\right)^{1/(1-\lambda)}\right]^{-\lambda}$, where $\lambda = 0.156$ and P = 0.03 MPa;
- tortuosity factor affecting water vapour diffusion of $\tau \approx 0.30$, calculated based on porosity and degree of saturation (Sr = 70%) considerations (Lai *et al.*, 1976).

Initial values of unknowns (in terms of absolute pressures) have been established for the first wetting step (initial matric suction of 1.9 MPa at 22°C and 1.6 at 80°C) as follows: u_a = 0.10 MPa, u_w = 0.15 MPa in the ceramic disc; u_a = 0.60 MPa, u_w = -1.3 MPa at 22°C and u_w = -1.0 MPa at 80°C in the high-porosity packing; and u_a = 0.60 MPa, u_w = -95 MPa at 22°C and u_w = -114 MPa at 80°C (corresponding to an initial $h_r \approx 50\%$). A constant initial temperature of 22°C (or 80°C) is assumed throughout the analysis domain. Initial conditions for the second wetting step (initial matric suction of 0.45 MPa) have been established as follows: u_a = 0.10 MPa, u_w = 0.40 MPa and T = 80°C for the ceramic disc; and with respect to the soil and coarse porous stone they have been established according to steady-state conditions arrived in the previous step. Flux problem boundary conditions prescribed on the ceramic disc are the following: u_a = 0.10 MPa, u_w = 0.15 MPa (for the first step with a target matric suction of 0.45 MPa) and u_w = 0.40 MPa (for the second step with a target matric suction of 0.20 MPa). For the coarse porous stone at 22°C, the following boundary conditions have been assumed (first wetting step with a target matric suction of 0.45 MPa): u_a = 0.60 MPa and $\omega_g^w = 1.32\times10^{-3}$ (mass fraction of water in gas is only prescribed for the open system to vapour corresponding to a constant relative humidity of ρ_v/ρ_{vs} = 0.50 with $\rho_{vs} = 1.948\times10^{-2}$ kg/m^3 at 22°C and ρ_{da} = 7.082 kg/m^3 at 0.60 MPa and 22°C). Variable boundary conditions have been prescribed with respect to mass fraction of water in gas, when performing first wetting path simulations at 80°C. Starting with a value of $\omega_{go}^w = 2.41\times10^{-2}$ (initial relative humidity of ρ_v/ρ_{vs} = 0.50 with $\rho_{vs} = 3.006\times10^{-1}$ kg/m^3 at 80°C and ρ_{da} = 5.919 kg/m^3 at 0.60 MPa and 80°C), mass fraction is progressively increased up to different target relative humidity (80%, 90%, 95%, 98%, 99% and 99.7%-nearly closed system), following an evolution similar to that under closed system conditions (refer to Fig. 4.38). Second wetting paths (target matric suction of 0.20 MPa at 80°C) have been started at $\omega_{go}^w = 4.87\times10^{-2}$ (ρ_v/ρ_{vs} = 0.95) and continued up to different target relative humidity (98%, 99%, 99.5% and 99.9%-nearly closed system), following a similar closed-system evolution (refer to Fig. 4.39). Maximum final relative humidity under closed-system conditions, corresponding to soil osmotic suction, is limited to 99.75%.

Calculated evaporative fluxes under steady-state conditions (end execution time is usually fixed at 100 days) are presented in Fig. 4.39 for the different target relative humidity values previously indicated. Measured range of evaporative fluxes are also represented in the previous figure, as well as the computed evaporative flux calculated at 22°C and constant h_r = 50%). The different results, both numerical and experimental, present comparable values, indicating an appropriate selection of soil

parameters controlling vapour diffusion as well as boundary conditions. The simultaneous evaporation and hydration of the soil sample give rise to a series of phenomena that interact with each other. Time evolution of matric suction for three representative points in the sample are shown in Fig. 4.40 for a target $(u_a\text{-}u_w) \rightarrow 0.45$ MPa (temperatures of 22°C and 80°C) and in Fig. 4.41 for a target $(u_a\text{-}u_w) \rightarrow 0.20$ MPa (temperature of 80°C). Matric suction isochrones (soil sample and upper coarse porous stone) are represented in Fig. 4.42 for a target $(u_a\text{-}u_w) \rightarrow 0.45$ MPa (temperatures of 22°C and 80°C) and in Fig. 4.43 for the second wetting step with a target $(u_a\text{-}u_w) \rightarrow 0.20$ MPa (temperature of 80°C). According to Fig. 4.40, near the top boundary (top: 1 mm below the upper coarse porous stone) water evaporation will cause an initial drying of the clay upper surface (due to the initial relative humidity of the air chamber), increasing matric suction (up to 4.20 MPa at 22°C and 3.78 MPa at 80°C) and causing a volume reduction (shrinkage that is not simulated), which can be associated with some lateral stress reduction. This drying is progressively slowed and reverted (approximately at elapsed times higher than 20 min) when soil vapour front advances inducing higher relative humidity in the air chamber (refer to Fig. 4.42). At this upper boundary, vapour diffusion is therefore a significant mechanism of moisture and heat transfer. Moving to the bottom boundary (bottom: 1 mm over the ceramic disc), the controlling condition is the higher water pressure of the ceramic disc with respect to the initial suction of soil specimen, implying a flux of water into the sample. This hydration process causes a monotonic suction reduction (refer to Fig. 4.40, bottom point), advancing progressively to the top of the specimen. Because of the lower water permeability of the soil compared to the ceramic disc, no significant boundary impedance is detected due to ageing effects at higher temperatures, and soil permeability will mainly control hydration times.

At the end of the different wetting steps and under steady-state conditions, full matric suction equalisation has not been achieved in the open system to vapour, due to free water evaporation. Isochrones presented in Fig. 4.42 and Fig. 4.43 show this effect on matric suction equalisation. In the closed-system, air becomes nearly vapour saturated at elapsed times higher than 1700 min at 80°C ($h_r > 99.0\%$) and around 17000 min at 22°C ($h_r > 98.4\%$), preventing further evaporation and allowing to arrive to the applied matric suction throughout the sample height. Fig. 4.44 presents final matric suction of three representative points of the sample under steady-state conditions and related to the evaporative flux in the open system. This way, evaporative fluxes are maintained between 1×10^{-6} $(mm^3/s)/mm^2$ and 1.5×10^{-7} $(mm^3/s)/mm^2$ in the initial wetting steps using air drainage lines of low cross-sectional area (inner diameter of 2 mm), in order to ensure a relative humidity higher than 98.5% in the open air chamber, which limits water vapour transfer at high temperatures and permits to attain matric suction equalisation over the entire sample height. The lower limit is obtained considering a rate of volume change resolution per day.

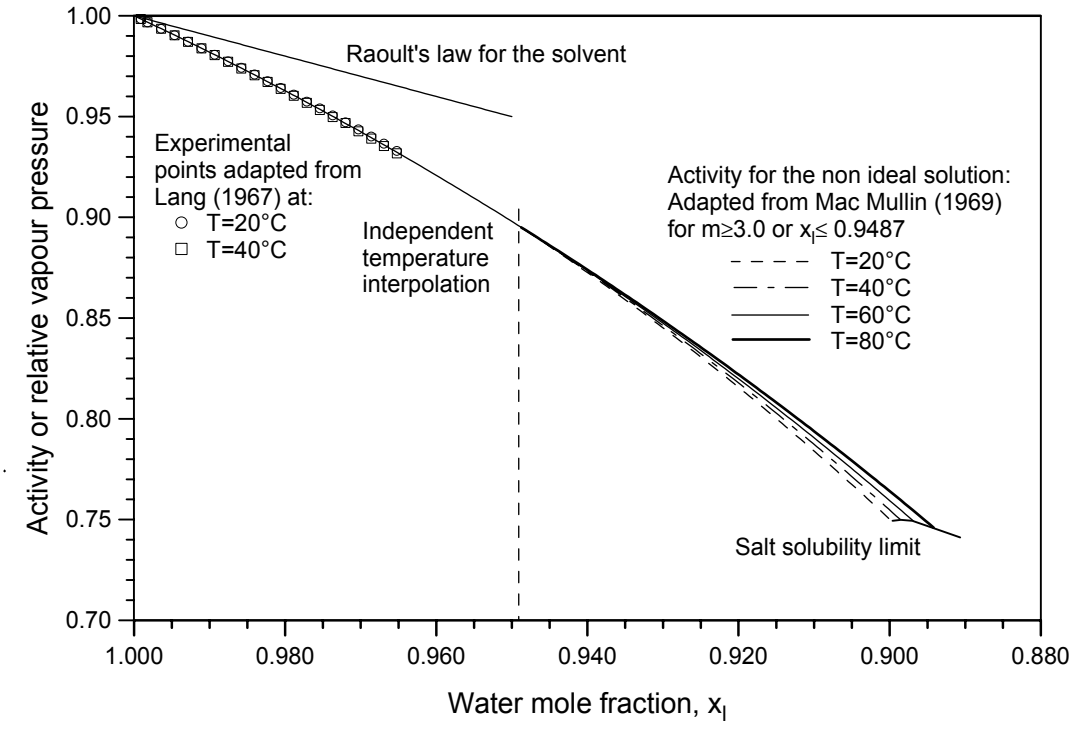

Figure 4.1 Activity of NaCl solution versus water mole fraction.

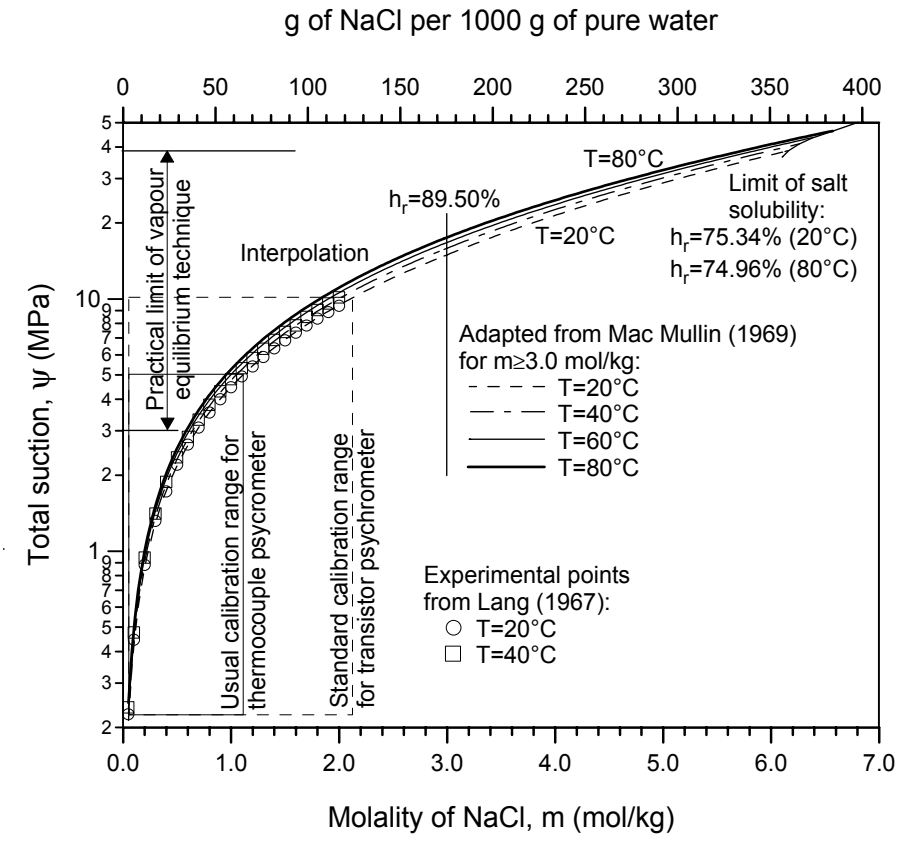

Figure 4.2 Soil total suction imposition at different temperatures with NaCl solutions.

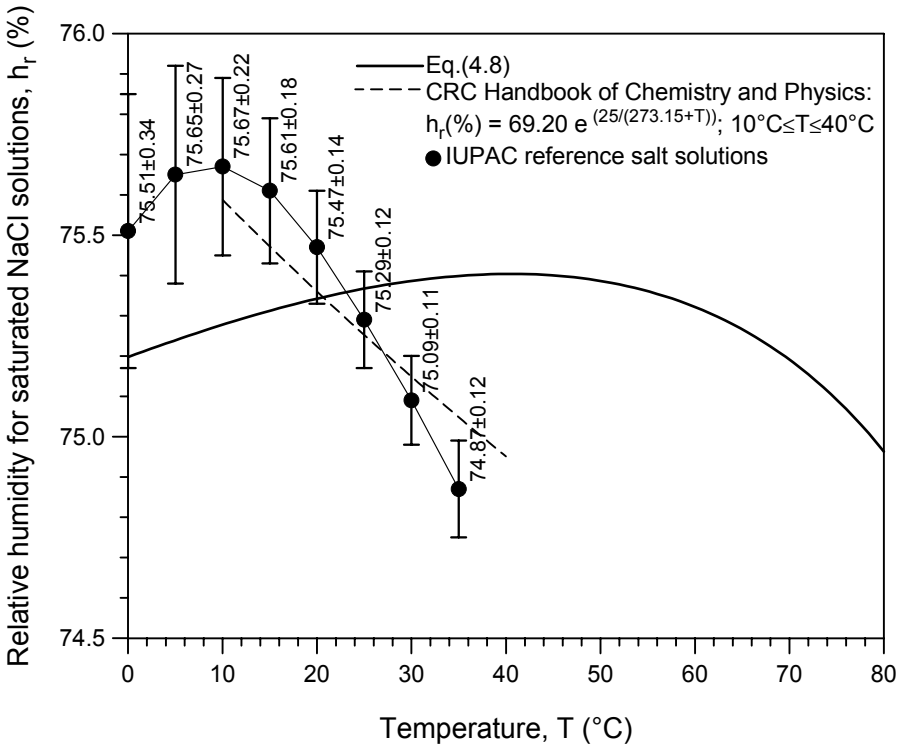

Figure 4.3 Relative humidity for saturated NaCl solutions at different temperatures.

Figure 4.4 Implements of vapour equilibrium tests.

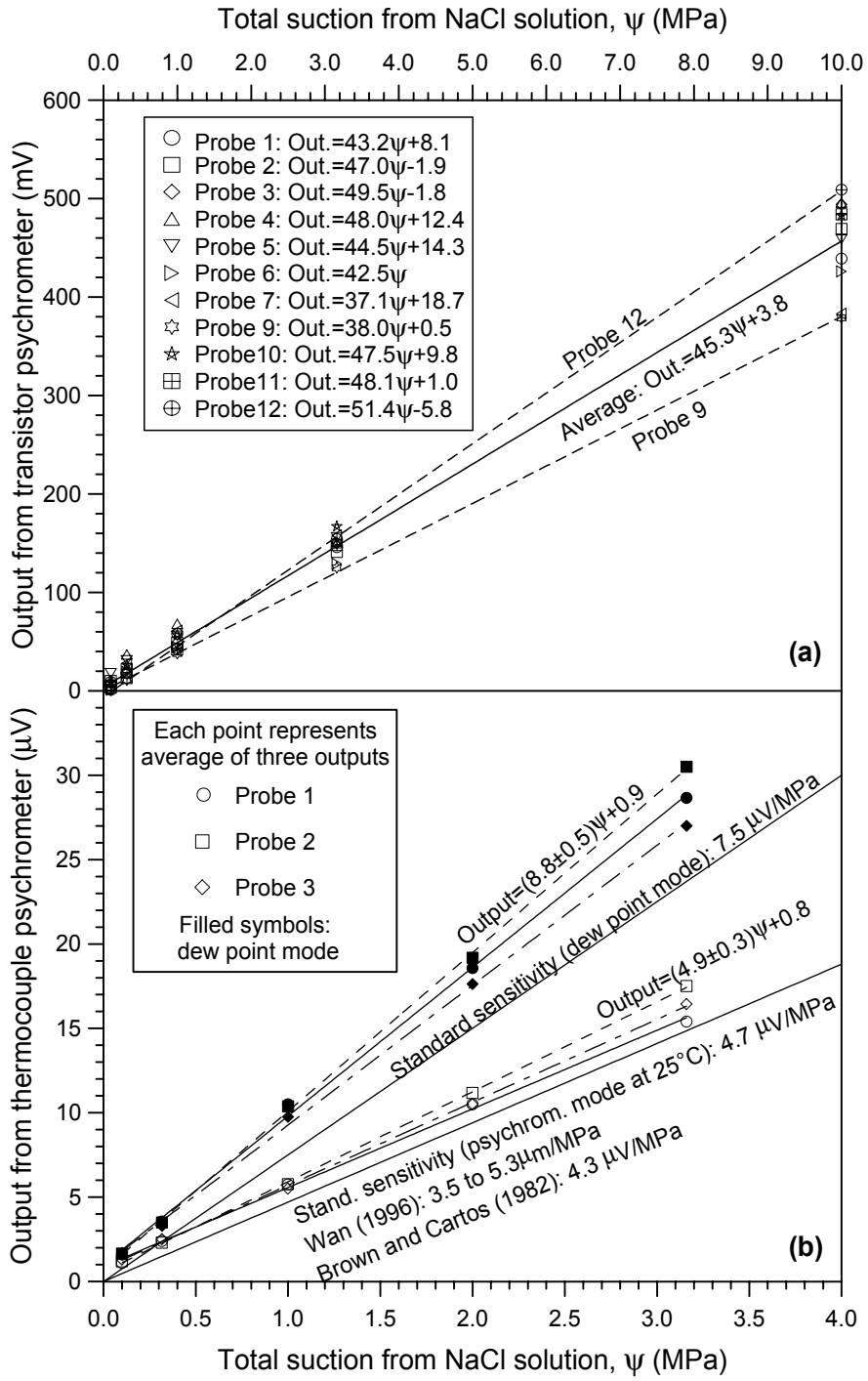

Figure 4.5 a) Calibration curves for transistor psychrometric probes. b) Calibration curves for thermocouple psychrometers (dew point and psychrometric modes).

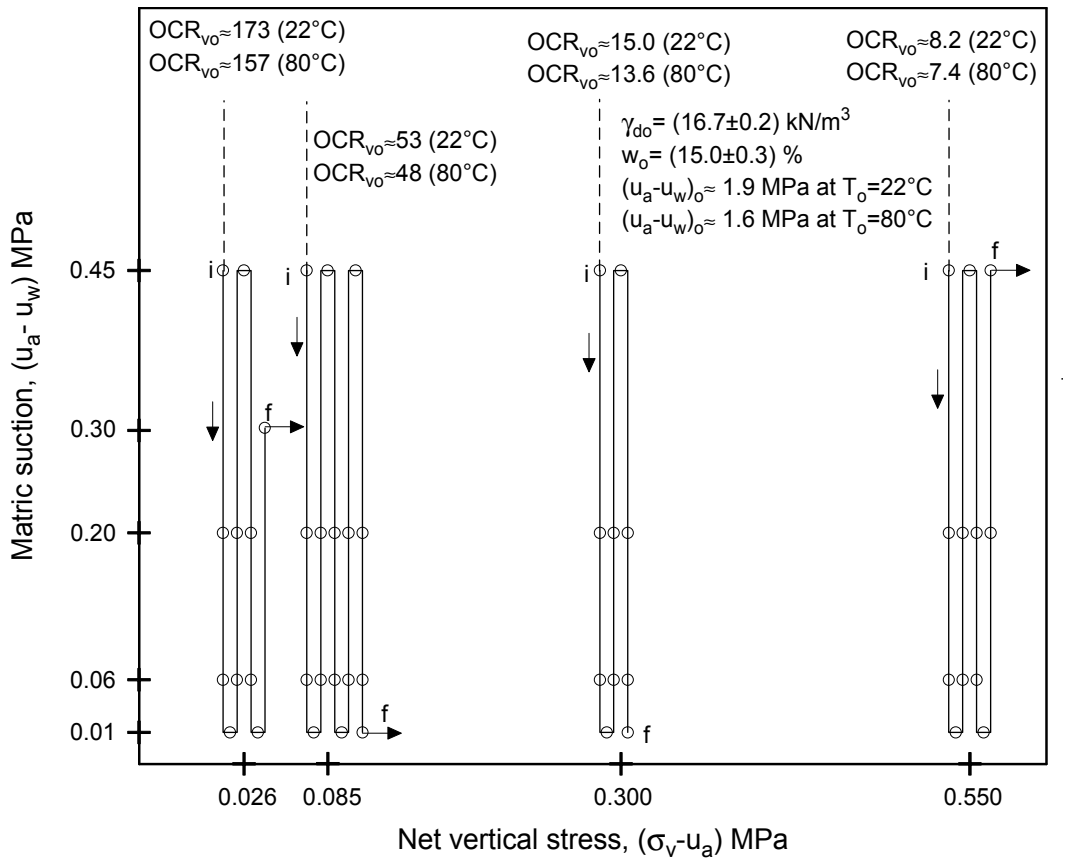

Figure 4.6 Oedometer isothermal (22°C and 80°C) wetting-drying cycles on dense (heavily overconsolidated) packings.

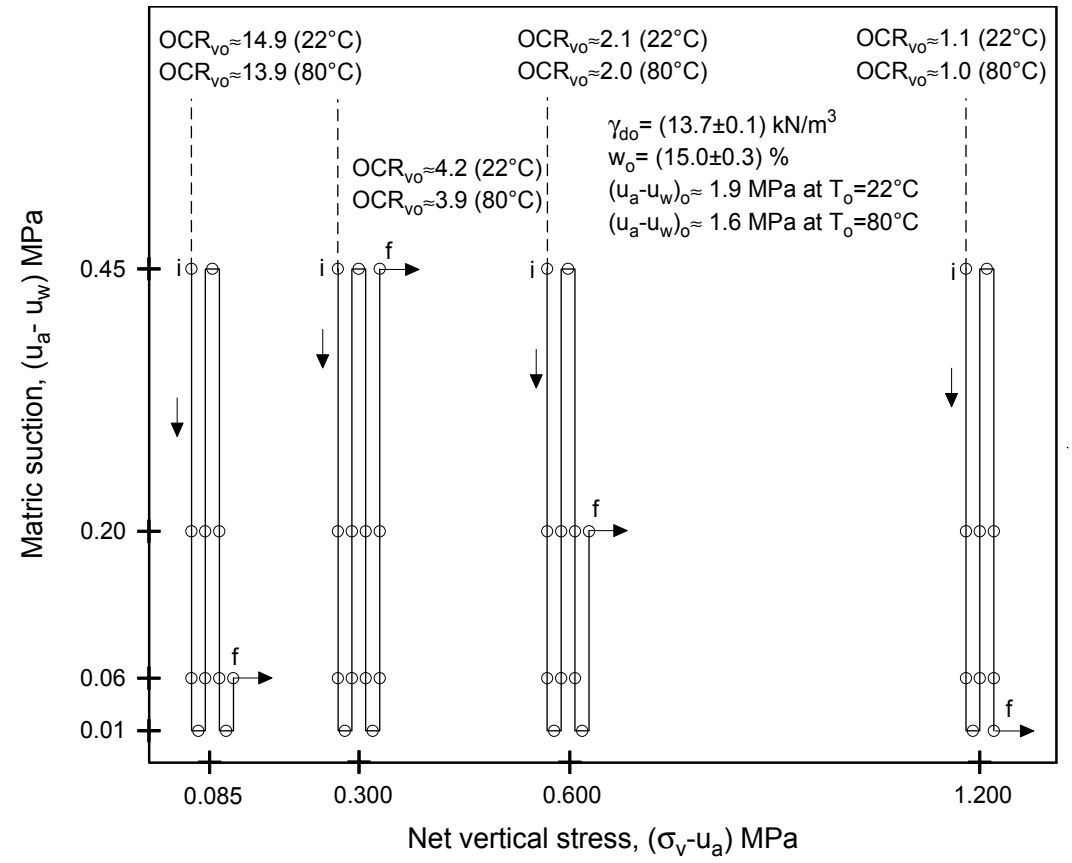

Figure 4.7 Oedometer isothermal (22°C and 80°C) wetting-drying cycles on high-porosity packings.

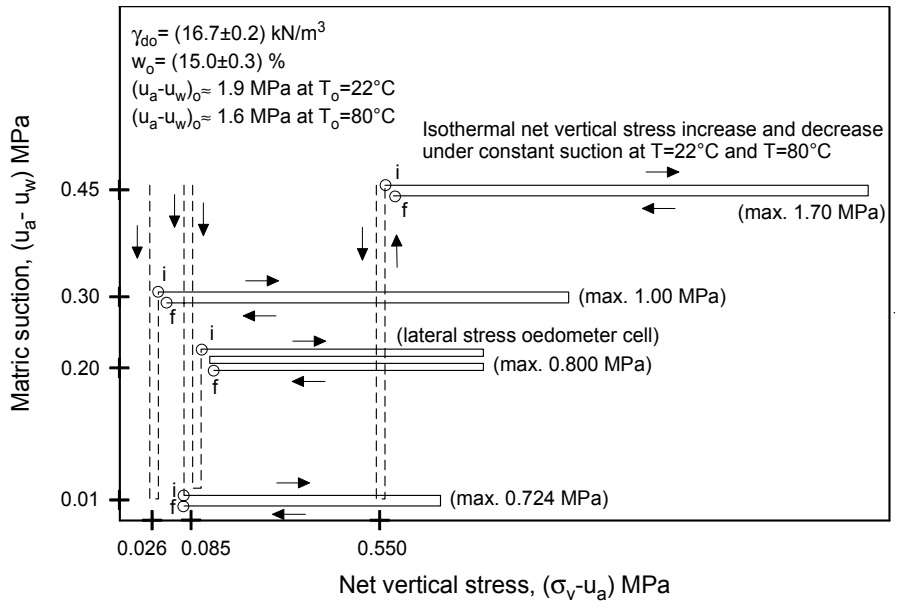

Figure 4.8 Oedometer loading-unloading paths at constant matric suction for the high-density packings.

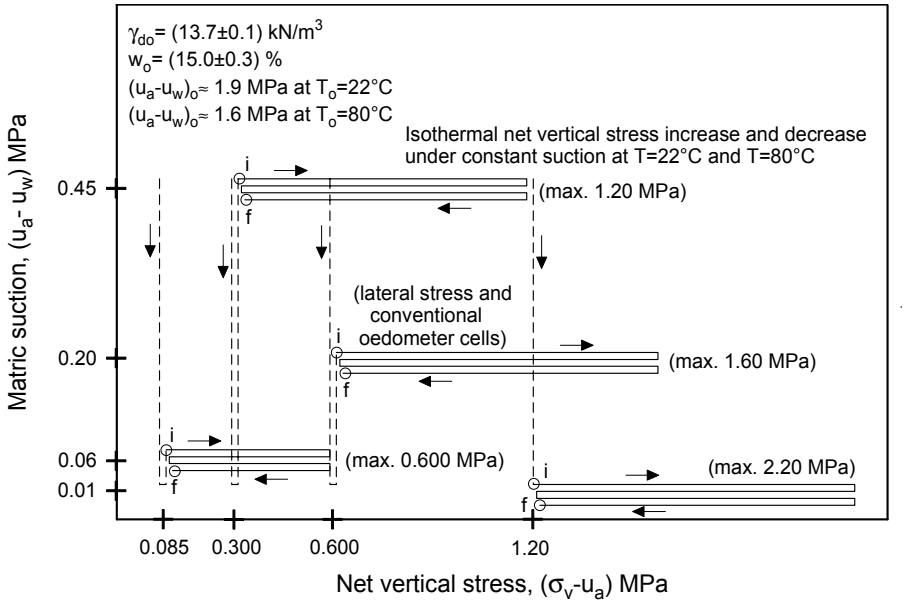

Figure 4.9 Oedometer loading-unloading paths at constant matric suction for the high-porosity packings.

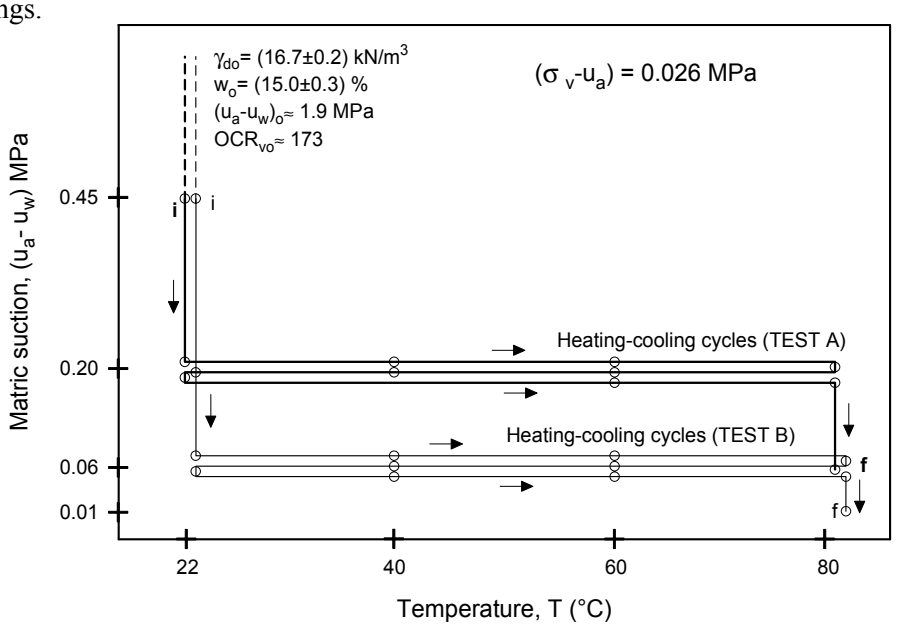

Figure 4.10 Oedometer non-isothermal paths at constant matric suction and net vertical stress.

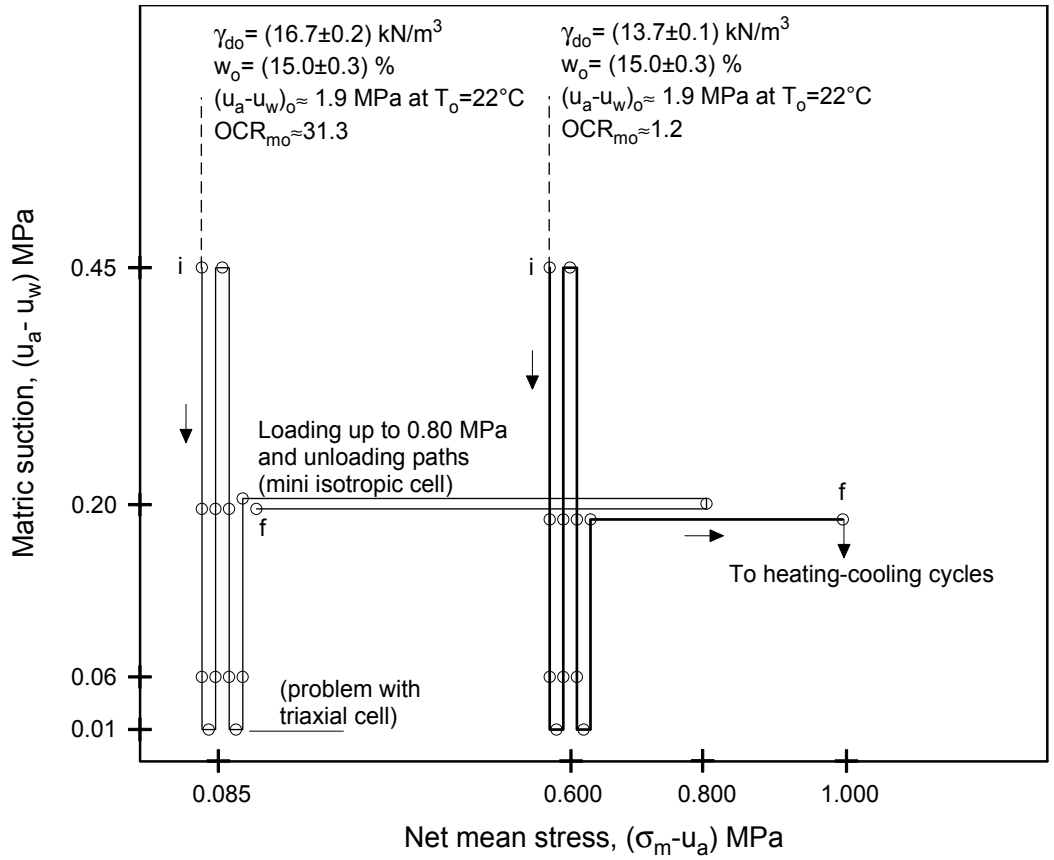

Figure 4.11 Isotropic wetting-drying cycles and loading-unloading paths on dense and high-porosity packings (mini isotropic and triaxial cells).

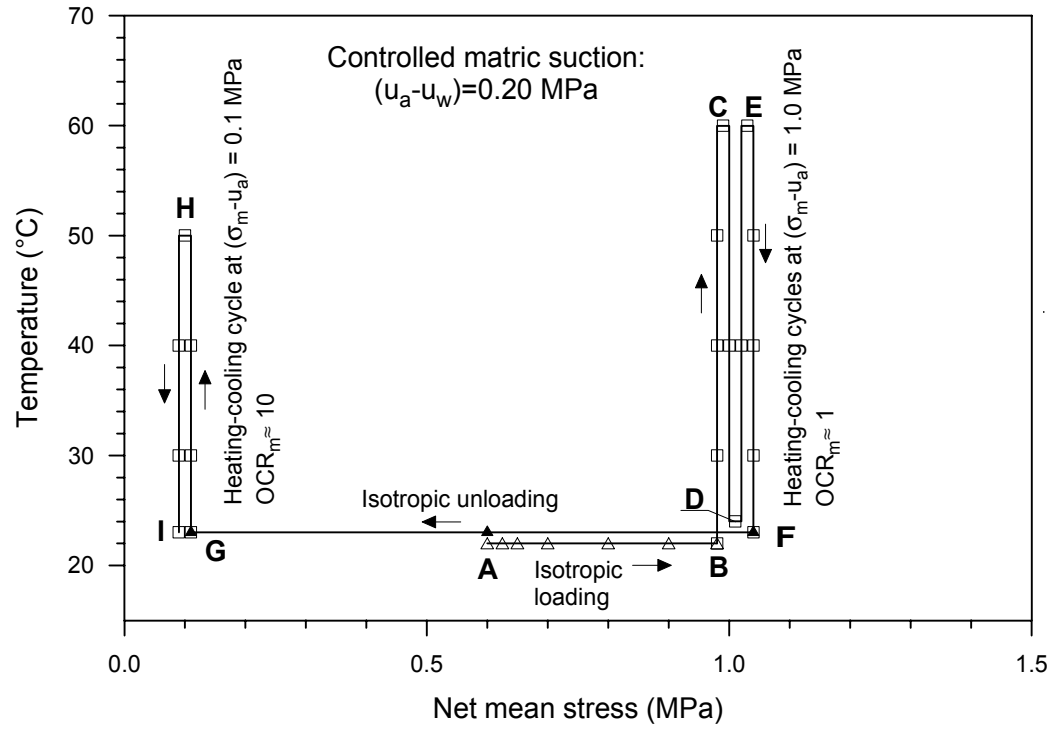

Figure 4.12 Non-isothermal paths under controlled matric suction and constant net mean stress (high-porosity packing).

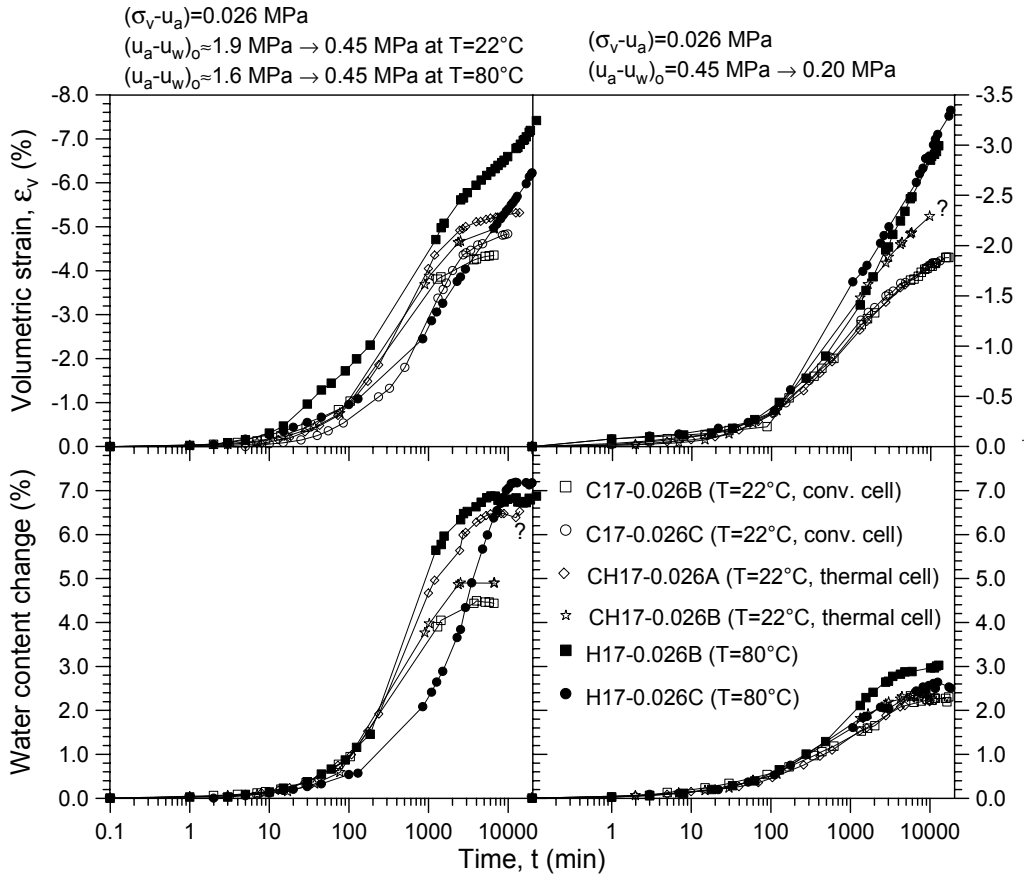

Figure 4.13 Repeatability and reproducibility features on high-density first wetting paths (expansive behaviour, suction steps 1.9 MPa → 0.20 MPa).

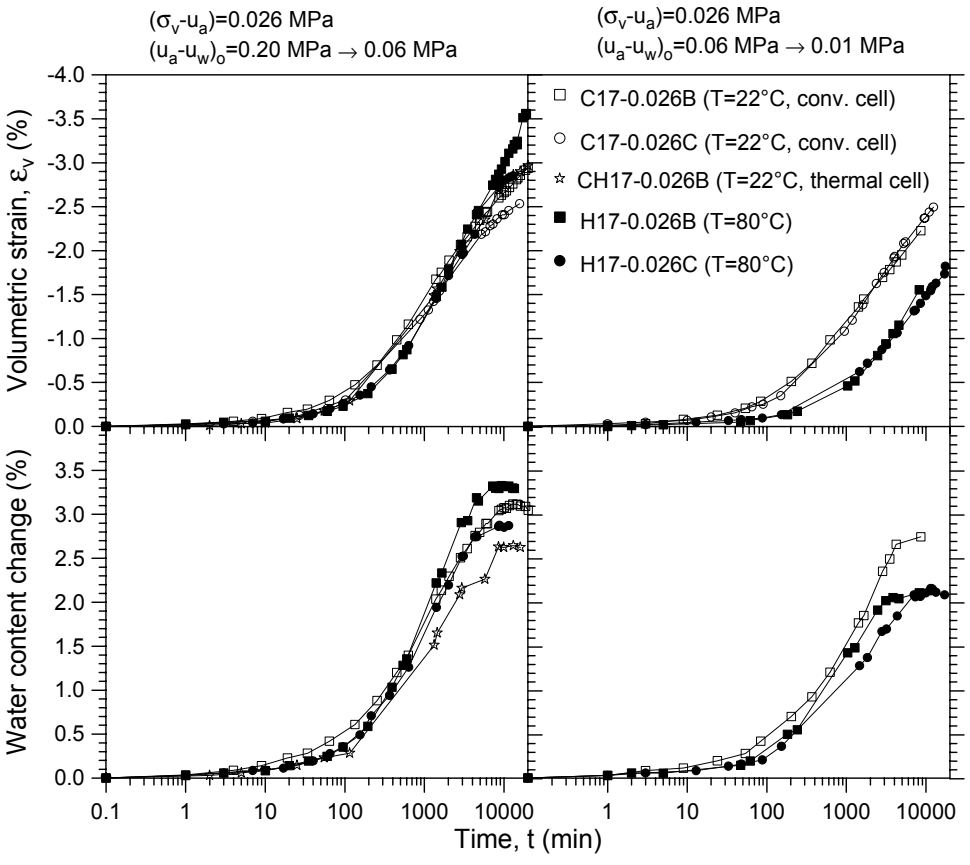

Figure 4.14 Repeatability features on high-density first wetting paths (expansive behaviour, suction steps 0.20 MPa → 0.01 MPa).

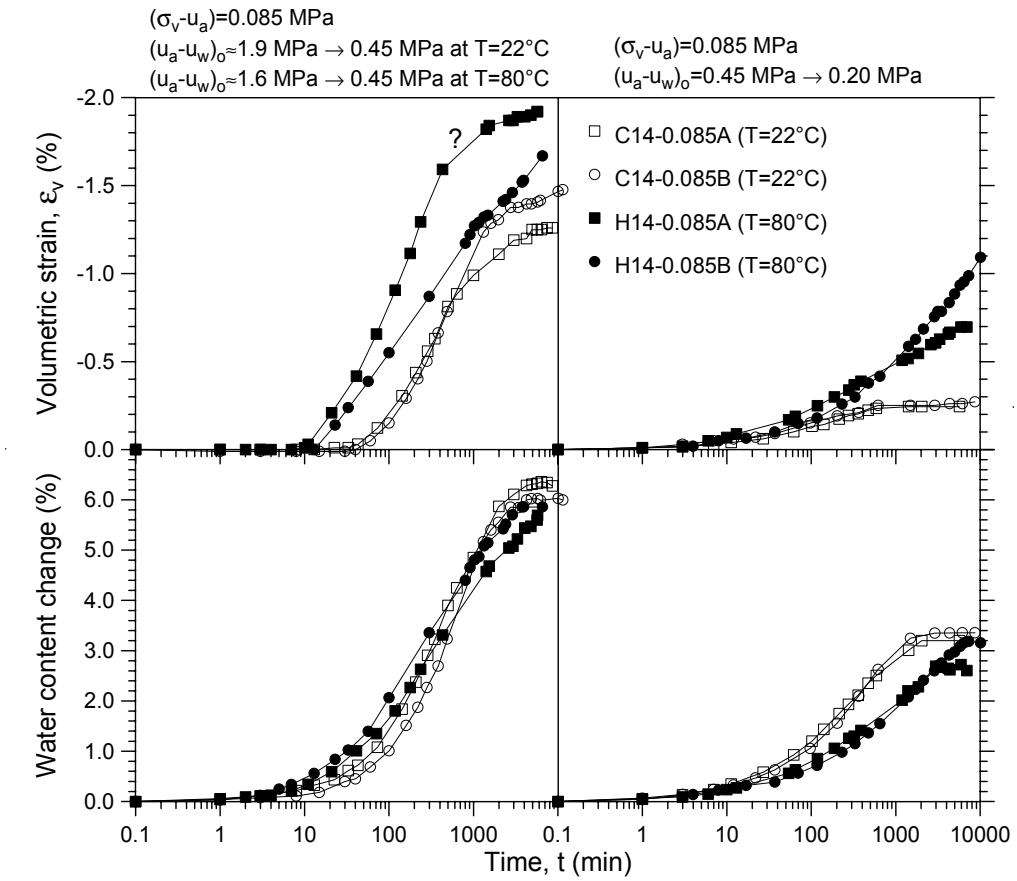

Figure 4.15 Repeatability features on high-porosity first wetting paths (suction steps 1.9 MPa → 0.20 MPa).

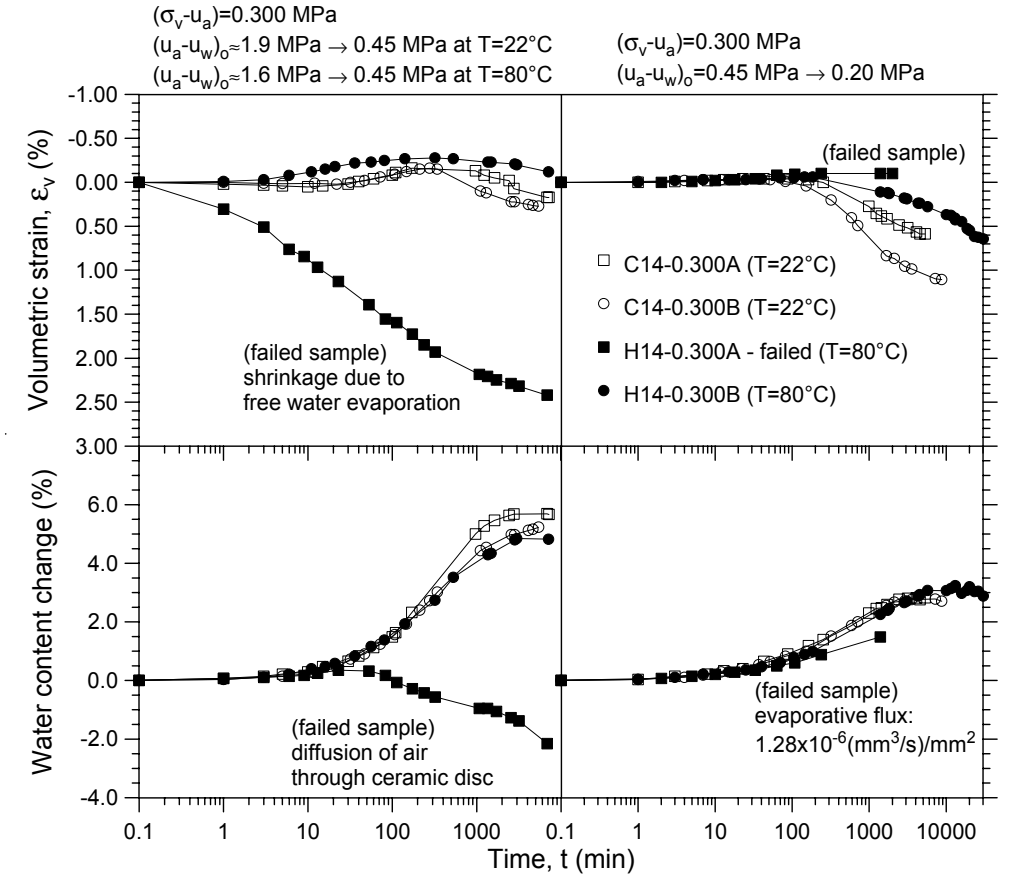

Figure 4.16 Repeatability features on high-porosity first wetting paths. Soil shrinkage due to water evaporation.

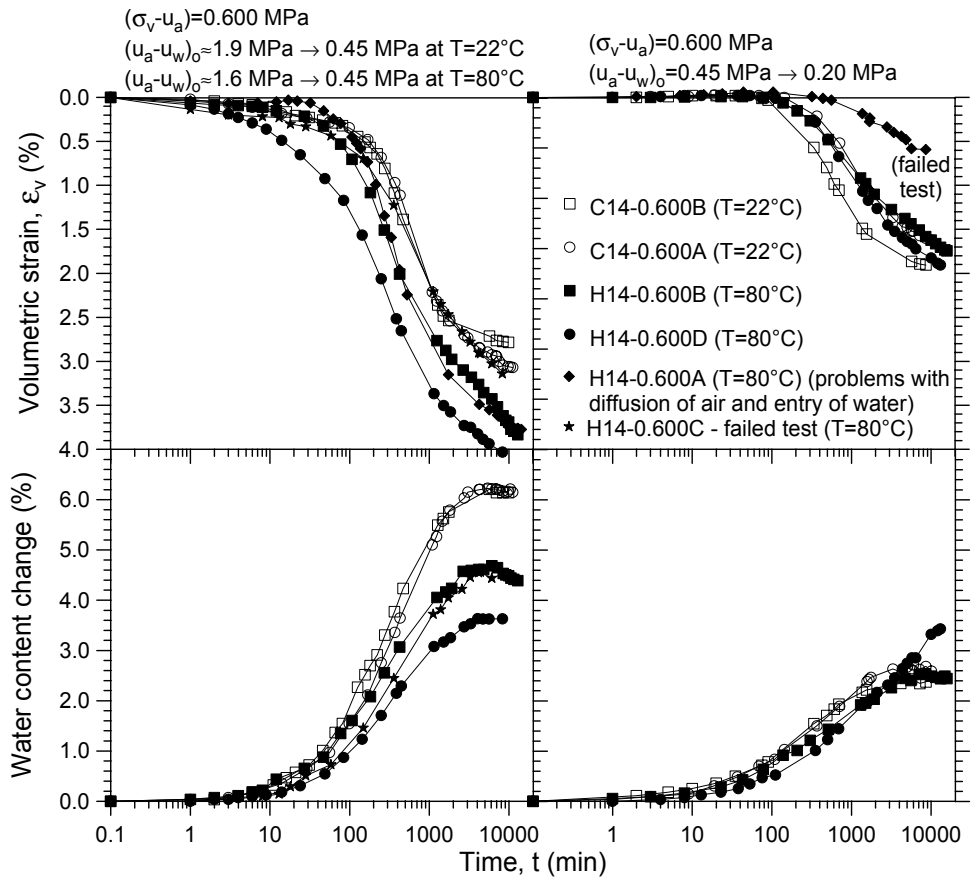

Figure 4.17 Repeatability features on high-porosity first wetting paths (collapsible behaviour, suction steps 1.9 MPa → 0.20 MPa).

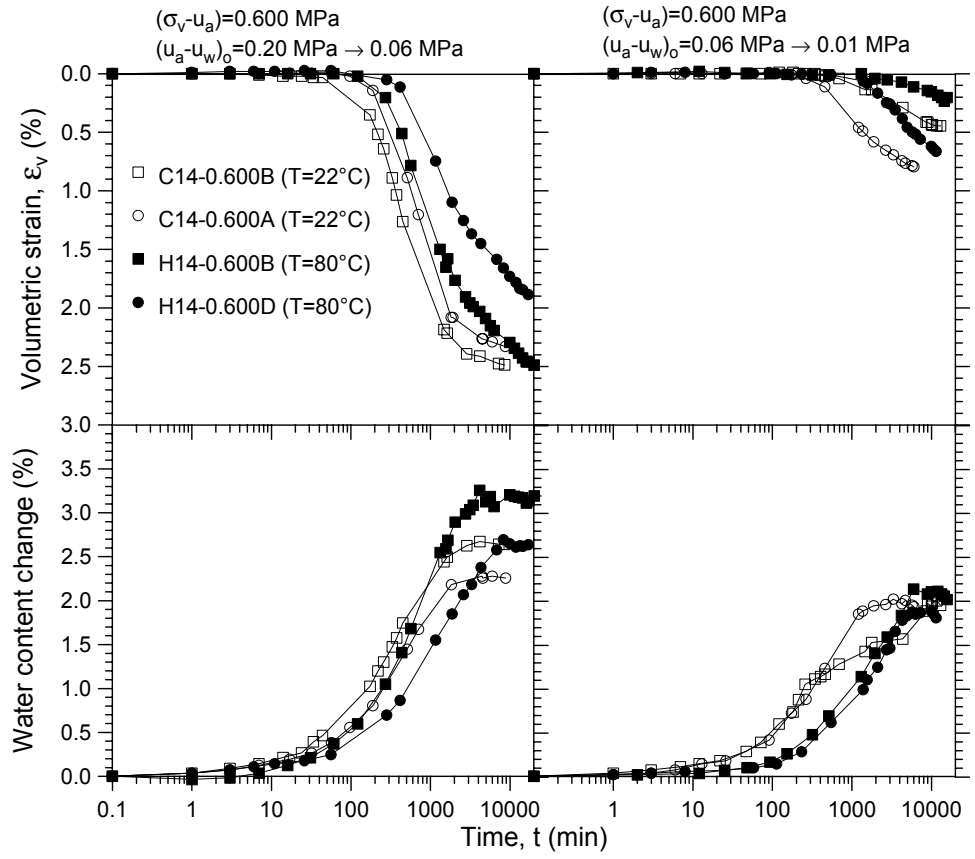

Figure 4.18 Repeatability features on high-porosity first wetting paths (collapsible behaviour, suction steps 0.20 MPa → 0.01 MPa).

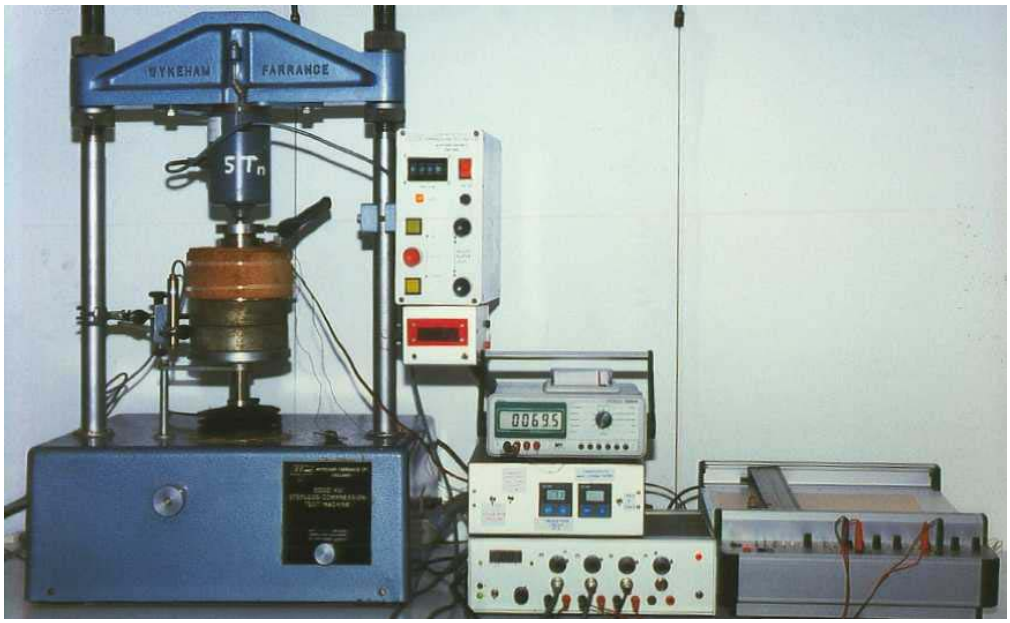

(a)

(b)

Figure 4.19 Experimental setup for static compaction tests: a) sample preparation in the hermetic mould inside the heating chamber, b) sample preparation in the lateral stress ring.

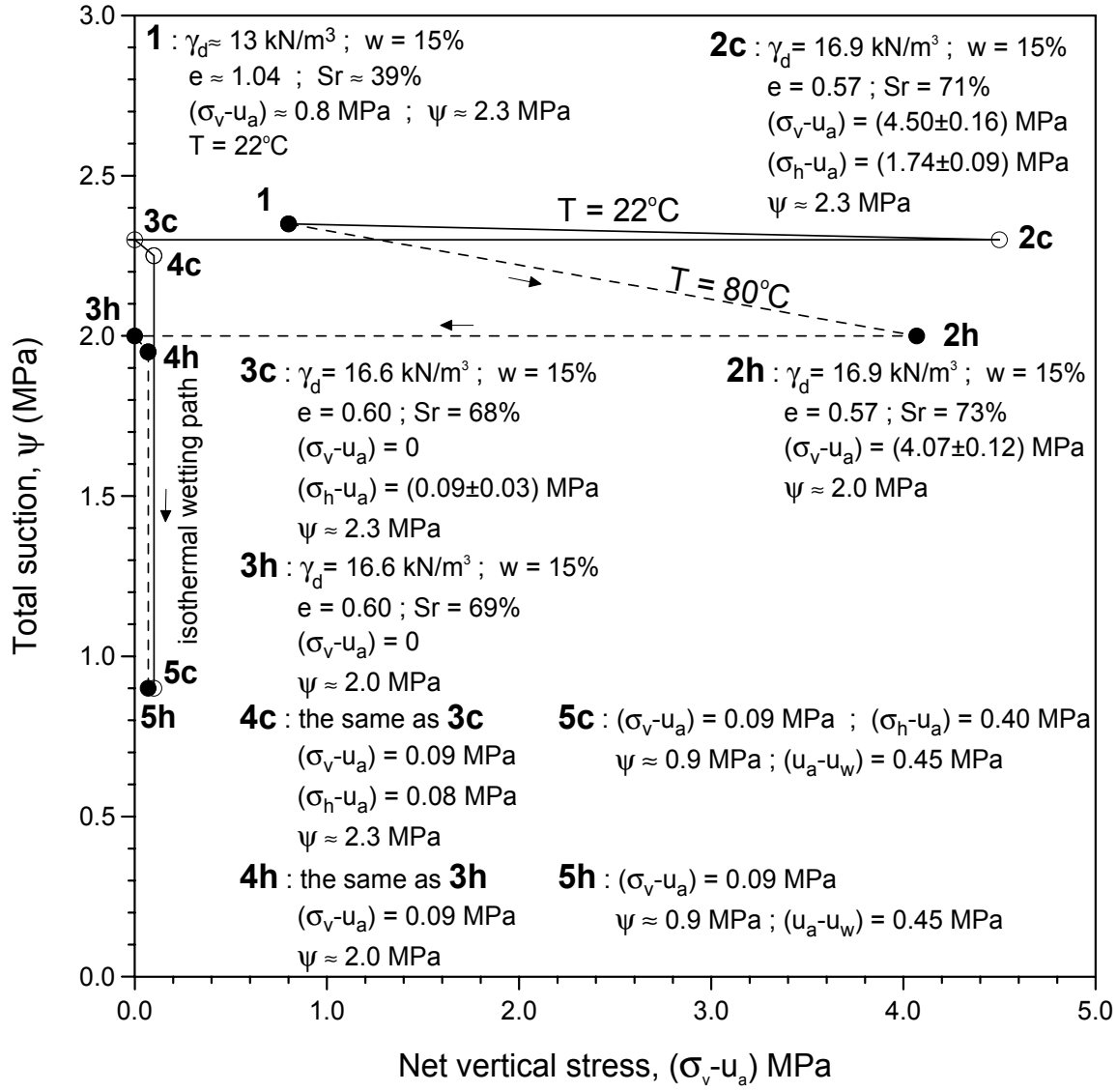

Figure 4.20 Stress paths, stress variable values and soil conditions for the high-density packing during sample preparation under different temperatures ('c' refer to 22°C and 'h' to 80°C).

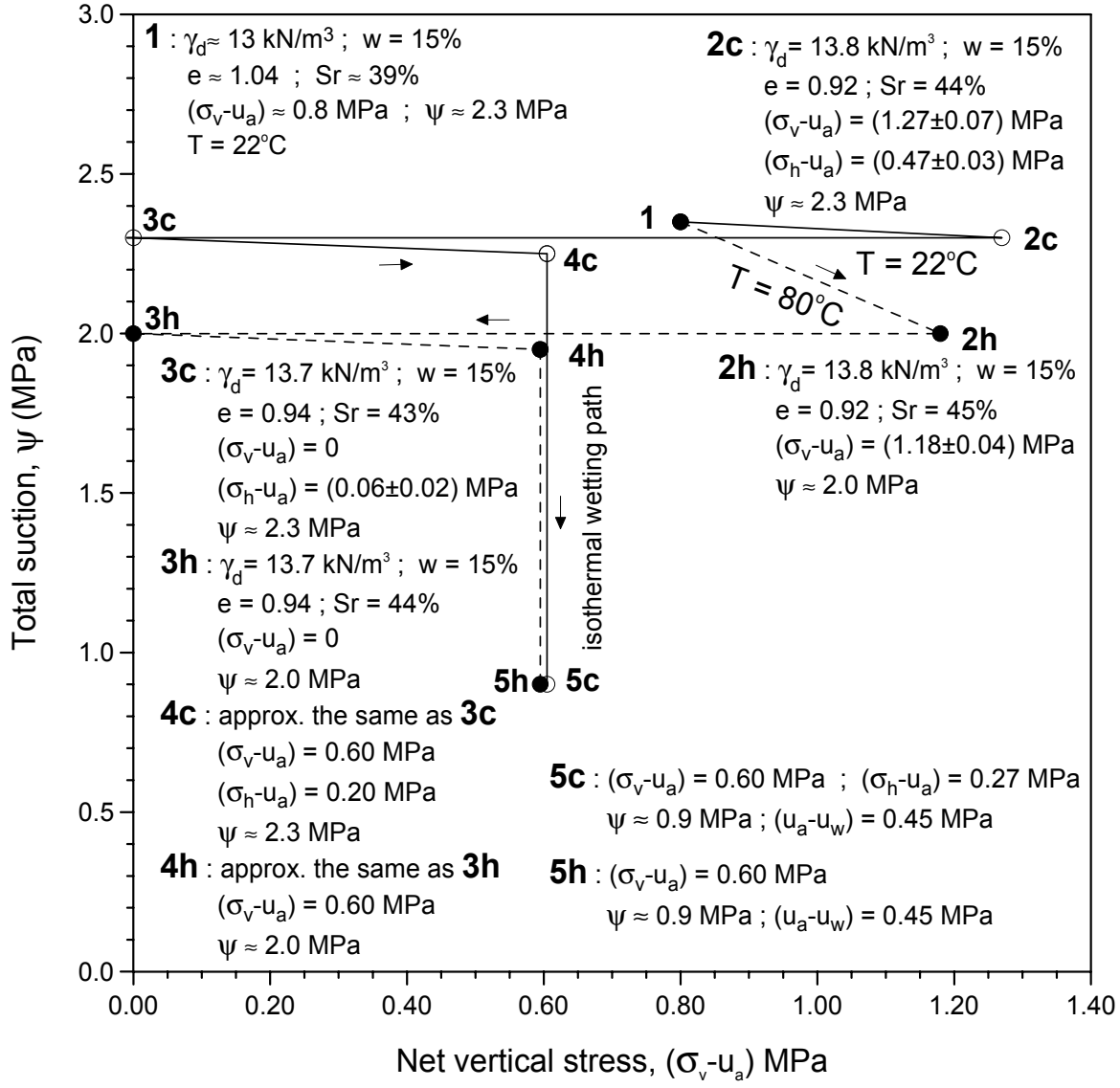

Figure 4.21 Stress paths, stress variable values and soil conditions for the high-porosity packing during sample preparation under different temperatures ('c' refer to 22°C and 'h' to 80°C).

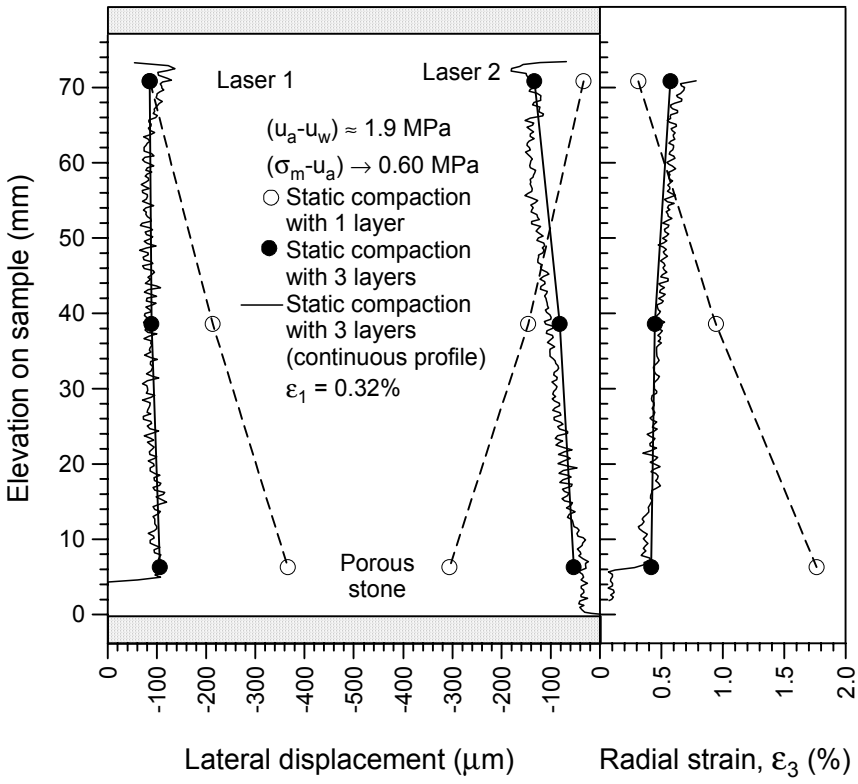

Figure 4.22 Examination of static compaction techniques for isotropic tests.

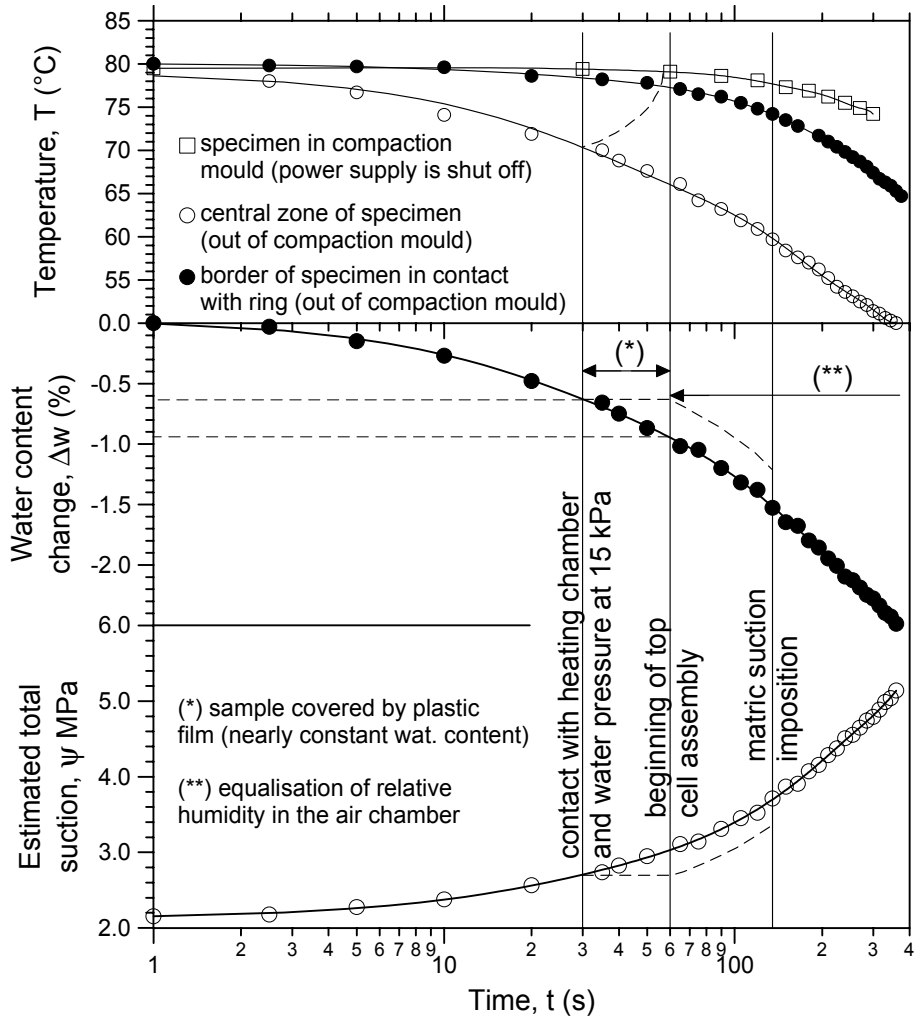

Figure 4.23 Temperature evolution of the high-density sample at two points (central zone and border in contact with the ring) and water content changes (or suction changes) during setting up.

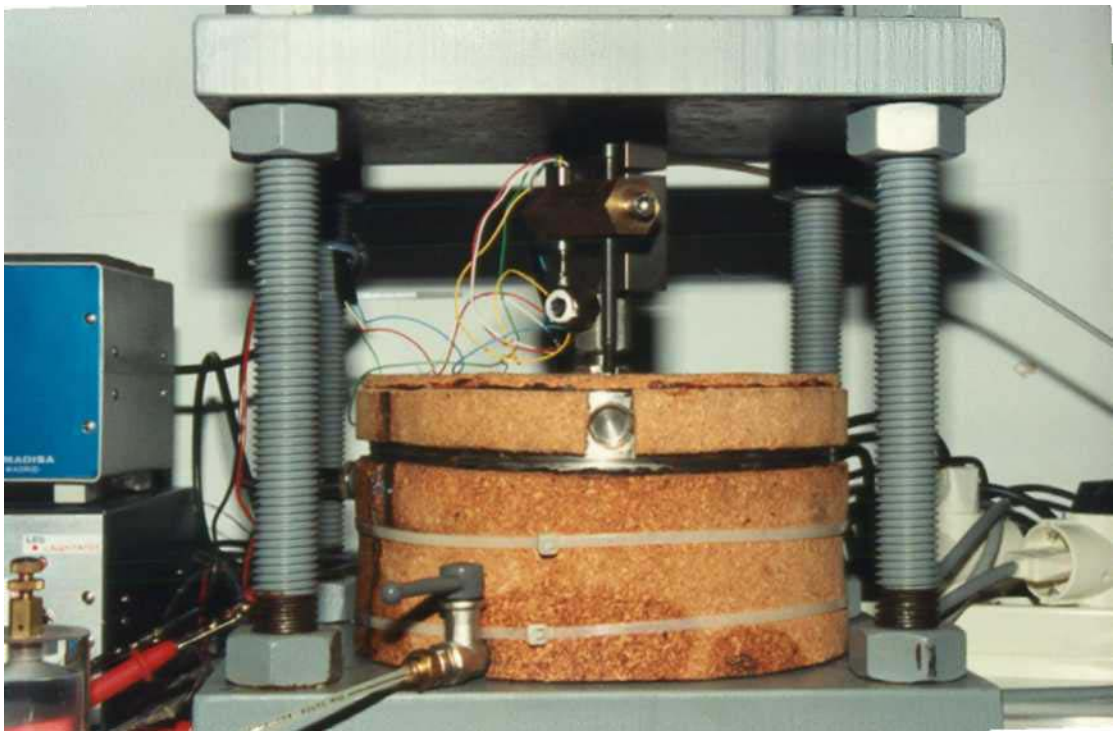

(a)

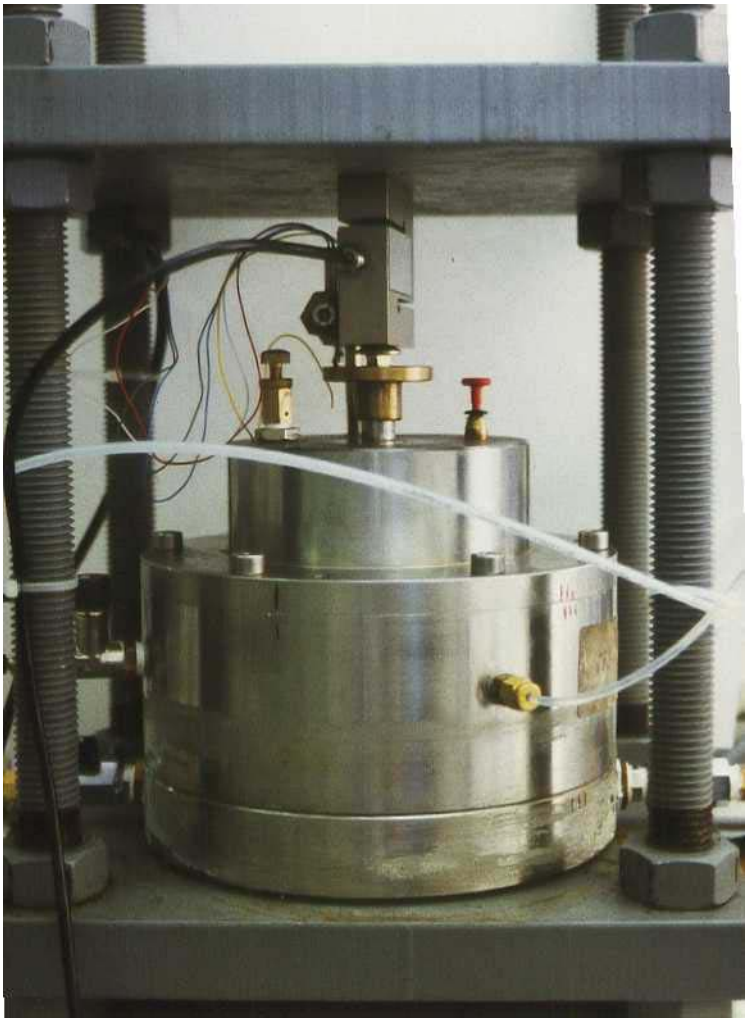

(b)

Figure 4.24 Layout of swelling pressure tests: a) thermal cell and b) lateral stress cell.

Figure 4.25 Silicone membrane inside the three-split fabrication mould.

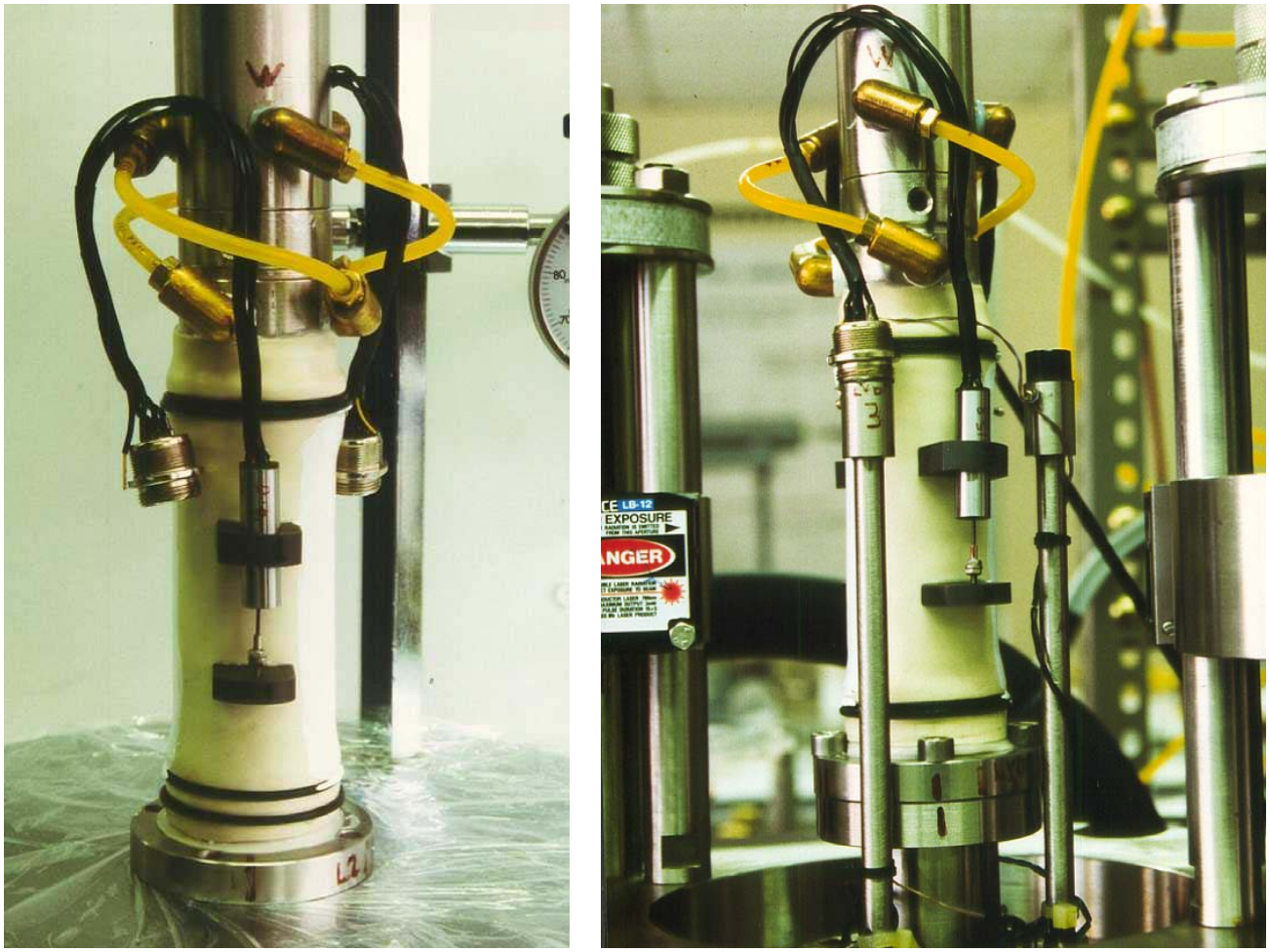

(a) **(b)**

Figure 4.26 Triaxial sample: a) LVDTs mounted on sample and b) partly assembled triaxial cell showing full internal instrumentation.

(c)

Figure 4.26 Triaxial sample: c) final conditions after testing period.

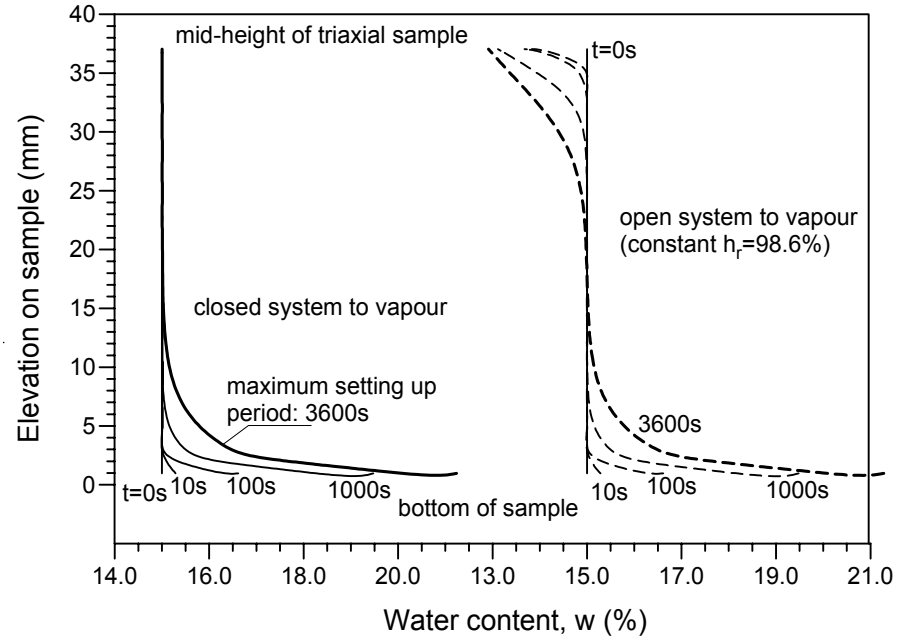

Figure 4.27 Isochrones of water content changes during sample (triaxial cell) setting up.

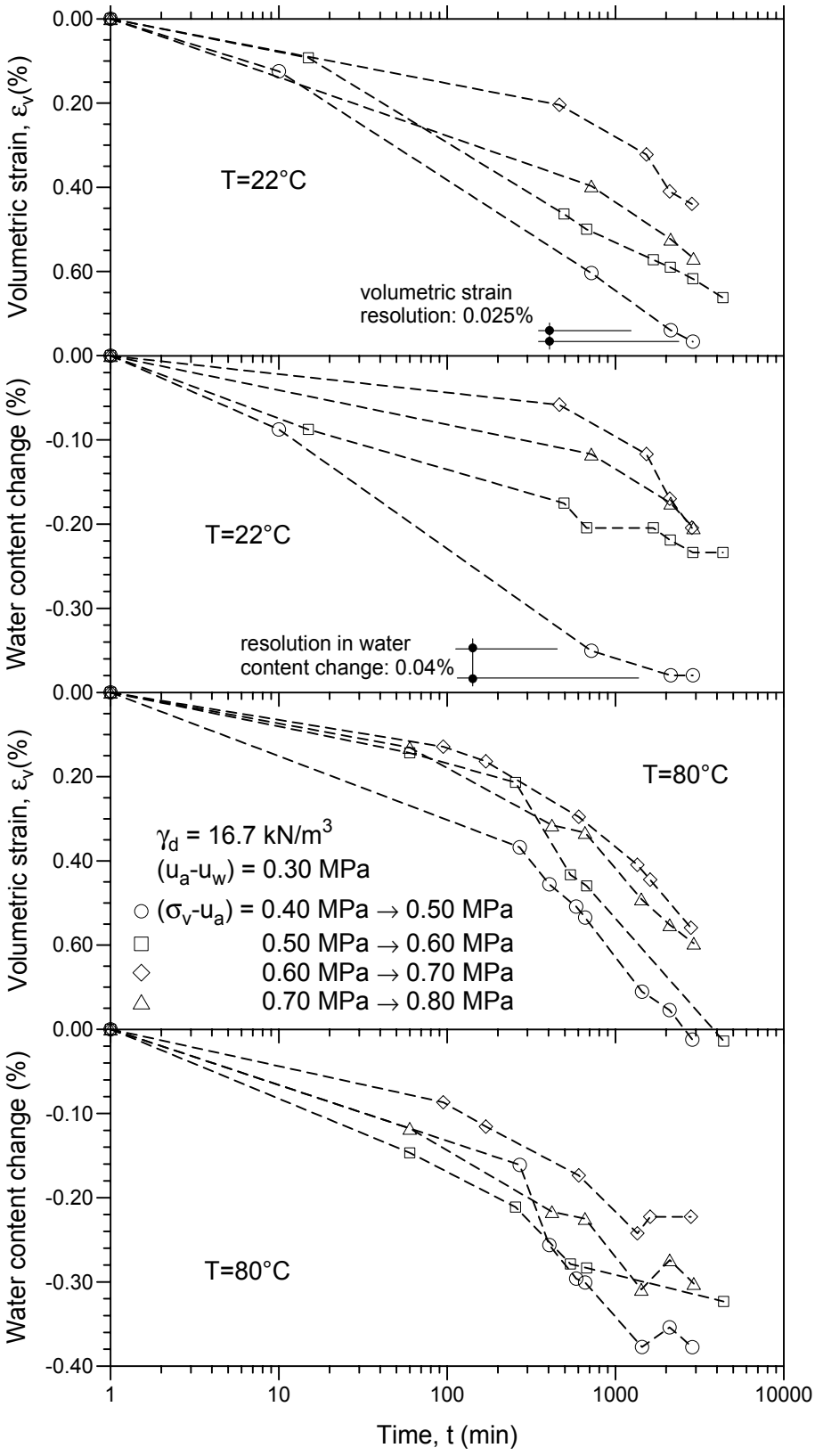

Figure 4.28 Equalisation periods for loading steps under controlled matric suction (oedometer tests with high-density packings at 22°C and 80°C).

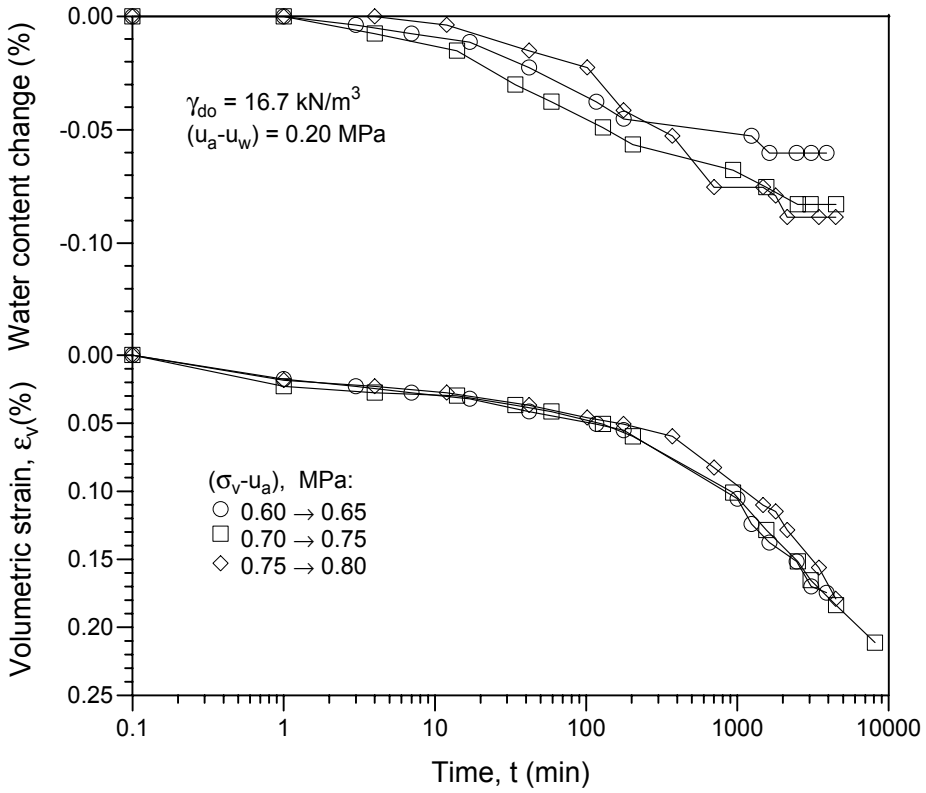

Figure 4.29 Equalisation periods for loading steps under controlled matric suction in the lateral stress cell (high-density packing).

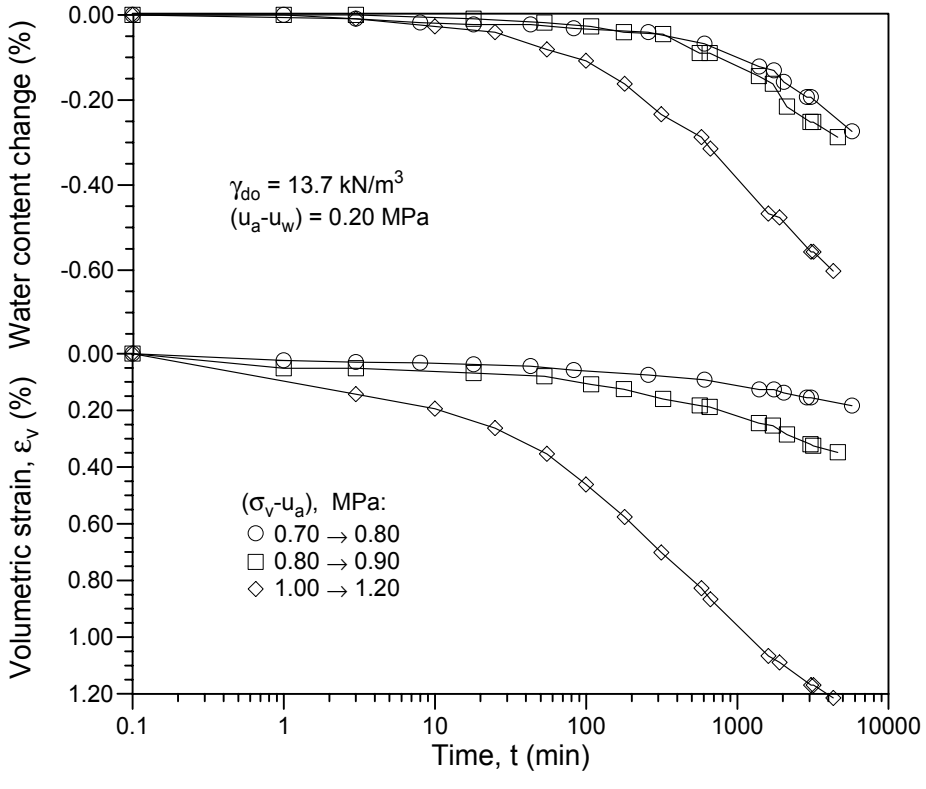

Figure 4.30 Equalisation periods for loading steps under controlled matric suction in the lateral stress cell (low-density packing).

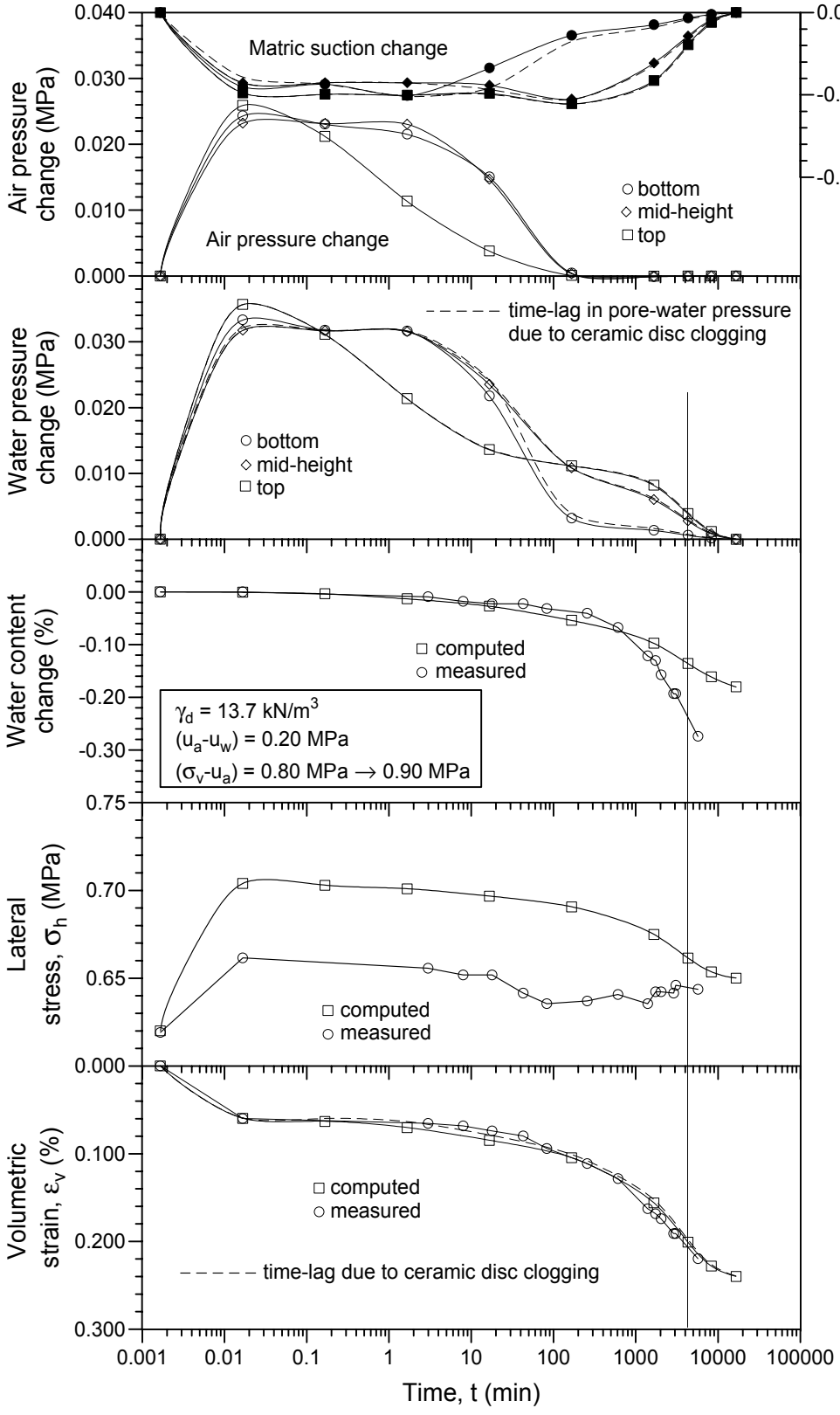

Figure 4.31 Time evolution at selected nodes of air and water pressure changes, average lateral stress within the sample height, volumetric strain and water content changes during the application of a step loading increment and during the subsequent consolidation period.

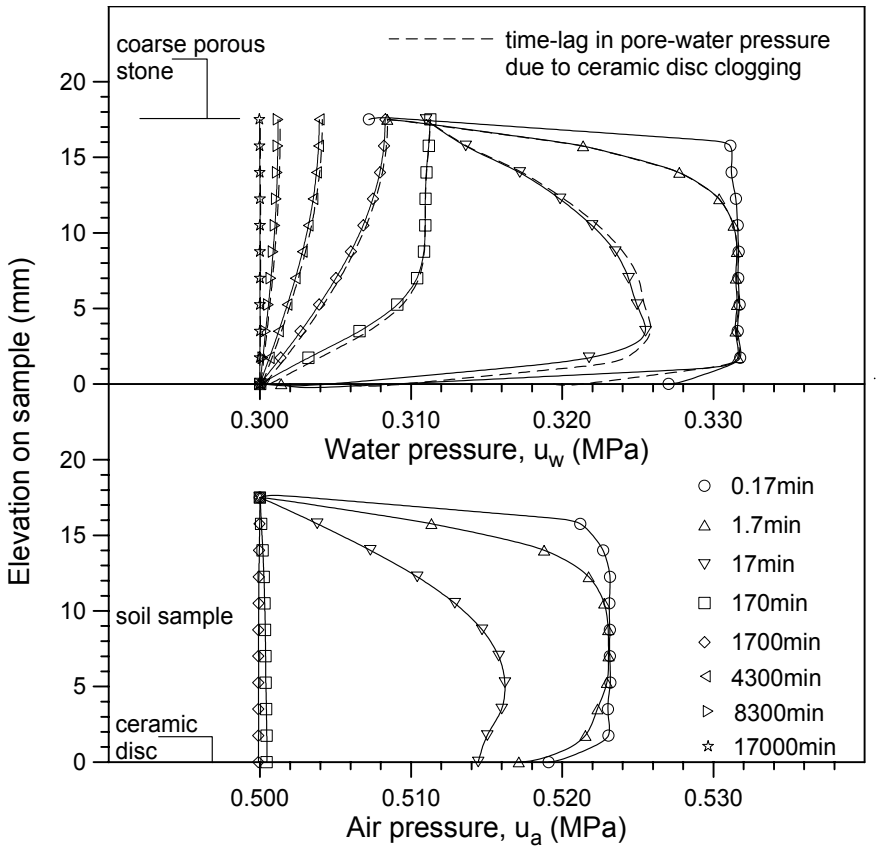

Figure 4.32 Isochrones of air and water pressure changes along sample height.

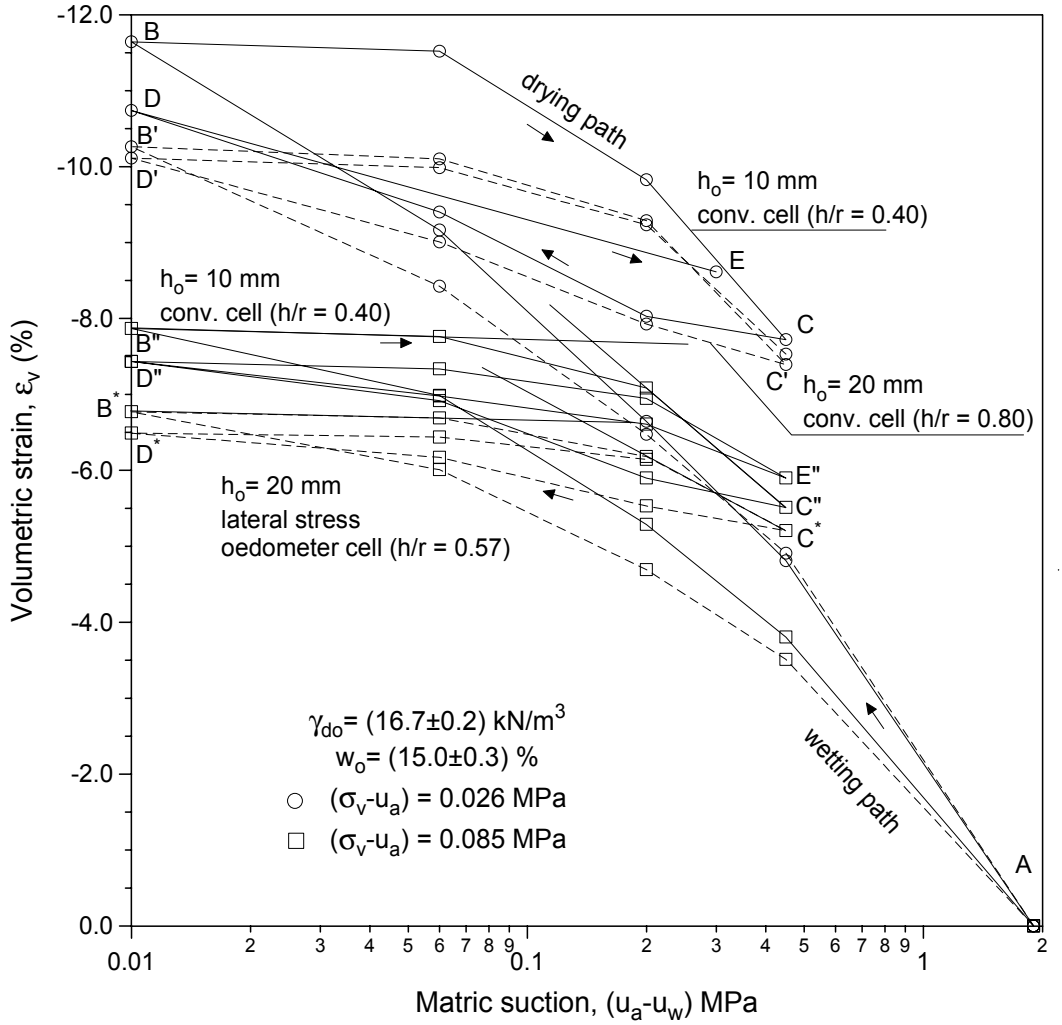

Figure 4.33 Ring friction effects in wetting-drying cycles (high-density packing).

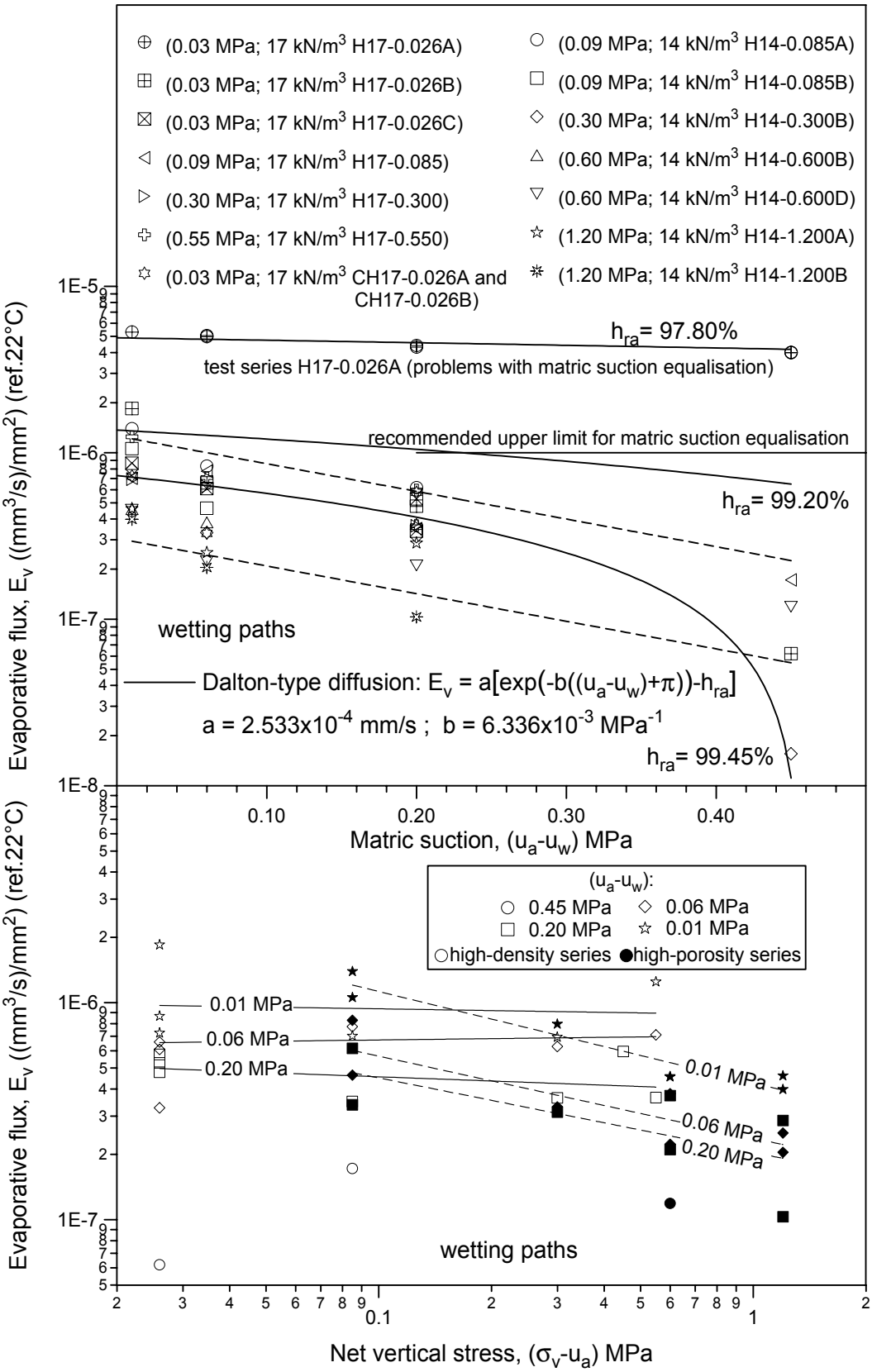

Figure 4.34 Measured evaporative fluxes under steady-state conditions in first wetting paths.

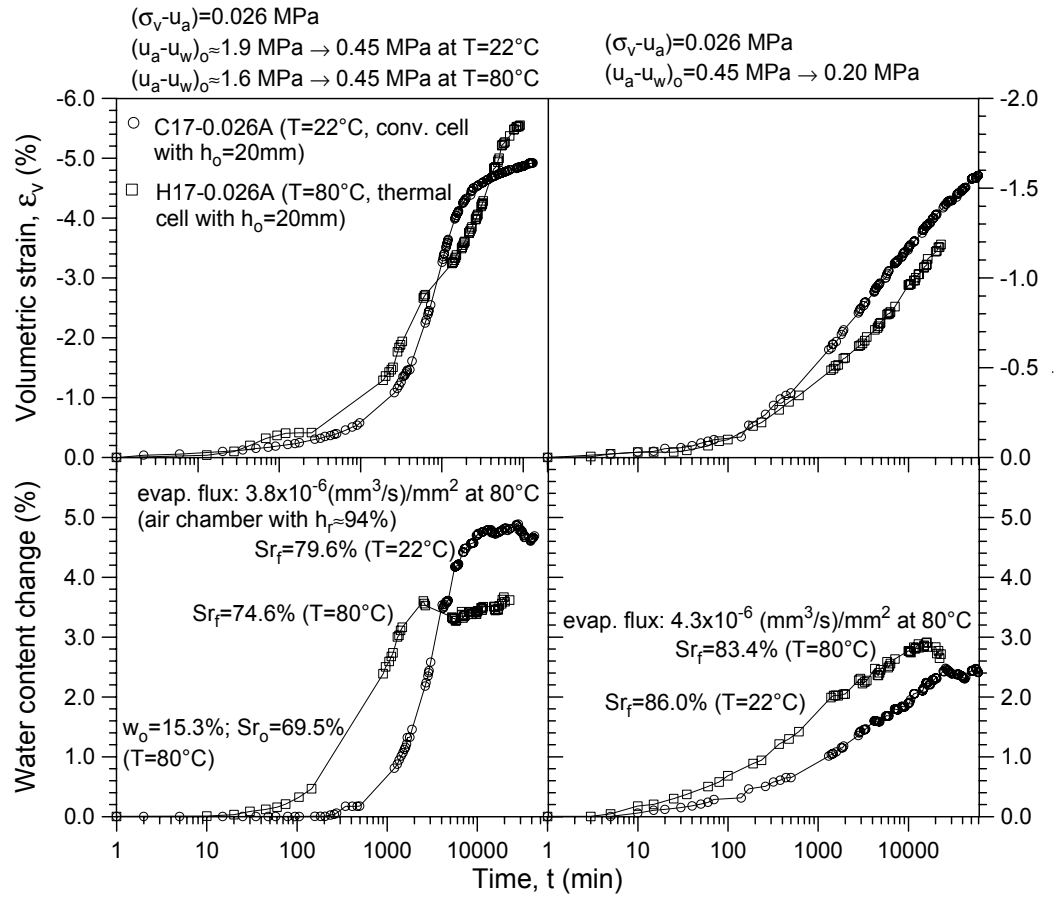

Figure 4.35 Problems with matric suction equalisation in test series H17-0.026A (first stages).

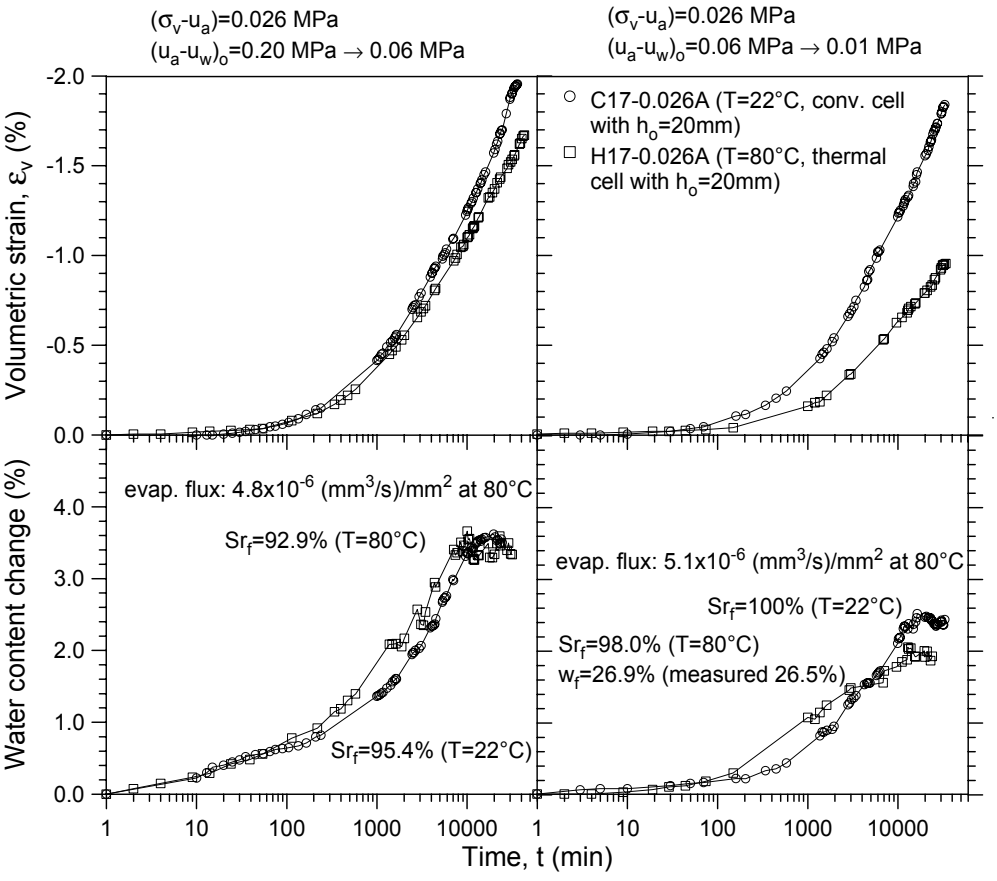

Figure 4.36 Problems with matric suction equalisation in test series H17-0.026A (last stages).

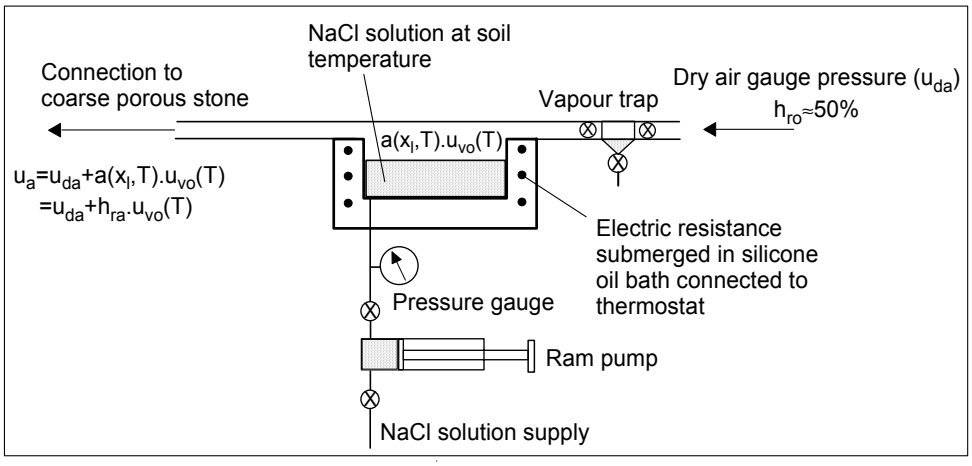

Figure 4.37 Proposed equipment to control vapour pressure in the dry air pressure line of the triaxial cell.

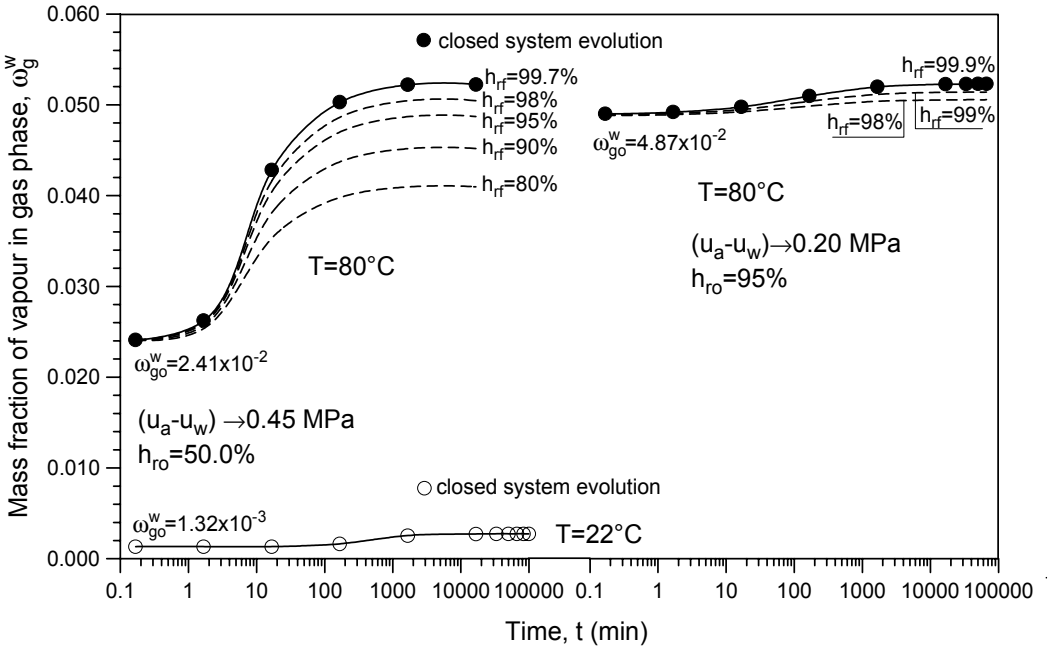

Figure 4.38 Variable boundary conditions for mass fraction of water in gas.

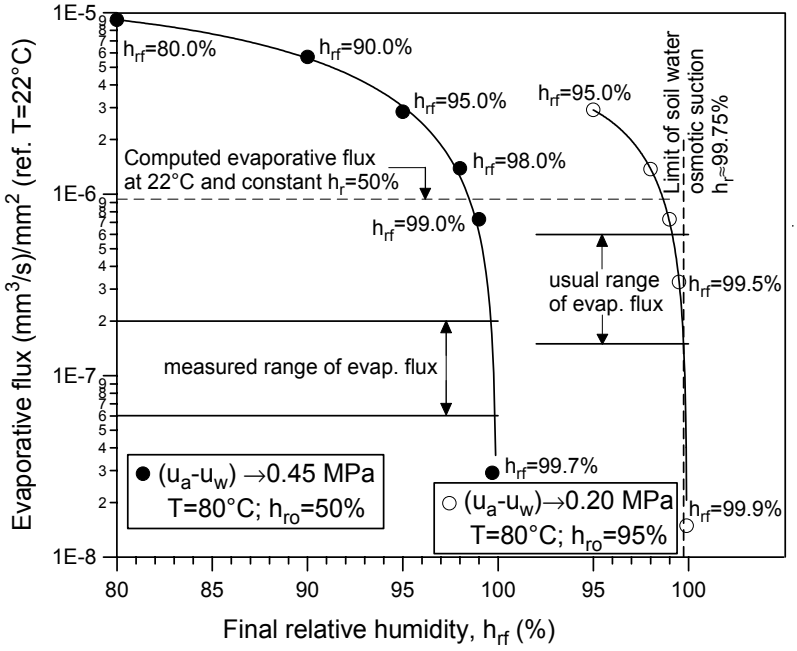

Figure 4.39 Computed evaporative fluxes under steady-state conditions for different final relative humidity.

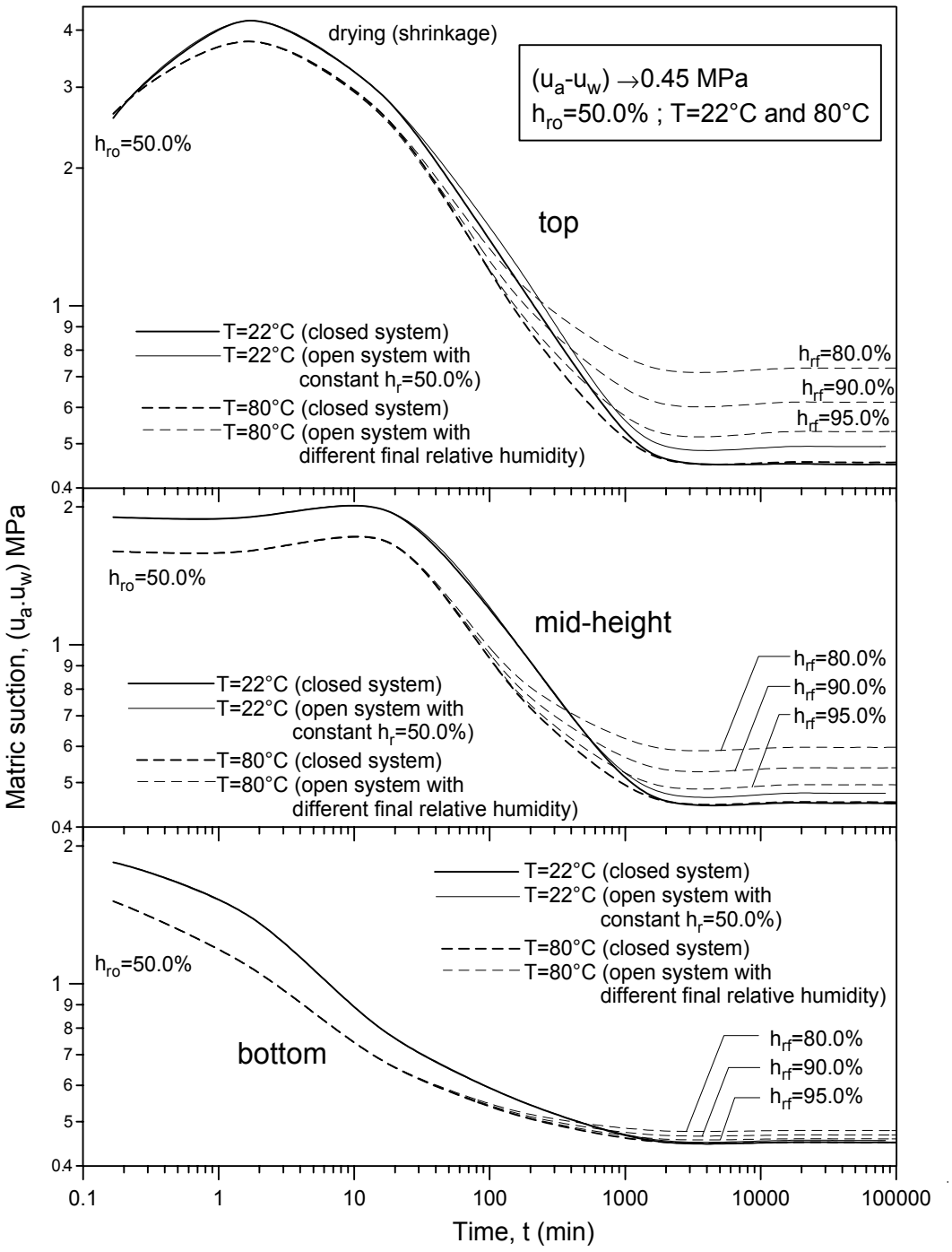

Figure 4.40 Matric suction evolution at selected nodes during first wetting step (target matric suction of 0.45 MPa).

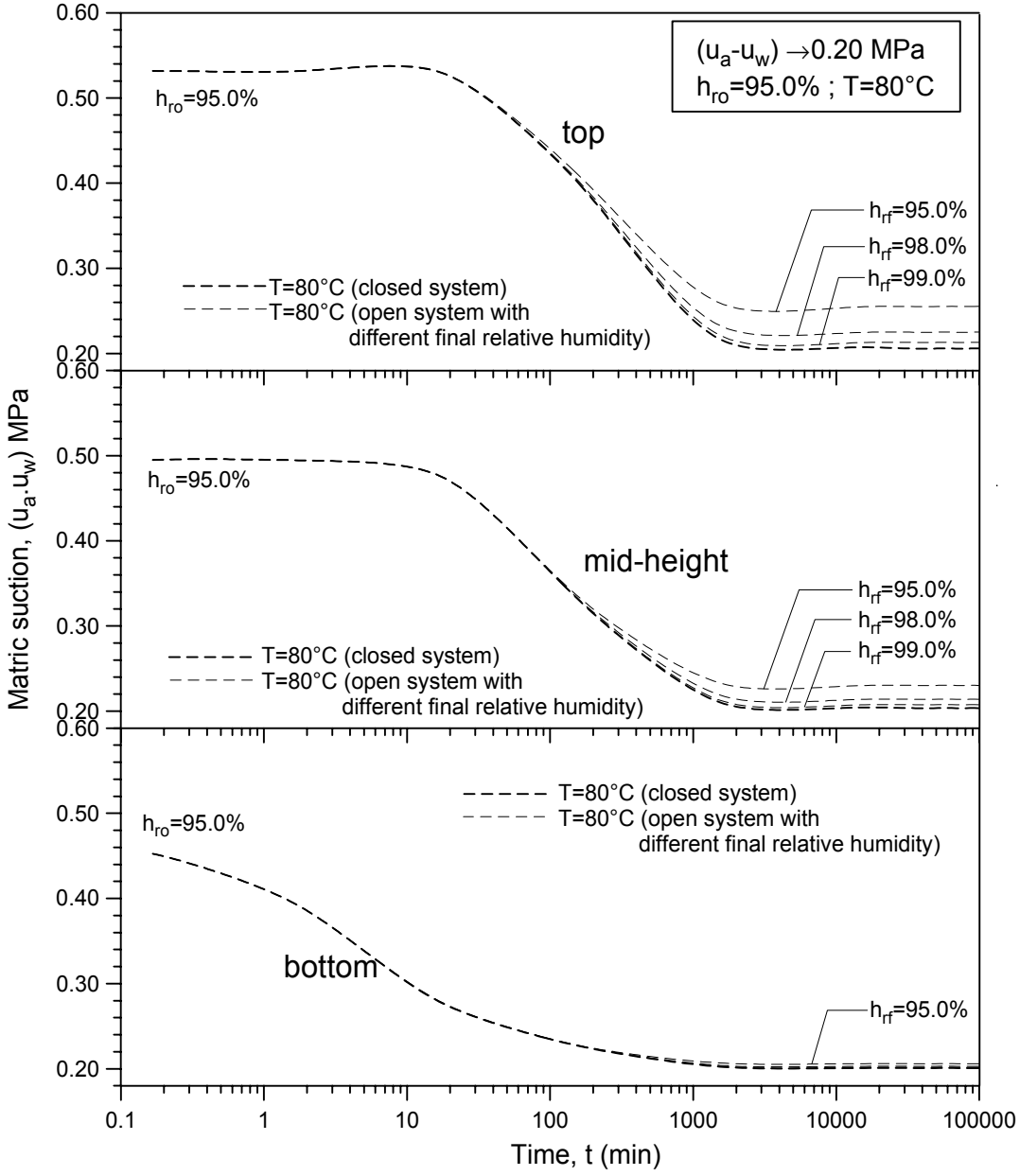

Figure 4.41 Matric suction evolution at selected nodes during second wetting step (target matric suction of 0.20 MPa).

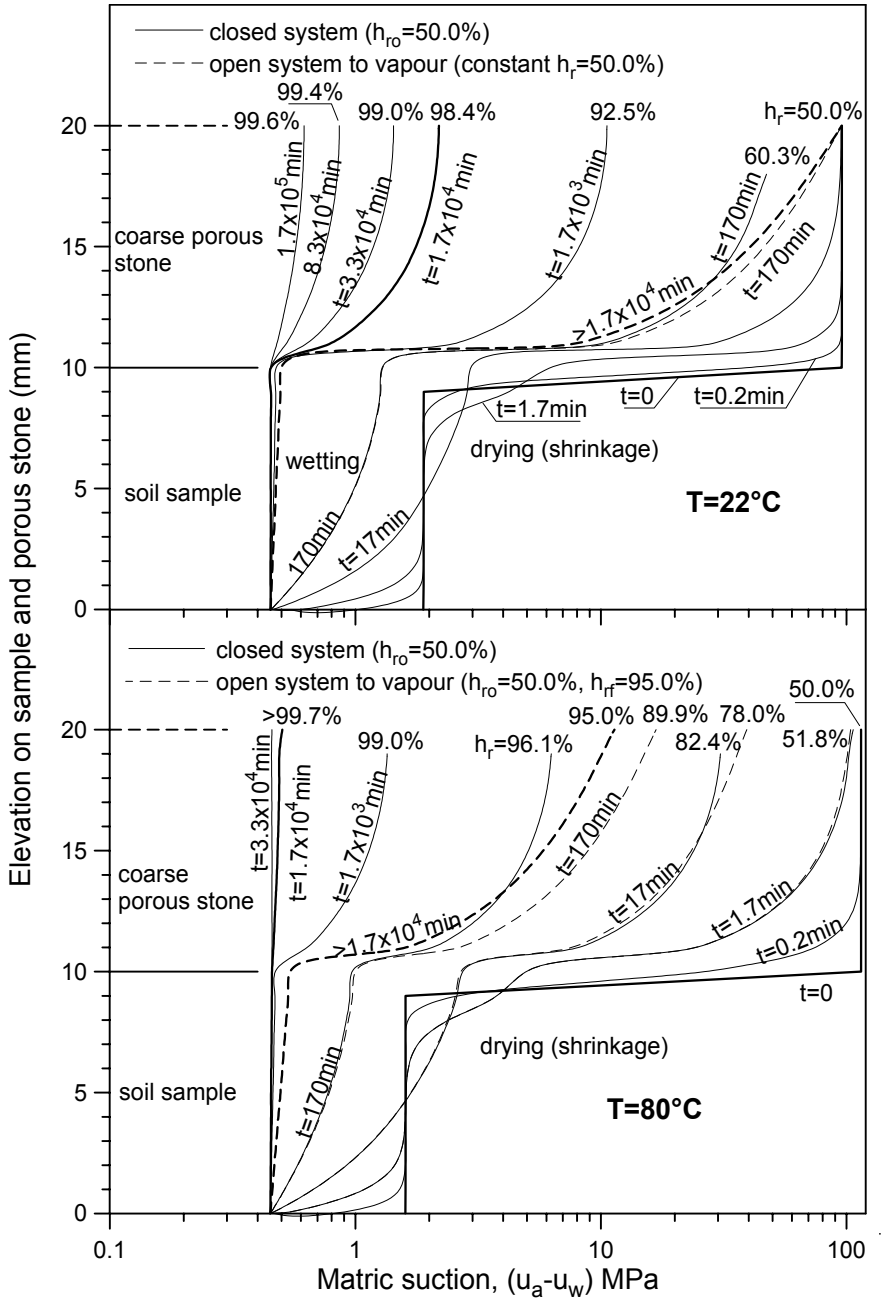

Figure 4.42 Matric suction isochrones for the first wetting step (target matric suction of 0.45 MPa).

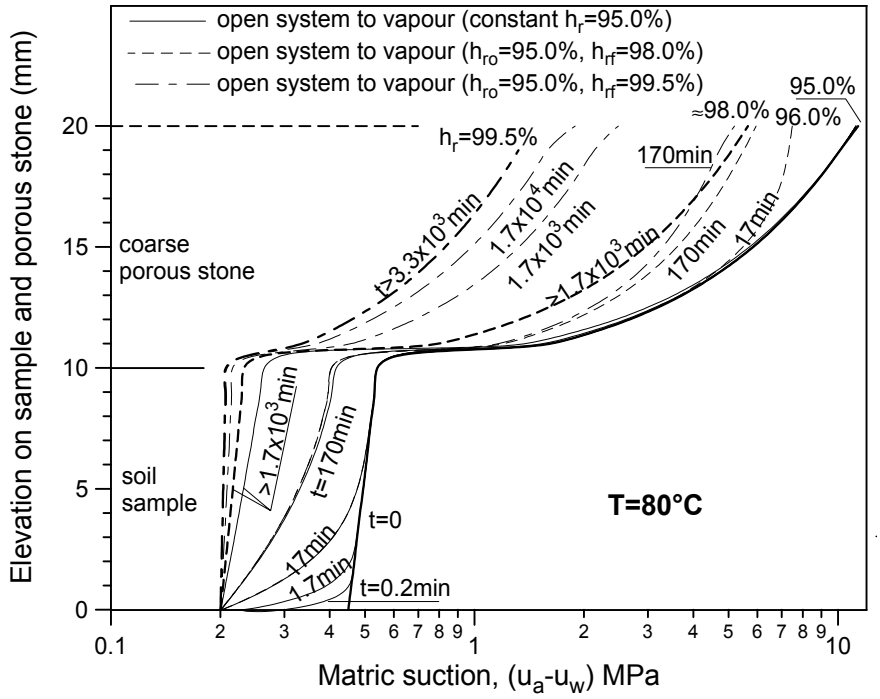

Figure 4.43 Matric suction isochrones for the second wetting step (target matric suction of 0.20 MPa).

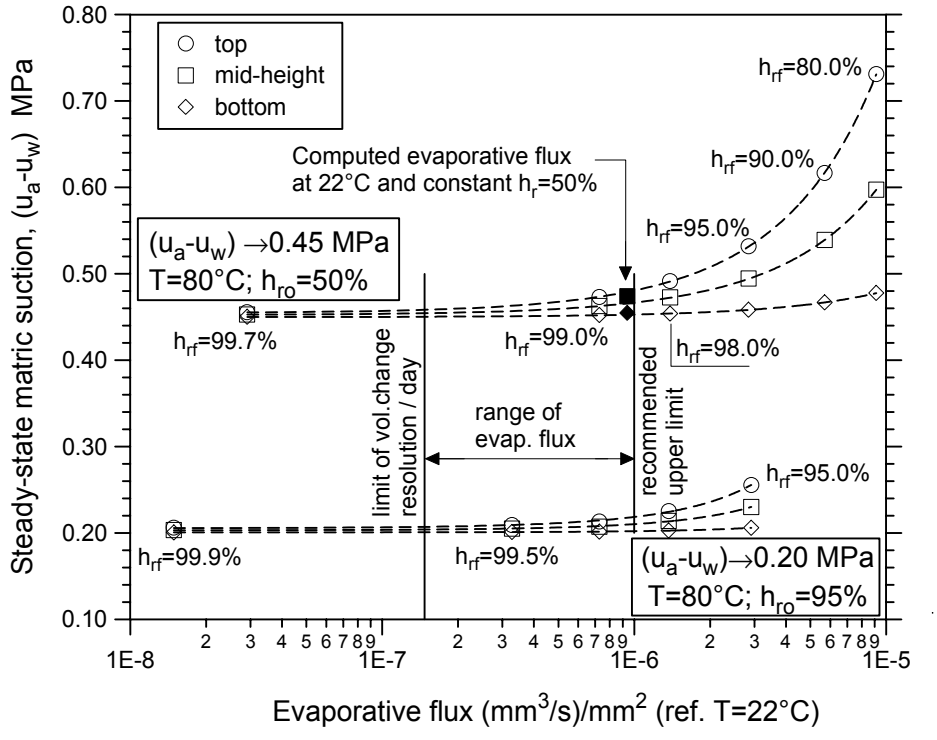

Figure 4.44 Final matric suction at selected points under steady-state conditions and related to the evaporative flux in the open system.